

UV Light Induced Surface Patterning and Recycling Strategies

Zur Erlangung des akademischen Grades eines
DOKTORS DER NATURWISSENSCHAFTEN

(Dr. rer. nat.)

von der KIT-Fakultät für Chemie und Biowissenschaften
des Karlsruher Instituts für Technologie (KIT)

genehmigte

DISSERTATION

von

M.Eng., Shuai Li

aus

Sichuan, China

1. Referent: Prof. Dr. Pavel A. Levkin

2. Referent: Prof. Dr. Patrick Théato

Tag der mündlichen Prüfung: 22.07.2022

Eidesstattliche Erklärung

Hiermit versichere ich, dass ich die vorliegende Arbeit selbständig verfasst und keine anderen als die angegebenen Quellen und Hilfsmittel verwendet, sowie Literaturzitate kenntlich gemacht habe. Die Satzung des Karlsruher Instituts für Technologie (KIT) zur Sicherung guter wissenschaftlicher Praxis wurde beachtet. Ich erkläre außerdem, dass diese Dissertation weder in gleicher oder ähnlicher Form bisher in einem anderen Prüfungsverfahren vorgelegen hat. Die elektroische Version der Arbeit stimmt mit der schriftlichen überein und die Abgabe und Archivierung der Primärdaten gemäß Abs. A (6) der Regeln zur Sicherung guter wissenschaftlicher Praxis der KIT beim Institut ist gesichert.

Ort, Datum

Unterschrift

Abstract

Surfaces exist in every aspect of our daily life, thus the modification of surfaces is of great significance in scientific research and in people's daily life. Over the past decades, great effort has been devoted to developing surfaces with various functionalities, such as controlled hydrophilicity, hydrophobicity, biocompatibility, antimicrobial activity, adhesiveness, non-adhesiveness, stimuli-responsiveness, or anti-icing properties. Surface patterning via photo-induced surface modification can create well-controlled physical or chemical patterns for use in a variety of fields, such as bioarrays, microfluidics, optical devices, healthcare materials, or sensors. At the same time, recycling and reuse are also meaningful for sustainable development due to the 368 million tons of polymers produced every year, 76% of which are discarded after single use. Recycling and reusing waste polymers and functionalized materials not only maintains sustainable economic development, but also reduces environmental pollution. This doctoral thesis focuses on reversible photo-induced surface patterning strategies, as well as photodegradation-induced gel patterning and recycling strategies.

In Chapter 1, an introduction is given to describe the recent progress in technologies for photo-induced surface and material patterning.

In Chapter 2, a facile and substrate-independent strategy for surface functionalization and patterning is introduced. This approach combines the advantages of three important coating methods: The substrate-independence of polydopamine coatings, the chemical reversibility of silane chemistry, and the rapid spatial control of thiol-ene photoclick chemistry. The unique simplicity of polydopamine coating and gas phase silanization allowed for the modification of different materials and complex surfaces without sophisticated equipment. Rapid UV-induced thiol-ene click chemistry enables patterning of silane functionalized polydopamine coating modified surfaces in minutes. The functionalization and patterning of diverse materials, such as glass, polytetrafluoroethylene (PTFE), aluminum, polypropylene or polyethylene are demonstrated. A controlled chemical removal of the patterns or surface functionalization by treatment with tetrabutylammonium fluoride allowed for the re-modification or the re-patterning of the substrate.

The developed universal surface modification for substrate independent and reversibly patternable coatings can facilitate the development of novel functional materials and devices useful in various applications.

In Chapter 3, the inherent UV photodegradability of poly(meth)acrylate organogels is introduced as a method to structure their surface. No additional photosensitizers are required to efficiently degrade organogels ($d \approx 1$ mm) on the minute scale. A low UV absorbance and a high swelling ability of the solvent infusing the organogel was found to be beneficial for a fast photodegradation, which is expected to be transferrable to other gel photochemistries. Organogel arrays, films, and structured organogel surfaces were prepared and the extraction ability and the slippery properties of the organogel were examined. Films of inherently photodegradable organogels on a copper circuit board served as the first ever positive gel photoresist: The spatially photodegraded organogel film protects the copper surfaces against an aqueous etchant ($\text{FeCl}_3_{\text{aq}}$).

In Chapter 4, a rapid approach to recycle crosslinked sodium polyacrylate is presented. This strategy is based on the inherent UV induced photodegradation of sodium polyacrylate. The recycle process does not require additional chemical reagents and the recovery of soluble sodium polyacrylate polymer from crosslinked sodium polyacrylate superabsorbers is practically quantitative. Recycled soluble sodium polyacrylate could be used as a thickener for aqueous paints or could be esterified to poly butyl acrylate (PBA) and poly 2-ethylhexyl acrylate (PEHA) for applications as a pressure sensitive adhesive. This rapid strategy provides the potential for the recycling of more than 2 million tons of waste superabsorbent materials per year.

In Chapter 5, a brief summary and outlook is presented. The substrate-independent reversible surface patterning strategy has important implications for the development of novel functional materials and devices. UV photodegradation of poly(meth)acrylates to pattern poly(meth)acrylate organogels is a potential alternative to soft lithography. The recycling of superabsorbent materials using UV photodegradation is of great significance for reducing environmental pollution and sustainable development.

Zusammenfassung

Oberflächen sind in jedem Aspekt unseres täglichen Lebens vorhanden, daher ist die Modifikation von Oberflächen von großer Bedeutung in der wissenschaftlichen Forschung und im täglichen Leben der Menschen. In den vergangenen Jahrzehnten wurden große Anstrengungen unternommen, um Oberflächen mit verschiedenen Funktionalitäten wie Hydrophilie, Hydrophobie, Biokompatibilität, antimikrobielle Aktivität, Haftvermögen, Anti-Haftvermögen, responsiven Eigenschaften und Vereisungsschutz zu entwickeln. Oberflächenstrukturierung durch photoinduzierte Oberflächenmodifikation kann gut kontrollierte physikalische oder chemische Muster zur Verwendung in einer Vielzahl von Bereichen erstellen, z. B. Bioarrays, Mikrofluidik, optische Geräte, Materialien für das Gesundheitswesen, oder Sensoren. Gleichzeitig sind Recycling und Wiederverwendung für eine nachhaltige Entwicklung von Bedeutung, da jährlich 368 Millionen Tonnen Polymere produziert werden, von denen 75 % nach einmaligem Gebrauch entsorgt werden. Das Recycling und die Wiederverwendung von Abfallpolymeren und funktionalisierten Materialien trägt nicht nur zu einer nachhaltigen wirtschaftlichen Entwicklung bei, sondern reduziert auch die Umweltverschmutzung. Diese Doktorarbeit konzentriert sich auf Strategien zur reversiblen photoinduzierten Oberflächenstrukturierung sowie auf durch Photodegradierung induzierte Gelstrukturierungs- und Recyclingstrategien.

In Kapitel 1 wird eine Einführung gegeben, um die jüngsten Fortschritte bei Technologien zur photoinduzierten Oberflächen- und Materialstrukturierung zu beschreiben.

In Kapitel 2 wird eine einfache und substratunabhängige Strategie zur Oberflächenfunktionalisierung und -strukturierung vorgestellt. Dieser Ansatz kombiniert die Vorteile von drei wichtigen Beschichtungsmethoden: Die Substratunabhängigkeit von Polydopaminbeschichtungen, die chemische Reversibilität der Silanchemie und die schnelle räumliche Kontrolle der Thiol-En-Photoklick-Chemie. Die einzigartige Einfachheit der Polydopaminbeschichtung und Gasphasensilanisierung ermöglichte die Modifizierung verschiedener Materialien und komplexer Oberflächen ohne komplizierte Ausrüstung. Die schnelle UV-induzierte Thiol-En-Klick-Chemie ermöglicht die Strukturierung von Silan-funktionalisierten

Polydopamin-beschichteten modifizierten Oberflächen in Minuten. Die Funktionalisierung und Strukturierung verschiedenster Materialien wie Glas, Polytetrafluorethylen (PTFE), Aluminium, Polypropylen oder Polyethylen wird demonstriert. Eine kontrollierte chemische Entfernung der Muster oder der Oberflächenfunktionalisierung durch Behandlung mit Tetrabutylammoniumfluorid ermöglichte die erneute Modifizierung oder Neustrukturierung des Substrats. Die entwickelte universelle Oberflächenmodifikation für substratunabhängige und reversibel strukturierbare Beschichtungen kann die Entwicklung neuartiger funktioneller Materialien und Geräte erleichtern, die in verschiedenen Anwendungen nützlich sind.

In Kapitel 3 wird die inhärente UV-Photoabbaubarkeit von Poly(meth)acrylat-Organogeln als Methode zur Strukturierung ihrer Oberfläche vorgestellt. Es sind keine zusätzlichen Photosensibilisatoren erforderlich, um Organogele ($d \approx 1 \text{ mm}$) im Minutenmaßstab effizient abzubauen. Eine geringe UV-Absorption und eine hohe Quellfähigkeit des Lösungsmittels, das das Organogel durchdringt, erwiesen sich als vorteilhaft für einen schnellen Photoabbau, von dem erwartet wird, dass er auf andere Gel-Photochemien übertragbar ist. Organogel-Arrays, Filme und strukturierte Organogel-Oberflächen wurden hergestellt und die Extraktionsfähigkeit und die Gleiteigenschaften des Organogels untersucht. Filme aus inhärent photoabbaubaren Organogelen auf einer Kupferleiterplatte dienten als erster positiver Gel-Photoresist: Der räumlich photoabbaubare Organogelfilm schützt die Kupferoberflächen vor einem wässrigen Ätzmittel ($\text{FeCl}_3 \text{ aq.}$).

In Kapitel 4 wird ein schneller Ansatz zum Recycling von vernetztem Natriumpolyacrylat vorgestellt. Diese Strategie basiert auf dem inhärenten UV-induzierten Photoabbau von Natriumpolyacrylat. Der Recyclingprozess erfordert keine zusätzlichen chemischen Reagenzien und die Gewinnung von löslichem Natriumpolyacrylat-Polymer aus vernetzten Natriumpolyacrylat-Superabsorbern ist praktisch quantitativ. Wiederverwertetes lösliches Natriumpolyacrylat könnte als Verdickungsmittel für wässrige Farben verwendet werden oder könnte für Anwendungen als Haftklebstoff zu Polybutylacrylat (PBA) oder Poly-2-ethylhexylacrylat (PEHA) verestert werden. Diese schnelle Strategie bietet das Potenzial für das Recycling von mehr als 2 Millionen Tonnen Superabsorber-Abfall pro Jahr.

In Kapitel 5 wird eine kurze Zusammenfassung und ein Ausblick gegeben. Die Strategie der substratunabhängigen reversiblen Oberflächenstrukturierung hat wichtige Auswirkungen auf die Entwicklung neuartiger funktioneller Materialien und Geräte. Der UV-Photoabbau von Poly(meth)acrylaten zu strukturierten Poly(meth)acrylat-Organogeln ist eine potenzielle Alternative zur weichen Lithographie. Das Recycling von superabsorbierenden Materialien durch UV-Fotoabbau ist von großer Bedeutung für die Verringerung der Umweltverschmutzung und eine nachhaltige Entwicklung.

Acknowledgement

Four years in Germany went by quickly! First of all, I would like to thank Prof. Dr. Pavel A. Levkin for giving me the opportunity to become a PhD student at Karlsruhe Institute of Technology. I learned a lot of scientific thinking from him and thank him for inspiring me in my project ideas. He gave me a lot of encouragement when I wanted to give up. Thank you, Pavel!

I would like to thank Prof. Dr. Patrick Theato for taking his time to be my second Referent.

I would like to thank my colleague Johannes M. Scheiger, who has been extremely helpful in almost all my projects. He helped me a lot in both my research and life in Germany. Thank you, Johannes!

I am thankful to my colleague and roommate Zhenwu, we spent three years together in Germany.

I am thankful to all my group members for your help, kindness, and patience. Thankful to Haijun, Yanxi, Wenxi, Zheqin, Ye, Farid, Changming, Anna, Konny, Janne, Maria, Shraddha, Alisa, Simon, Tina, Marius, Gerile, Julius, Max, Sida, Yaqi, Weiyi, Juning, Qianyu, Xiaotao, Dorothea, Razan, Joaquin offering me a friendly working environment. I am very happy to work with you all!

I would like to thank PD Dr. Dr. Michael Hirtz, Dr. Alexander Welle, Dr. Vanessa Trouillet, Birgit Huber and Maxi Hoffmann for their help with measurements!

I would like to thank Prof. Dr. Patrick Theato and Dr. Gary Davidson for being my TAC members and for their valuable suggestions!

I would like to thank Prof. Dr. Stefan Bräse and all colleagues at IBCS for the good public environment you provide!

I would like to thank BIF-IGS school for providing many useful courses and opportunities to communicate with researchers in other fields!

I would like to thank the China Scholarship Council for their financial support!

I would like to thank my parents and wife for their support and tolerance!

Table of Contents

Abstract.....	I
Zusammenfassung.....	III
Acknowledgement	VII
1 Introduction.....	1
1.1 Surface Modification.....	1
1.1.1 Silane Chemistry	2
1.1.2 Polydopamine.....	3
1.1.3 Click Chemistry	5
1.2 Reversible Surface Modification.....	7
1.2.1 Non-covalent Reversible Modification	7
1.2.2 Covalent Reversible Modification	8
1.3 Surface Patterning and Photopatterning.....	11
1.3.1 Bottom-Up Photopatterning	12
1.3.2 Top-Down Photopatterning.....	15
1.3.2.1 Photochromic Patterning.....	16
1.3.2.2 Photodegradation Patterning.....	18
1.4 Photodegradation of Poly(meth)acrylate Gel	21
1.5 Summary and Perspectives	23
2 Results and Discussion	25
2.1 Substrate-Independent and Re-Writable Surface Patterning by Combining Polydopamine Coatings, Silanization and Thiol-Ene Reaction.....	25
2.1.1 Introduction	25
2.1.2 Results and Discussion	26
2.1.3 Summary.....	43
2.1.4 Experimental Details.....	43
2.2 Inherently UV Photodegradable Poly(meth)acrylate Gels	47
2.2.1 Introduction	47

2.2.2 Results and Discussion	48
2.2.3 Summary.....	63
2.2.4 Experimental Details.....	64
2.3 Pampers to Paints and Pressure Sensitive Adhesives: Recycling of Superabsorbers via UV Degradation.....	69
2.3.1 Introduction	69
2.3.2 Results and Discussion	70
2.3.3 Summary.....	80
2.3.4 Experimental Details.....	81
3 Conclusions and Outlook	83
4 Appendix	87
4.1 Abbreviations.....	87
4.2 Curriculum Vitae	89
4.3 Publications.....	90
References	91

1 Introduction

1.1 Surface Modification

Surface modification is a widely studied topic in materials science.¹⁻³¹ It can be used to introduce a variety of properties in materials, such as hydrophilicity,¹⁻³ hydrophobicity,⁴⁻⁷ biocompatible property,⁸⁻¹⁰ antibacterial property,¹¹⁻¹³ adhesive property,¹⁴⁻¹⁶ non-adhesive,¹⁷⁻¹⁹ antifouling property,²⁰⁻²² stimuli-responsiveness,²³⁻²⁷ anti-icing property,²⁸⁻³¹ and so on. The approaches to surface modification can be divided into physical and chemical. A typical example of physical modification is bioinspired self-repairing slippery surfaces. Aizenberg et al. reported synthetic liquid-repellent surfaces, ‘slippery liquid-infused porous surfaces’ (SLIPS), that each consist of a film of lubricating liquid locked in place by a micro/nanoporous substrate (Figure 1.1). SLIPS are self-repairing by wicking into damaged sites in the underlying substrate and can repel immiscible liquids of virtually any surface tension.⁴ For chemical modification, a variety of chemical reactions can be used in the surface modification of materials.^{20,21,32-43} Among the most commonly used are silane chemistry,^{20,32-35,42} polydopamine chemistry,³⁶⁻³⁸ click chemistry,³⁹⁻⁴² free radical polymerization grafting,^{20,21,43} etc.

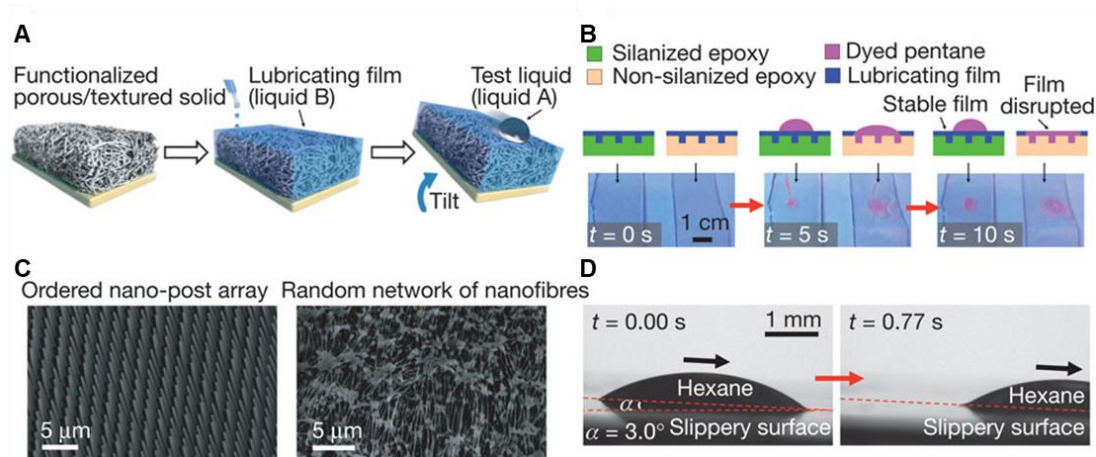


Figure 1.1 (A) Schematics showing the fabrication of a slippery liquid-infused porous surfaces by infiltrating a functionalized porous/textured solid with a low-surface-energy, chemically inert liquid to form a physically smooth and chemically homogeneous lubricating film on the surface of

the substrate. (B) Comparison of the stability and displacement of lubricating films on silanized and non-silanized textured epoxy substrates. (C) Scanning electron micrographs showing the morphologies of porous/textured substrate materials. (D) Optical micrograph showing the flow of low surface tension liquid hydrocarbon-hexane on slides. Adapted from Ref.⁴

1.1.1 Silane Chemistry

Trichlorosilane, trimethoxysilane or triethoxysilane are often used to form alkylsiloxane monolayers on substrates.^{34,44} The reaction of alkylsilane-modified surfaces can usually be carried out in solution or in the gas phase and it is easier to obtain dense monolayers in gas-phase reactions than in solution.⁴⁵ Water plays an important role in anchoring the silane to the substrates, the hydrolyzed molecule of chlorosilane reacts with the hydroxyl group on the substrate.^{46,47} Subsequently, the silane molecules form a polymeric network, partly covalently bound to the substrate. As shown in Figure 1.2, the other end of the silane chain can be various functional molecules or active group that reacts with other chemical reagents.³⁵ When connecting functional molecules, silane chemistry modification can directly endow materials with hydrophilicity-hydrophobicity,⁴⁸⁻⁵⁰ biocompatible property,^{32,51} adhesive property,⁵² antifouling property,⁵³ antibacterial property,⁵⁴ etc. When the other end of silanes are reactive molecules, they can serve as linking molecules for the secondary modification of the material surfaces.³⁴

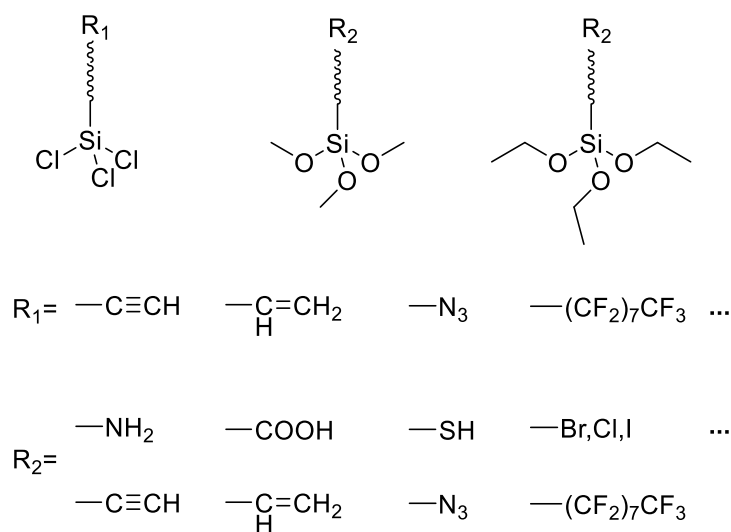


Figure 1.2 Chemical structures of trichlorosilane, trimethoxysilane and triethoxysilane. The other end of the silane chain can be various functional molecules or active group that reacts with other chemical reagents.

1.1.2 Polydopamine

Surface functionalization through polydopamine (PDA) coating was introduced by Lee and Messersmith in 2007 is a unique method inspired by the adhesive properties of the mussel foot (Figure 1.3).⁵⁵ The advantages of this technique include its simplicity, substrate-independence, robustness and universality.⁵⁶⁻⁵⁹ This substrate-independent coating method has been widely used in various applications, including surface patterning,⁶⁰⁻⁶² improving biocompatibility of substrates,⁶³⁻⁶⁵ and rendering surfaces superhydrophobic^{66,67} or antibacterial.^{68,69} The possibility of secondary modification, patterning or the ability to re-functionalize PDA coatings is important to broaden the scope of applications of this coating method.⁷⁰⁻⁷² Various methods for the secondary modification of PDA coating, utilizing the presence of activated double-bonds, multiple catechol groups and amino functionality in the PDA, have been introduced, including the use of thiols, amines, silanes or various metal ions.^{70,73-77}

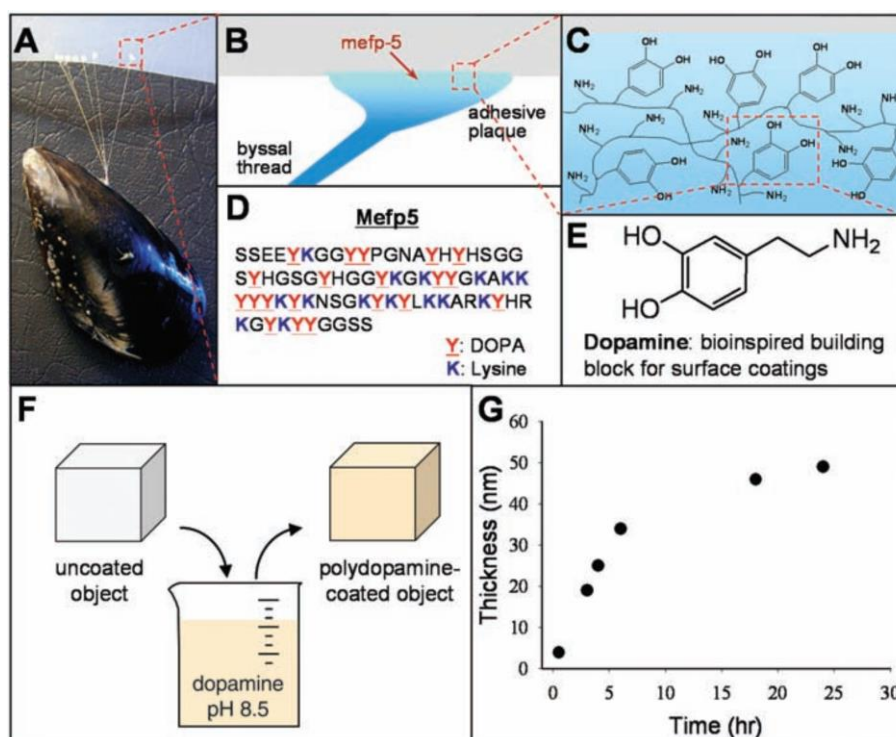


Figure 1.3 (A) Photograph of a mussel attached to commercial PTFE. (B, C) Schematic illustrations of the interfacial location of Mefp-5 and a simplified molecular representation of characteristic amine and catechol groups. (D) The amino acid sequence of Mefp-5. (E) Dopamine contains both amine and catechol functional groups found in Mefp-5 and was used as a molecular building block for polymer coatings. (F) A schematic illustration of thin film deposition of polydopamine by dip-coating an object in an alkaline dopamine solution. (G) Thickness evolution of polydopamine coating on Si as measured by AFM of patterned surfaces. Adapted from Ref.⁵⁵

Dopamine undergoes a series of oxidative reactions to form 3,4-dihydroxyindole (DHI), as shown in Figure 1.4 is a widely accepted primary building block.^{55,78} Second, there is a large amount of uncyclized oxidized dopamine on the surface of the coating, which contains significant levels of amino groups.⁷⁹ After the formation of dopamine-quinone, it reacts with DHI or dopamine through the coupling of catechol-catechol.⁷⁸ In the formation of polydopamine, the catechol-catechol dimerization process is important because it presents amine groups on the surface for further functionalization.⁸⁰ A new class of self-assembling physical trimers, (dopamine)₂/DHI, incorporates polydopamine chains.⁷⁹ For a long time, hydrogen bonding and π - π stacking were considered to be the main intermolecular interactions in the formation of polydopamine coatings. The latest study shows that the cation- π interaction is also the main force for interchain

deposition.⁸¹ These interactions mediate the deposition of polydopamine, which increases coating thickness.⁷⁸

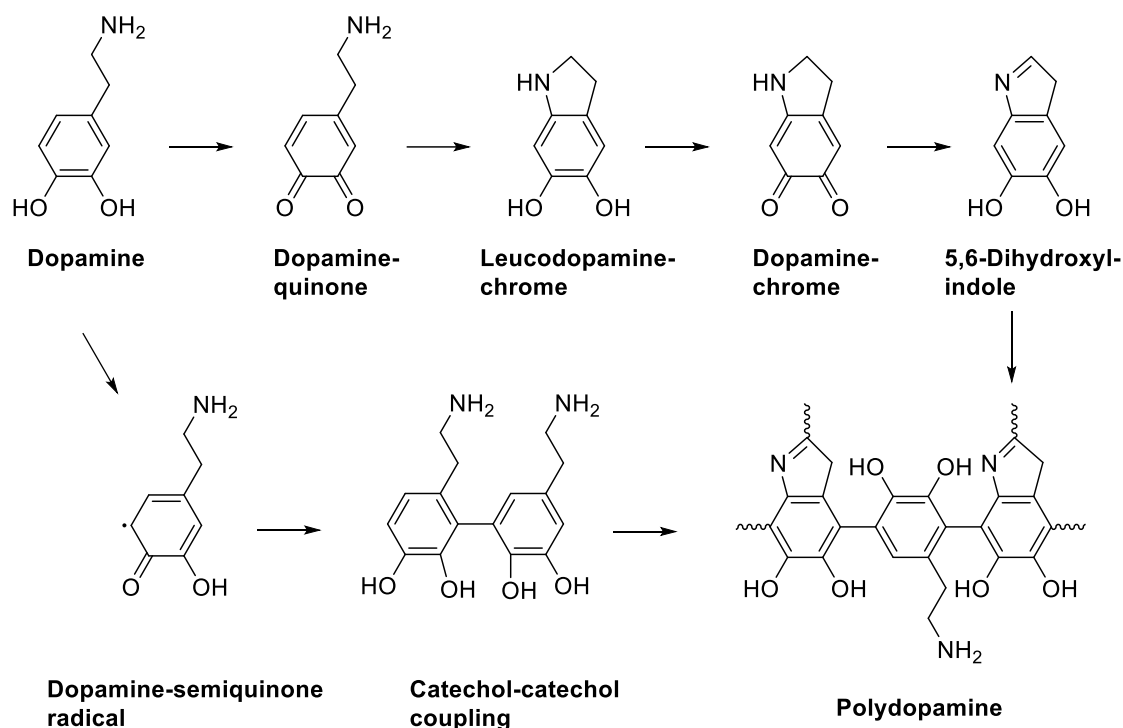


Figure 1.4 Polymerization and interaction mechanisms of dopamine. As reported by Lee and Messersmith in 2007, 3,4-dihydroxyindole (DHI) spontaneously generated by a series of oxidation steps from dopamine.⁵⁵ Second, there is a significant level of uncyclized form of oxidized dopamine presenting primary amine groups on the surface. Through the formation of dopamine-quinone, it subsequently reacts with DHI or dopamine through the coupling of catechol to catechol. The backbone of polydopamine is mainly 4,7-catechol-catechol coupling with uncyclized primary amine and cyclized secondary pyrrole amine.⁷⁸

1.1.3 Click Chemistry

Click chemistry was proposed by Sharpless et al. in 2001.³⁹ Click chemistry vividly describes the chemical reaction process as simple, efficient, and versatile like clicking a mouse. It mainly has the following characteristics: (1) the reaction raw materials are readily available, (2) the reaction is very reliable, insensitive to oxygen and water, (3) the product stereoselectivity is good, the yield

is high, (4) the post-reaction treatment and product separation are simple and convenient, (5) the reaction by-products are environmentally friendly.^{39,40,42} Due to these advantages of click chemistry, it is widely used in surface modification in recent years. Common click chemistry reactions for surface modification include azide-alkyne cycloaddition,^{82,83} thiol-ene/yne click reactions,^{41,84-90} tetrazole-ene reactions,⁹¹⁻⁹³ Diels-Alder cycloaddition,⁹⁴ and oxime/hydrazone formation⁹⁵. Collman et al. applied click chemistry to the study of electrode surface modification for the first time.^{82,83} They formed a monolayer of the azide ligand on the surface of the gold electrode, and then modified the acetylenic ferrocene to the surface of the electrode and investigated the electrode performance by cyclic voltammetry. As shown in Figure 1.5, Atsushi et al. modified vinyl bearing metal substrates with various thiol molecules to endow metal substrates with different surface wettability.⁴¹ Sun et al. used functionalized polyvinyl alcohol as a connector to immobilize complex functional molecules such as biotin, carbohydrates and proteins on the glass surface through Diels-Alder and click reactions.⁹⁴ The specific adsorption of various functional molecules and biomolecules immobilized on the surface was investigated.

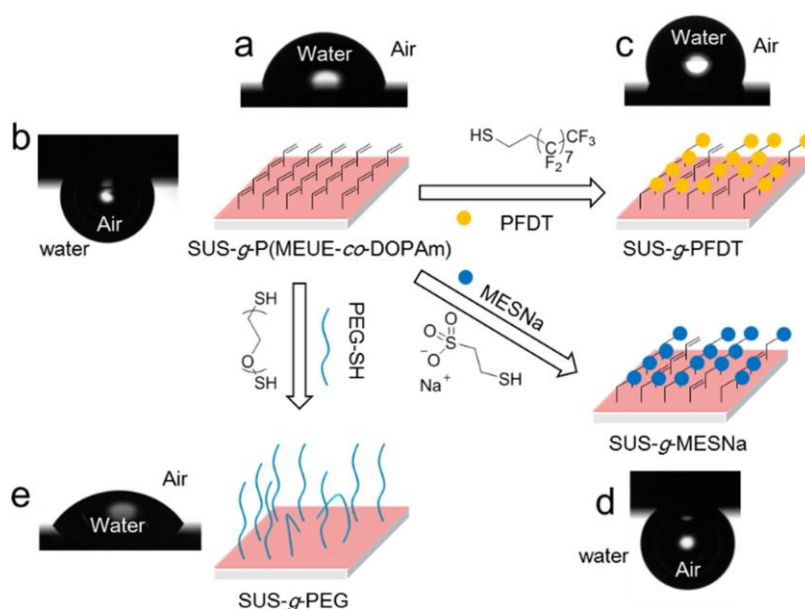


Figure 1.5 Schematic of the post functionalization of metal surface with vinyl groups using various thiols. Adapted from Ref.⁴¹

1.2 Reversible Surface Modification

Surface modification enables materials to be applied with a new surface property, while reversible surface modifications can impart one or more surface properties to materials multiple times.⁹⁶⁻¹¹¹ Reversible surface modification allows material substrates to be recycled and reused, which is sustainable and environmentally friendly. Many related reversible surface modification processes have been reported, including reversible hydrogen bond formation,⁹⁶ electrically assisted ionoprinting,¹⁰¹ metal complexation,⁹⁸ host-guest chemistry,⁹⁷ sulfur chemistry,^{100,102,103} reversible silane chemistry,¹¹² Schiff-base chemistry,^{99,113} Diels-Alder chemistry,¹⁰⁴⁻¹⁰⁷ and reversible photochemistry¹⁰⁸⁻¹¹⁰. The reversible modification can be roughly divided into the following two categories, non-covalent reversible modification and covalent reversible modification.

1.2.1 Non-covalent Reversible Modification

Non-covalent reversible modifications are based on non-covalent bonding forces, the modified layer can be removed by stimuli such as light, heat, pH changes, solvents, etc.^{96-98,101} Non-covalent reversible modification strategies reported in recent years include reversible hydrogen bond formation,⁹⁶ electrically assisted ionoprinting,¹⁰¹ metal complexation,⁹⁸ host-guest chemistry.⁹⁷ Christopher et al. report a patterned and rewritable surface system that relies on synthetic hydrogen-bonding motifs (symmetrical oligoamide-asymmetric oligoamides pairs, SOA-AOA pairs).⁹⁶ The maleimide-functionalized amide asymmetric oligoamides (AOA) was first immobilized on the substrate, and the symmetrical oligoamides (SOA) sequence with functional groups could form a dimer with AOA through hydrogen bonding (Figure 1.6). The SOA was removed by the destruction of the dimer structure by methanol and chloroform mixture solvents. The formation and destruction of AOA-SOA dimers are the main mechanisms of surface reversible processes. Luc Brunsveld et al. reported a strategy to facile, robust and reversible immobilization of supramolecular proteins via selective monovalent interaction of ferrocene with cucurbituril immobilized on gold surfaces. Proteins can be printed as uniform monolayers that are resistant to washing conditions and removed by competition with excess ferrocene ligand.⁹⁷ Schubert et al. reported the reversible functionalization of surface by exploiting the reversible formation of terpyridine bicomplexes.⁹⁸

The reversible formation of terpyridine bicomplexes, based on monolayers functionalized with terpyridine ligands, was used as a versatile supramolecular binding motif. Ligand-modified monolayers can be obtained by decomplexing the formed supramolecular complexes. These monolayers were then used for additional complexation reactions, leading to reversible functionalization of the substrate.⁹⁸



Figure 1.6 Schematic representation of the synthetic route to the patterned immobilization of symmetrical oligoamide-asymmetric-polymethylmethacrylate (SOA-PMMA) on a silicon wafer. The wafer was globally functionalized with tetrazoles (S1) and partly functionalized with AOA-Mal (4) via a photo-induced NITEC reaction employing a shadow mask resulting in S2. SOA-PMMA (P1) was repeatedly immobilized and washed off the AOA-functionalized part of S2/S3. Adapted from Ref.⁹⁶

1.2.2 Covalent Reversible Modification

Covalent reversible modification strategies are based on reversible chemical reactions or dynamic bonds.^{102,103,105-110,113} Compared with non-covalent modification, covalent bonding modified surfaces are more chemically stable and robust. Covalent reversible modification strategies reported in recent decades involve Schiff-base chemistry,^{99,113} reversible silane chemistry,¹¹² sulfur chemistry,^{100,102,103,114} Diels-Alder chemistry,¹⁰⁴⁻¹⁰⁷ and reversible photochemistry¹⁰⁸⁻¹¹⁰. Zhao et al. reported a reversible polymer brush coating based on Schiff-base chemistry, achieved dynamic

control of nanoparticle surface properties.⁹⁹ They first immobilized aldehyde-functionalized ATRP initiator molecules to the surface of amine-functionalized nanoparticles, and then grew polymer brushes through ATRP. The dynamic nature of the imine bond allows the polymer brushes to be removed, allowing exchange reactions between different aldehyde-functional molecules. This allows the introduction of small molecule fluorophores or the production of hybrid polymer brushes.⁹⁹ A typical reversible silanization modification is presented in Figure 1.7.¹¹² Marius et al. combined synthetic and surface chemistry to achieve variable control of surface wettability by either coupling a fluorinated alkyl silane to the naturally hydrophilic surface of a nanoporous polymer coating to achieve superhydrophobicity or by removing it from the surface by application of fluoride anions to regain hydrophilicity.¹¹² Figure 1.8, a typical reversible modification strategy based on light-induced disulfide exchange reaction is presented, achieving reversible photo functionalization, patterning, and exchange and removal of surface functional groups.¹¹⁴ This surface shows reversible and rewritable functionality under UV irradiation. A uniform fluorescent surface is produced by using fluorescent FITC-disulfide, photopatterning was demonstrated by masked illumination. This method is versatile, fast and various functional groups can be introduced onto the disulfide-functionalized surfaces and removed reversibly by light-induced disulfide exchange.¹¹⁴ Kowollik et al. reported an example of use Diels-Alder chemistry for reversible surface modification with polymers.¹⁰⁴ Diels-Alder reaction allows for the covalent linkage of various dienophile with cyclopentadiene functionalized surface under ambient temperature. After the system was heated to 90 °C, a reversible reaction was triggered. This method can be used to modify surfaces with polyisobornyl acrylate, polystyrene, and polyethylene glycol, demonstrating the versatility of this chemical approach for surface modification.¹⁰⁴

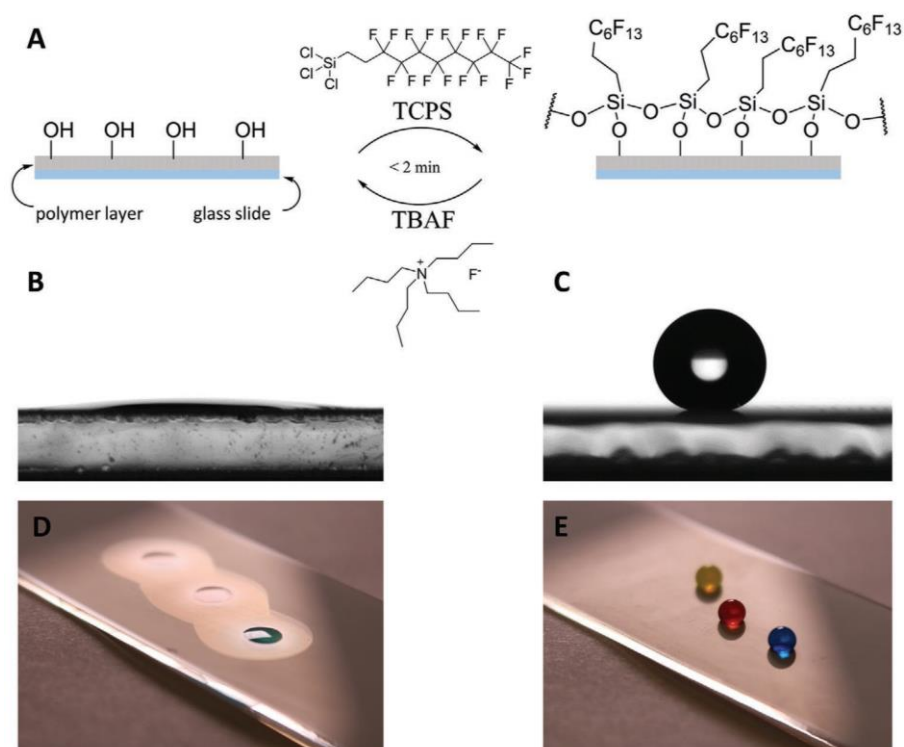


Figure 1.7 General overview of the method as a reaction scheme (A) and images of water droplets on hydrophilic (B, D) and superhydrophobic (C, E) polymer surfaces. Adapted from Ref.¹¹²

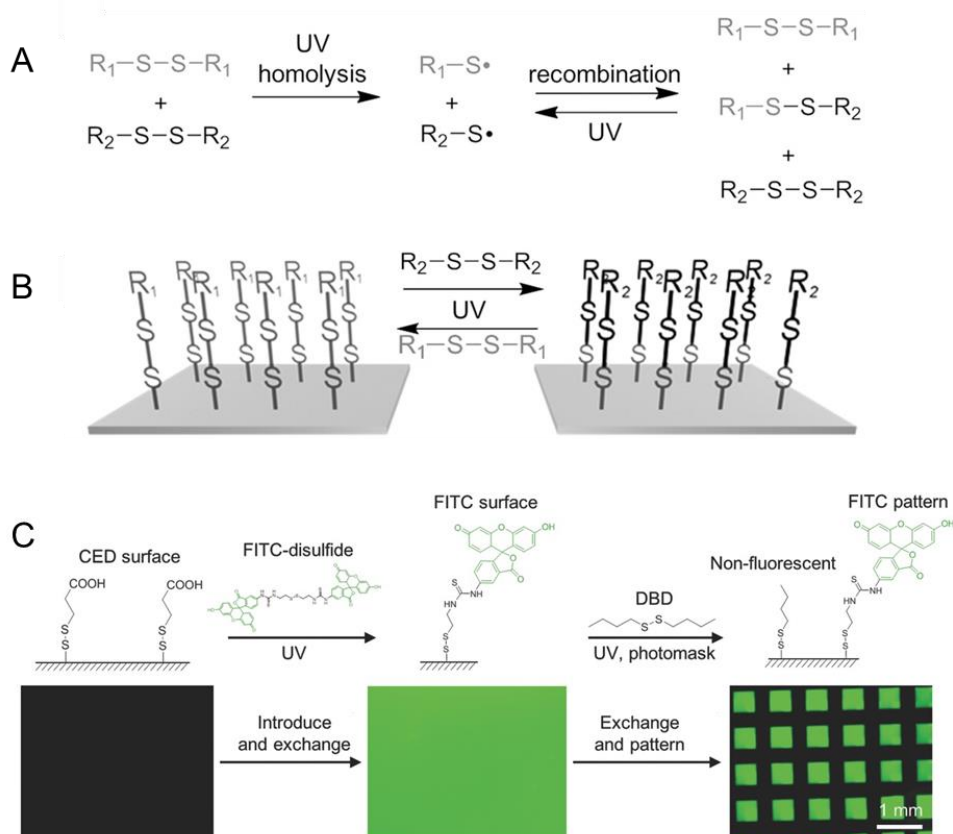


Figure 1.8 (A) Schematic representation of a photodynamic disulfide exchange reaction (PDDE). Disulfides are converted into two sulfenyl radicals under UV irradiation, which can combine to form new disulfides. The new disulfides can again be activated to become sulfanyl radicals and thus the process is reversible. (B) Schematic representation of the reversible surface modification based on the PDDE. (C) The surface modification using photoinduced disulfide exchange and corresponding fluorescence microscopy images. Adapted from Ref.¹¹⁴

1.3 Surface Patterning and Photopatterning

As a branch of surface modification, surface patterning is accessible which achieves well-controlled physical or chemical patterns on the surface.¹¹⁵⁻¹²⁶ Patterned surfaces can be used in a variety of research and industrial fields, such as bioarrays,¹¹⁸⁻¹²⁰ microfluids,¹²³⁻¹²⁵ optical devices,^{121,122} medical science,¹²⁶ sensors,¹¹⁵⁻¹¹⁷ and so on. Over the past few decades, researchers have developed a large variety of surface patterning strategies, including laser writing,^{127,128} scanning probe lithography,¹²⁹⁻¹³¹ two-photon polymerization,^{132,133} micro-contact printing,^{134,135} inkjet printing,¹³⁶ microfluidic patterning,¹³⁷ photopatterning^{100,102,103,114,138} and so on. Usually, for the same surface material, there can be many different patterning techniques to achieve the purpose. For example, self-assembled monolayers (SAMs) on planar metal surfaces were first reported by Allara and Whitesides et al.^{139,140} This system has been widely studied due to its facile preparation, wide commercial availability, and self-assembly to form organic molecular nanoarrays.^{139,140} Typical strategies for fabricating patterned SAMs are microcontact printing, scanning probe lithography, and photo-induced patterning (Figure 1.9).¹³⁵ The elastic stamp is made of polydimethylsiloxane (PDMS) and is used to transfer the SAM molecules to the substrate. The PDMS stamp is removed from the solution and contacted with the surface, causing the adsorbed molecules to transfer from the stamp to the substrate in the contact area. Thereby reproducing the pattern information encoded in the surface profile of the stamp.¹⁴¹ (Figure 1.9A) In scanning probe lithography, probe tips are used not only to visualize nanoscale surface structures, but also to manipulate atoms and molecules on the surface.¹⁴² (Figure 1.9B) SAM patterns can also be

prepared with photo-induced patterning by irradiating SAM functionalized surface through photomask without the use of photoresist. (Figure 1.9C)¹³⁵

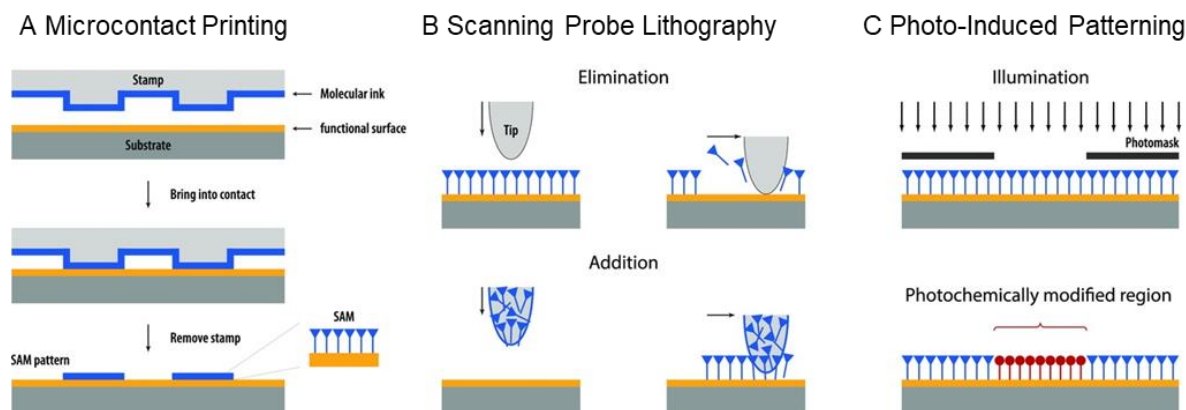


Figure 1.9 Overview of patterning techniques for self-assembled monolayers. (A) In microcontact printing, SAMs patterns are achieved by region-selectively transferring a molecular ink onto a substrate via an elastomeric stamp. (B) By utilizing nanoscopic probe tips to locally eliminate or add molecules, highly resolved SAMs features can be generated by scanning probe lithography. (C) Illuminating SAMs through a photomask can result in photochemical modification of the non-covered areas. This photolithographic approach allows for the subsequent removal or functionalization of the modified regions. Adapted from Ref.¹³⁵

In these patterning strategies, photopatterning is one of the most convenient techniques. As a non-contact energy source, light can not only spatially control the modification position of the material surface, but also realize temporal control by adjusting the wavelength, energy density, and exposure time.^{100,102,103,114,138} The photo-patterning strategies can be roughly divided into two categories, the first is a photo-induced bottom-up strategy of growing patterns from substrates, and the second is top-down patterns formed by light-induced material changes on a uniform surface.

1.3.1 Bottom-Up Photopatterning

Bottom-up photopatterning strategies are based on the photo induced surface modification methods, including photo induced click chemistry reaction (Figure 1.10),^{84-86,88,138,143} photoinitiated radical polymerization,¹⁴⁴⁻¹⁴⁷ and photo assisted oxidation.¹⁴⁸ These photo induced modification methods

require substrates with specific reactive groups such as hydroxyl group,¹⁴⁸ alkene group,^{84-86,88,138} alkyne group,⁹⁰ azides group,^{82,83} free radical polymerization initiators,¹⁴⁴⁻¹⁴⁷ etc. It is necessary to modify these active groups onto the substrate in advance. Silane chemistry and polydopamine are two simple and widely applicable substrate modification methods.³²⁻³⁸ A typical example of photopatterning based on silane chemistry is the modification of alkenyl group to glass slides via chlorosilanes followed by the photo induced thiol-ene click reaction to prepare hydrophilic and hydrophobic patterns (Figure 1.11). Organic droplet arrays fabricated on flexible polymer substrates were also realized.¹³⁸

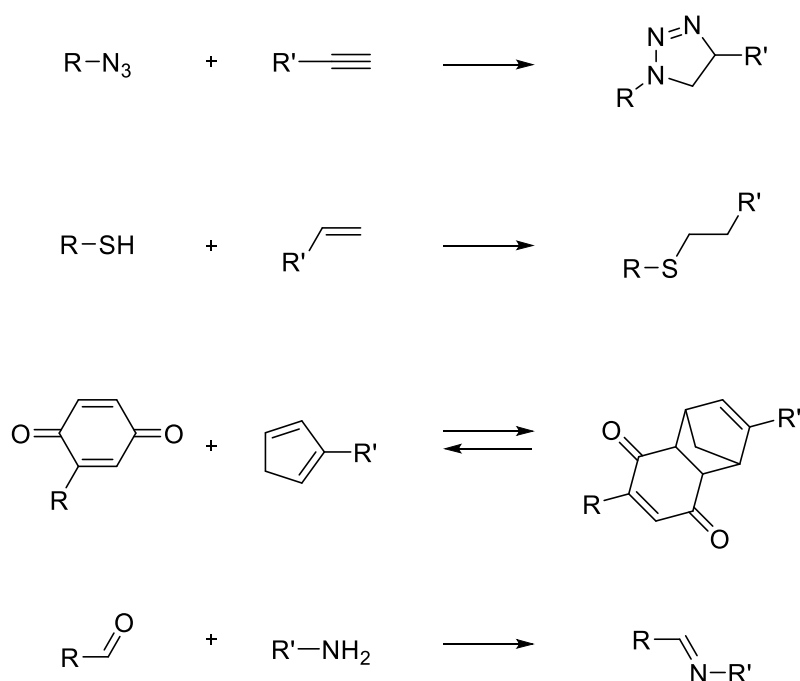


Figure 1.10 Examples of “click” reactions employed for monolayer modification, from top to bottom: Huisgen 1,3-cycloaddition, thiol-ene reaction, Diels-Alder cycloaddition, and imine and oxime formation.

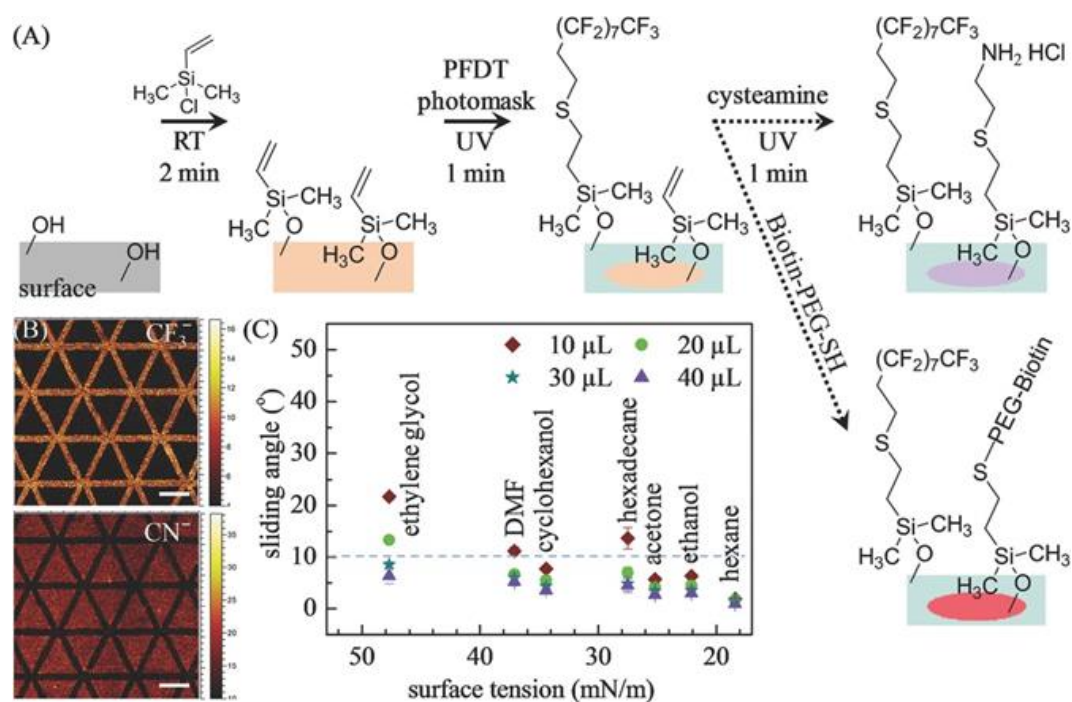


Figure 1.11 (A) Schematic representation of the silanization reaction and UV-induced thiol-ene photo-click reactions for creating the wetting-dewetting micropatterns. (B) ToF-SIMS 2D graphs of negative CF₃⁻ and the CN⁻ secondary ions, showing the patterning of PFDT and cysteamine, respectively. Scale bar: 500 μm. (C) Sliding angles of low-surface-tension solvents on PFDT-modified glass. Adapted from Ref.¹³⁸

Polydopamine is another popular choice for building connection layer between the substrate and functional layer for further bottom-up patterning. The controllable aspects of the PDA coating secondary modification, including temporal and spatial control, are not as developed as the coating methods themselves.^{149,150} Both spatial and temporal control play an important role in the subsequent application of such materials. In recent years, researchers have proposed new solutions to accelerate the secondary modification of PDA coatings. As shown in Figure 1.12, Gu et al. accelerated the reductive deposition and oxidative removal of metal ions on a polydopamine coating by ultraviolet irradiation to control the deposition of metal nanoparticles both spatially and temporally. Due to the spatial and temporal controllability of light, the metallization of PDA surface could be well controlled, allowing the construction of a grayscale patterned metallic surface. Reversible depositing and removing metal nanoparticles enabled them to recycle metals from wastewater and electric circuits. Thus, this method demonstrates rapid, controllable and reversible

secondary modification of PDA coatings.¹⁵¹ Several approaches for the patterning of PDA coatings have also been reported. Wu et al. demonstrated patterning of hydrophobic surfaces by negative microcontact printing of PDA.⁶⁰ Du et al. achieved patterning of PDA coatings on different materials through UV-triggered dopamine polymerization.¹⁴⁹ Behboodi-Sadabad et al. succeeded in patterning of different phenolic compounds, which have similarities with dopamine.¹⁵²

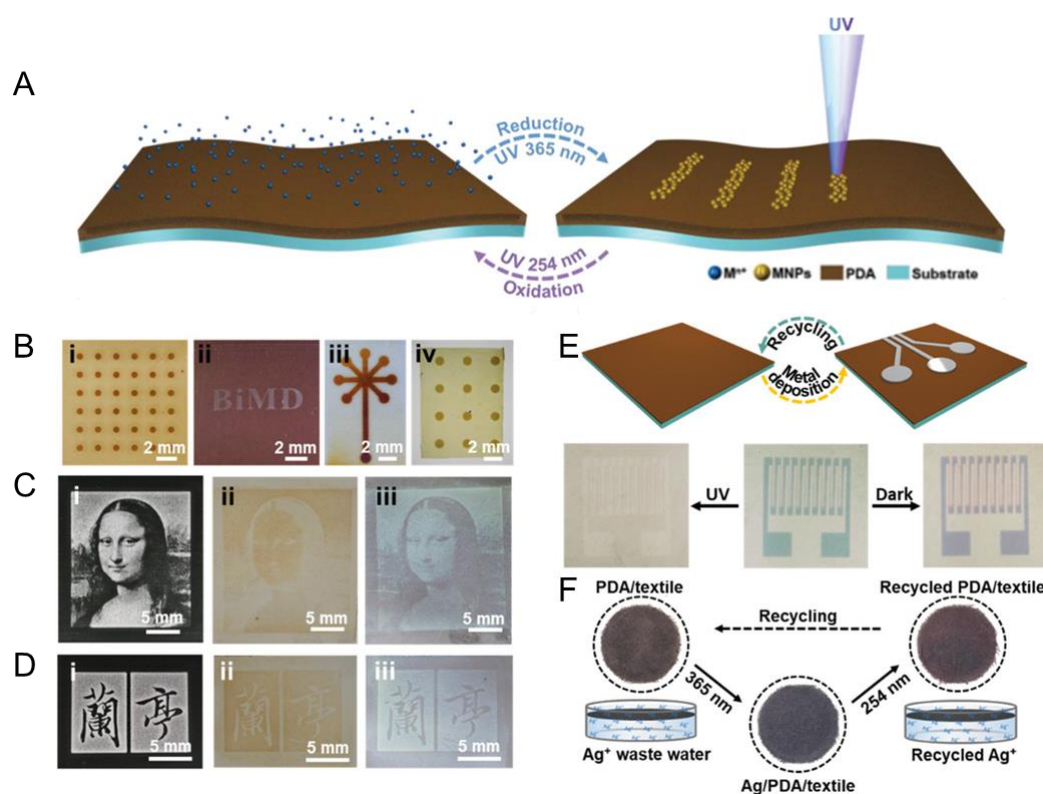


Figure 1.12 (A) Schematic representation of polydopamine-assisted deposition and removal of metal nanoparticles (MNPs). (B-D) Various metallic patterns fabricated on various PDA-coated substrates by using corresponding photomasks. (E) A PDA surface was used to recycle electronic circuit. (F) A PDA-coated textile (diameter 60 mm) was utilized for wastewater treatment. Adapted from Ref.¹⁵¹

1.3.2 Top-Down Photopatterning

The difference between the top-down photopatterning strategy and the bottom-up photopatterning strategy is that top-down photopatterning begins with a uniformly modified surface, which is

modified by light irradiation to produce patterns.¹⁵³⁻¹⁵⁹ The top-down photopatterning strategies can be roughly divided into two categories, photochromic patterning,¹⁵³⁻¹⁵⁵ and photodegradation patterning.¹⁵⁶⁻¹⁵⁹

1.3.2.1 Photochromic Patterning

Photochromic patterning of surface was achieved via the modification of surfaces with photo switchable molecules such as azobenzene,¹⁵⁵ diselenide bond,¹⁵⁴ liquid crystal,¹⁵³ etc. By irradiating the surface containing the structure-change material with light, combined with a photomask, patterns with extremely high resolution can be generated on the surface, and these top-down patterns are reversible. As shown in Figure 1.13, a typical example of photoinduced structure transition patterning is reported by Wu et al.¹⁵⁵ They introduced a new type of nanocomposite material with good processing properties that can be easily applied to banknotes, wine, pharmaceuticals and other products. It is composed of photo responsive azobenzene-containing polymers (azopolymers), and upconverting nanoparticles (UCNPs). Azo polymers exhibit photochromism, photo-switchable glass transition temperature (T_g) values, and photo-induced orientation due to reversible cis-trans photoisomerization. These light-responsive properties cause the material to change color when exposed to light, which in combination with the photomask forms a pattern. Xu et al. reported a structural color material with reversible stimuli-responsiveness to visible light (Figure 1.14).¹⁵⁴ In their system, the structural color comes from the birefringence of the stretched material, whose shape can be fixed while maintaining mechanical stress. The fixation stress is released by diselenide metathesis by visible light irradiation. Adjusting the wavelength or irradiation time using a commercial projector can achieve tunable structural color patterns, and the structural color patterns can be arbitrarily erased and rewritten.¹⁵⁴

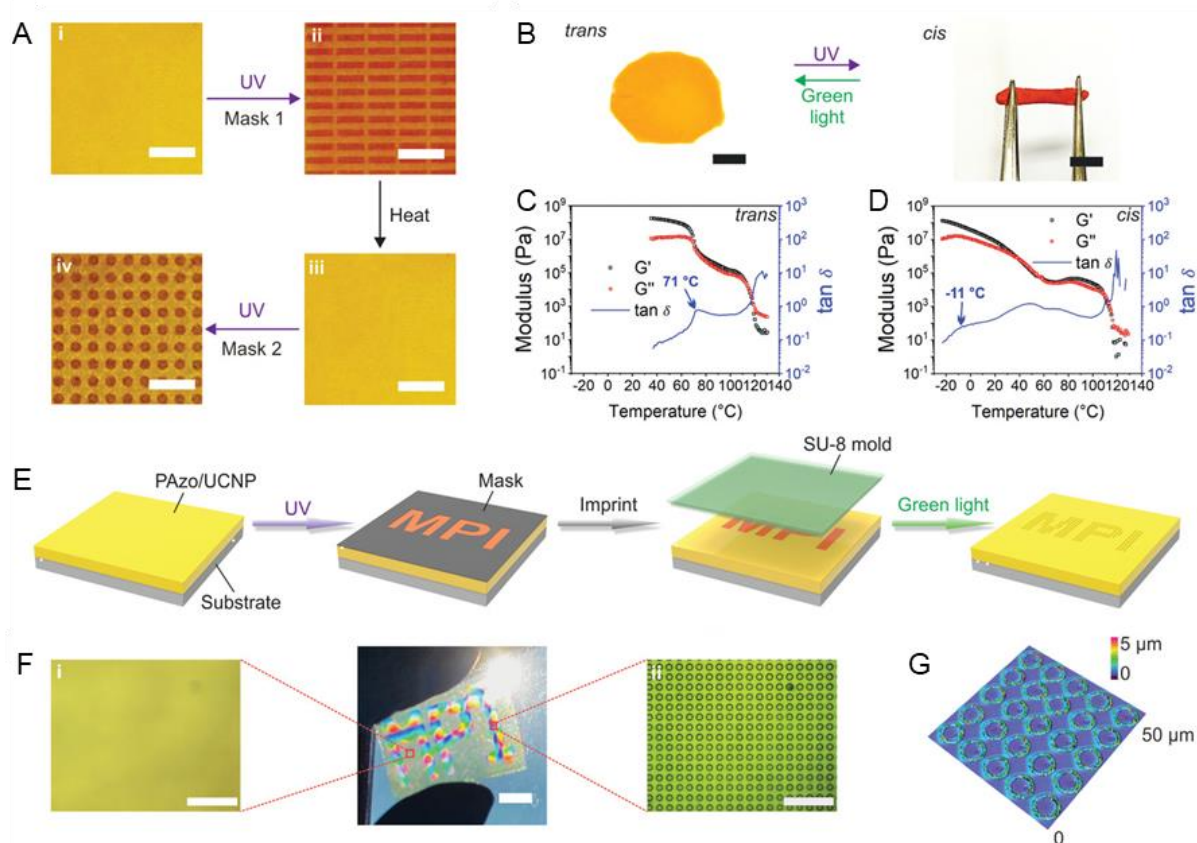


Figure 1.13 (A) Reversible writing and erasure of color-changing patterns on a PAzo/UCNP nanocomposite film. Scale bars: 5 mm. (B) Photographs of *trans* and *cis* PAzo/UCNP nanocomposites. Scale bars: 5 mm. (C, D) Dynamic mechanical analysis (DMA) data of (C) *trans* and (D) *cis* PAzo/UCNP nanocomposites. (E) Schematic of the fabrication of imprinted microstructures with structural colors. (F) Photograph of a PAzo/UCNP nanocomposite film with imprinted microstructures on a polyethylene terephthalate substrate. Scale bar: 1 cm. (G) Confocal microscopy image of imprinted microstructures on a PAzo/UCNP nanocomposite film. Adapted from Ref.¹⁵⁵

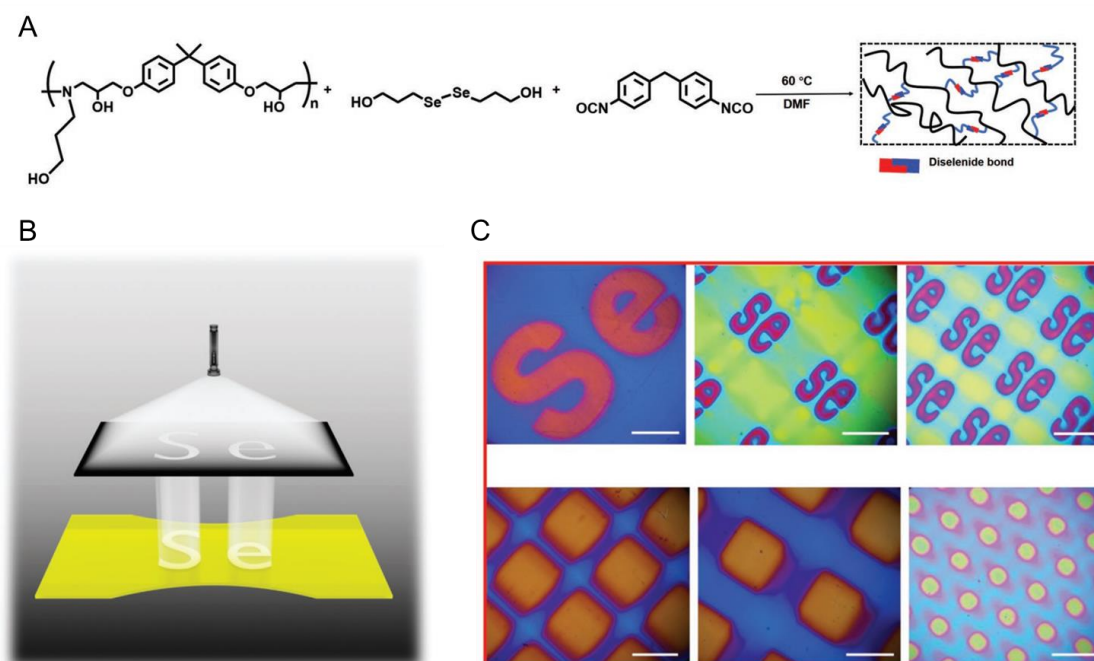


Figure 1.14 (A) Synthesis of diselenide-containing polymeric network. (B) Patterning strategy with photomask. (C) Various patterns with different structural colors realized by photomask. The scale bar is 500 μm . Adapted from Ref.¹⁵⁴

1.3.2.2 Photodegradation Patterning

Photodegradation means that the modification layer or material is detached from the substrate or degraded under the irradiation of light. For achieving patterning with photodegradation, the photomask or controlled light source is chosen to be used in this strategy. When the photomask is covered on the surface, a part of the surface is protected by the dark area of photomask. Degradation happens in the other part, where the surface properties are changed to form a pattern.^{156,159} Without photomask, the light source with controllable projected pattern is also able to achieve photodegradation patterning.^{157,158} The photodegradation patterning strategy can form surface patterns with different wettability by degrading the modified monolayer on substrate,¹⁵⁶ or directly degrade the material to form three-dimensional patterns¹⁵⁷⁻¹⁶⁰. The most common strategy for degrading monolayers to form surface patterns is to use plasma to eliminate organic monolayers on the surface of materials.¹⁵⁶ The strategy of patterning by photodegrading bulk material, also known as soft lithography, was first proposed by Whiteside's et al.¹⁶⁰ This strategy forms patterns

by directly degrading part of the material using laser or ultraviolet light.¹⁵⁸⁻¹⁶⁰ A typical example of laser-degraded materials to form patterns is reported by Ko et al, they introduced a "successive laser pyrolysis" strategy, a novel on-demand laser PDMS patterning process that exploits the phenomenon of self-sustained continuous photothermolysis guided by a continuous wave laser (Figure 1.15).¹⁵⁸ In turn, the increased laser absorption of pyrolysis byproducts generates increased photothermal energy, which facilitates successive iterations of PDMS pyrolysis. After proper removal of by-products from pyrolysis, SLP enables rapid digital patterning of 2D and even 3D high-quality PDMS microstructures that can be used directly without additional post-processing.¹⁵⁸ Compared with lasers, ultraviolet light is a less energy-consuming and milder energy source, and is also commonly used for photodegradation patterning of hydrogels or organogels.^{159,161-167} Researchers usually speed up the degradation rate of gels under UV by adding photolabile groups to the polymer cross-linked network. The photolabile groups used for the patterning of gel photodegradation include disulfide bonds,^{164,165} diselenide bonds,¹⁶⁷ o-nitrobenzyl ester,^{161,162} coumarins,¹⁶³ Ru^{II} polypyridyl complexes,¹⁶⁶ etc. In these photodegradation patterning strategies, complex structural design is often required to incorporate photolabile groups into the gel, which greatly limits its application range. Recently, Levkin et al. reported photodegradation patterning using the most commonly used hydrophilic methacrylate hydrogels (Figure 1.16).¹⁵⁹ They demonstrate UV-induced degradation of hydrophilic methacrylate hydrogels without any external photosensitizers. This opens the possibility of constructing conventional hydrogels using traditional photolithographic methods, i.e., creating complex hydrogel patterns, hydrogel particles using various types of commercially available hydrophilic methacrylate monomers and cross-linking agents or hydrogel gradients.¹⁵⁹

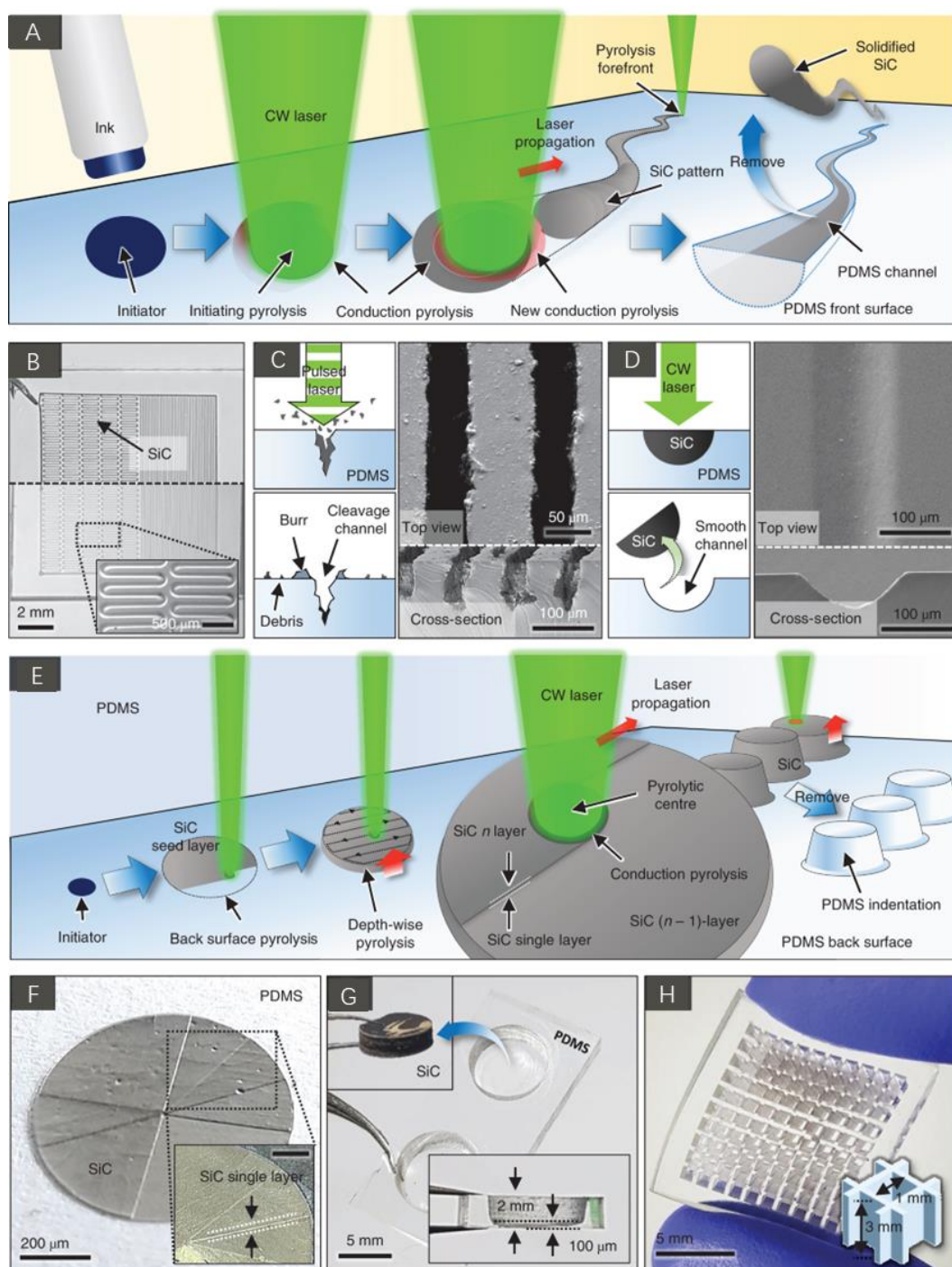


Figure 1.15 (A) The process flow of the front-surface scanning scheme. (B) Optical images of pattern. (C) Schematics and scanning electron microscopy (SEM) images of the laser ablation technique using a pulsed laser. (D) Schematics and SEM images of the successive laser pyrolysis highlighting the smooth inner surface. (E) The process flow of the back surface scanning (BSS) scheme showing the opaque initiating point, seed layer formation, repeated overlay scanning and removal of silicon carbide (SiC). (F) A highlighted SiC single layer created by semicircular overlay

scanning. Inset scale bar, 100 μm . (G) Deep cylindrical pattern (depth, 2 mm) and extracted SiC chunk. (H) High-aspect-ratio monolithic well arrays fabricated by the BSS. Adapted from Ref.¹⁵⁸

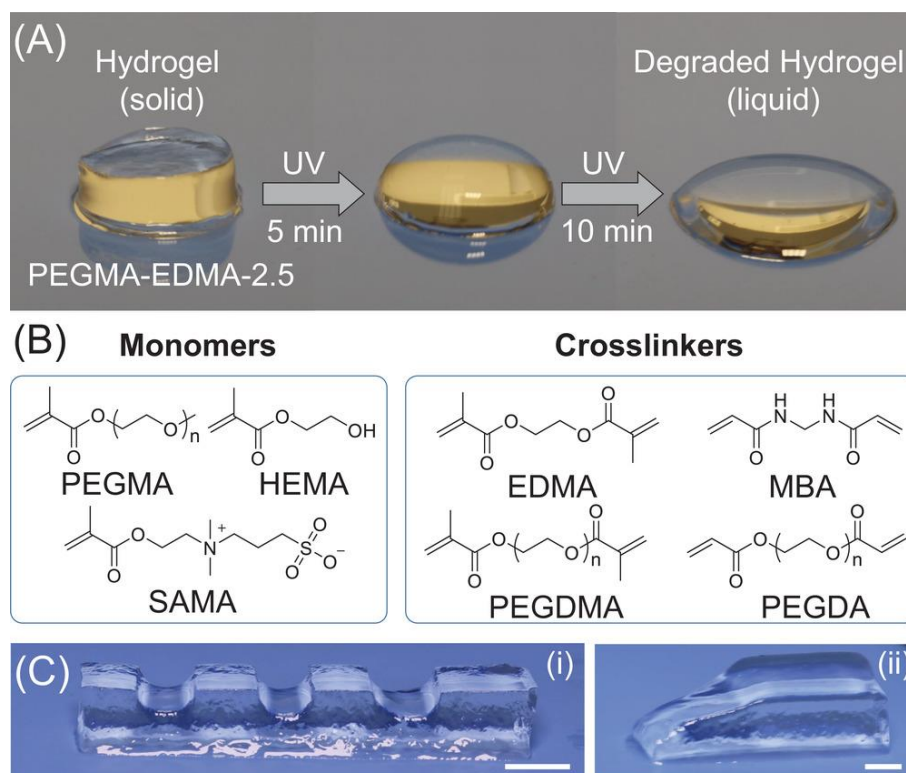


Figure 1.16 (A) Time-lapse images of a 3 mm thick hydrogel block exposed to UV irradiation. (B) Molecular structures of monomers and crosslinkers used for the formation of inherently photodegradable hydrogels. (C) Digital images of hydrogel channels (I), and hydrogels with thickness gradient (by moving the photomask during UV irradiation) (II). Scale bars are 5 mm. Adapted from Ref.¹⁵⁹

1.4 Photodegradation of Poly(meth)acrylate Gel

The inherent photodegradability of poly(meth)acrylate polymers has been studied for several decades. Motivated by applications such as coatings or photoresists, researchers investigated various factors relevant for the photodegradation properties of poly(meth)acrylates, such as the wavelength, the irradiation time, the molecular weight, the length of the (meth)acrylic ester chain, or *co*-monomers.¹⁶⁸⁻¹⁷² Photodegradation of poly(meth)acrylates requires UV light with a

wavelength below 320 nm, reaching a maximum quantum yield at ca. 280 nm.¹⁷³ Depending on the atmosphere (i.e. vacuum, air, or inert gas) the mechanism of photodegradation can involve photooxidative processes, namely the formation of peroxy radicals (R-O-O•), hydroperoxyls (R-O-OH), oxyl radicals (R-O•), and peroxides (R-O-O-R).¹⁷⁴ Photoinduced bond scissions can result in direct main chain scission or cleavage of the methacrylate's ester groups, i.e. the side chains (Figure 1.17).¹⁷⁵

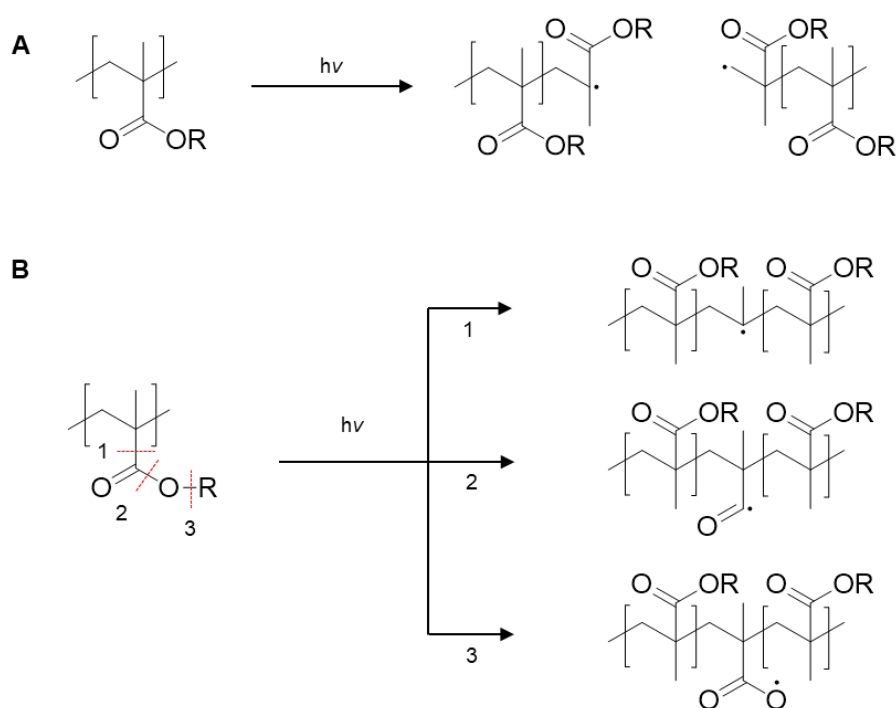


Figure 1.17 Possible UV light induced bond scissions of poly(meth)acrylate. (A) Main chain scissions. (B) Side chain scissions. Adapted from Ref.¹⁷⁵

The amount of photocrosslinking can simply be quantified by determining the weight of the insoluble fraction of the formerly soluble polymer. This insoluble fraction is termed the “gel fraction” due to its covalently crosslinked nature.¹⁷³ However, this “gel fraction” is not infused with a solvent and does not have a controllably low degree of crosslinking and is thus fundamentally different from common swollen poly(meth)acrylate gels.

A generally observed trend is that poly(meth)acrylates with longer alkyl ester side chains (e.g. butyl, hexyl, lauryl) tend to undergo photocrosslinking rather than photodegradation, which was explained by their low glass transition temperatures (T_G). A lower T_G enables a polymer radical

mobility and thus faster recombination of polymer radicals.¹⁷⁴ Poly(meth)acrylates were found to undergo less photocrosslinking reactions than polyacrylates.

Previous photodegradation studies were mainly conducted on films of the bulk polymers and the illumination times are in the range of hours or even hundreds of hours until measurable photodegradation processes occurred. Degradation of a swollen poly(meth)acrylate gel reduces the illumination time down to tens of minutes until photodegradation is visible with the bare eye. It is due to the spatial separation of polymer chains in a swelled polymer network, reducing “cage” effects causing polymer-based radicals to recombine (photocrosslinking).¹⁷⁶ A similar effect was found for the photodegradation of a *co*-polymer of methyl methacrylate and methyl acrylate in methyl acetate solution.¹⁷⁷

1.5 Summary and Perspectives

Surface modification and patterning techniques have developed significantly over the past few decades. Through various patterning techniques such as microcontact printing, inkjet printing and photopatterning, two-photon polymerization, micro-contact printing, inkjet printing, microfluidic patterning, and photopatterning, researchers have created patterns with various functions on the surface of materials. Patterned surfaces are widely used in bioarrays, microfluids, optical devices, medical science, sensors, and other scientific research and application fields. Photopatterning is one of the most convenient techniques, various photo-induced strategies have been widely developed by researchers, including photo-induced click chemistry, photo-induced polymerization, photodegradation, etc. At the same time, recycling and reuse are also meaningful for sustainable development and reduce environmental pollution. The application of various reversible surface modification techniques, including reversible hydrogen bond formation, electro-assisted ion printing, metal complexation, host-guest chemistry, sulfur chemistry, reversible silane chemistry, Schiff base chemistry, Diels-Alder chemistry, and reversible photochemistry, enables materials to be reused. Despite advances in these areas, combining multiple surface modification techniques to create reversible surfaces remains an attractive research direction. On the other hand, few studies have focused on exploiting the inherent UV photodegradability of polymethacrylates for photo-

induced surface patterning and polymer recycling. Recycling and reuse are meaningful for sustainable development due to the 368 million tons of polymers produced every year, 76% of which are discarded after single use. Recycling and reusing waste polymers and functionalized materials not only maintains sustainable economic development, but also reduces environmental pollution.

2 Results and Discussion

2.1 Substrate-Independent and Re-Writable Surface Patterning by Combining Polydopamine Coatings, Silanization and Thiol-Ene Reaction*

*This chapter and associated sections were published previously. Figures and tables also have been published and reproduced for use in this chapter. Copyright has been acquired from the publisher. Li, S., Scheiger, J. M., Wang, Z., Dong, Z., Welle, A., Trouillet, V., & Levkin, P. A. (2021). *Advanced Functional Materials*, 31(50), 2107716.

2.1.1 Introduction

Surface functionalization through polydopamine (PDA) coating was introduced by Lee and Messersmith in 2007 and is a unique method inspired by the adhesive properties of the mussel foot.⁵⁵ The advantages of this technique include its simplicity, substrate-independence, robustness and universality.⁵⁶⁻⁵⁹ This substrate-independent coating method has been widely used in various applications, including surface patterning,^{60,62,178} improving biocompatibility of substrates,⁶³⁻⁶⁵ and rendering surfaces superhydrophobic^{66,67} or antibacterial.^{68,69} The possibility of secondary modification, patterning or the ability to re-functionalize PDA coatings is important to broaden the scope of applications of this coating method.^{71,72} Various methods for the secondary modification of PDA coating, utilizing the presence of activated double-bonds, multiple catechol groups and amino functionality in the PDA, have been introduced, including the use of thiols, amines, silanes or various metal ions.^{70,73-77}

The controllable aspects of the PDA coating secondary modification, including temporal and spatial control, are not as developed as the coating methods themselves. However, both spatial and temporal control play an important role in the subsequent application of such materials. In recent years, some researchers have proposed new solutions to accelerate the secondary modification of PDA coatings. Gu et al. accelerated the reductive deposition and oxidative removal of metal ions

on a polydopamine coating by ultraviolet irradiation to control the deposition of metal nanoparticles both spatially and temporally.¹⁵¹ Several approaches for the patterning of PDA coatings have also been reported. Wu et al. demonstrated patterning of hydrophobic surfaces by negative microcontact printing of PDA.⁶⁰ Du et al. achieved patterning of PDA coatings on different materials through UV-triggered dopamine polymerization.⁶² Behboodi-Sadabad et al. succeeded in patterning of different phenolic compounds, which have similarities with dopamine.¹⁵² In addition, Gu et al. achieved UV-assisted reversible deposition of metal ions on PDA coatings.¹⁵¹ However, a reversible covalent modification of PDA coatings, which can greatly improve their reusability, has not been reported yet.

In this chapter, I present a rapid and reversible strategy for the secondary modification and patterning of PDA coatings. This method is based on the secondary modification of PDA coatings by chlorosilanes, which allows fine-tuning of the surface energy and renders the surface patternable via the thiol-ene photoclick reaction. In addition, we demonstrate the feasibility of selectively removing the siloxane layer from the PDA modified surface using tetrabutylammonium fluoride (TBAF) solution. We provide a complete characterization of the method through contact angle (CA) measurement, atomic force microscopy (AFM), X-ray photoelectron spectroscopy (XPS), and time-of-flight secondary ion mass spectrometry (ToF-SIMS) analyses. Finally, we demonstrate the feasibility of functionalization and patterning of complex large-scale objects, which facilitates the practical application of the method. Thus, this strategy is an effective method for substrate-independent functionalization and patterning of a variety of surfaces.

2.1.2 Results and Discussion

2.1.2.1 Deposition of polydopamine

The PDA coating was applied using the dipping method according to a previously reported oxidation deposition process.⁵⁵ In this step, we selected polytetrafluoroethylene (PTFE), polypropylene (PP), polyethylene (PE), aluminum (Al) and glass as substrates since these are commonly used industrially relevant materials (Figure 2.1A). All substrates appeared brown or light brown after modification with PDA (Figure 2.1B and 2.2). Evaluation of the surface

morphology of the coating on a silicon wafer by AFM showed an increase in surface roughness after modification with PDA, with an increased R_q value from 0.14 ± 0.01 nm to 0.90 ± 0.04 nm (Figure 2.1C). The thickness of the PDA coating on the silicon wafer was measured as 14.1 ± 0.4 nm using the scratch method. In all cases, the static water contact angle (CA) after the modification with PDA was similar and varied from 40° to 50° (Figure 2.3). The XPS characterization also confirmed the successful functionalization (Figure 2.4). In the PTFE/PDA sample, the C 1s peak from C-N for the PDA coating on PTFE was detected at 286.4 eV, while the C 1s peak from CF_2 at 292.4 eV was dramatically attenuated.

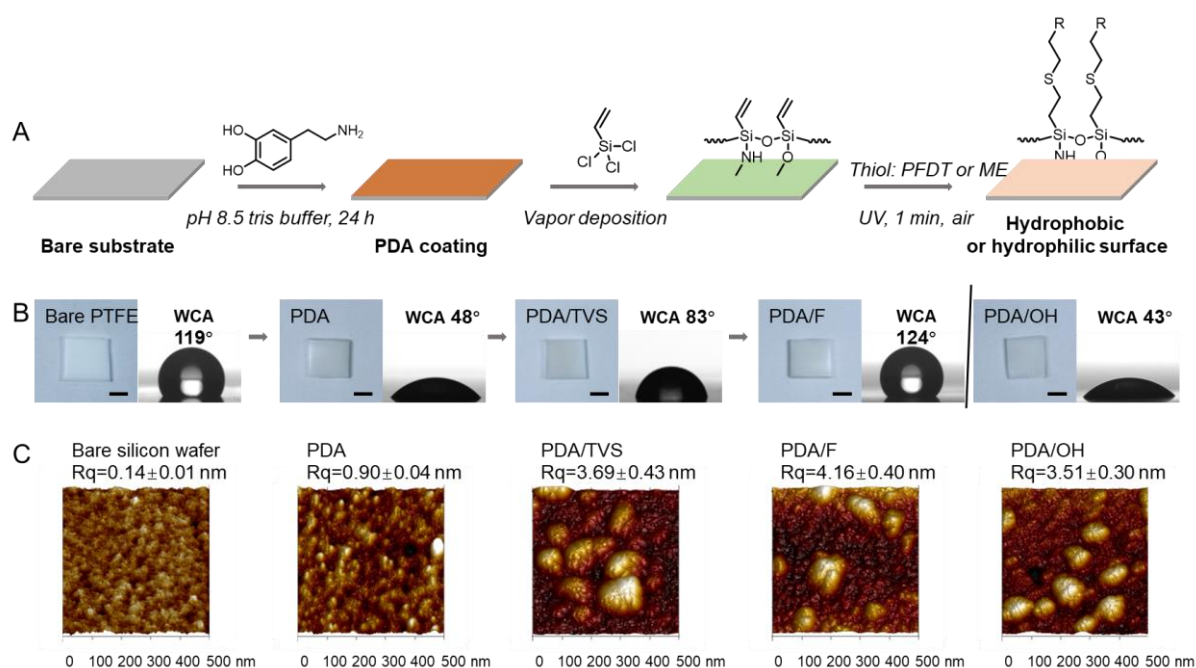


Figure 2.1 Substrate-independent surface functionalization by combining polydopamine coating, silanization by TVS (trichlorovinylsilane) and UV-induced thiol-ene reaction. (A) Schematic representation of the PDA deposition, TVS silanization and UV-induced thiol-ene photoclick processes. (B) Digital images of modified PTFE slides and 2- μL water droplets on modified PTFE slides. Scale bar: 5 mm. (C) AFM 3D images of different modified silicon wafers. Scale bars: 100 nm. Bare: bare substrates; PDA: PDA modified surface; PDA/TVS: PDA and TVS-modified surface; PDA/F: 1H,1H,2H,2H-Perfluorodecanethiol (PFDT) click on PDA/TVS surface; PDA/OH: 2-mercaptoethanol (ME) click on PDA/TVS surface. Copyright 2022, Wiley-VCH.

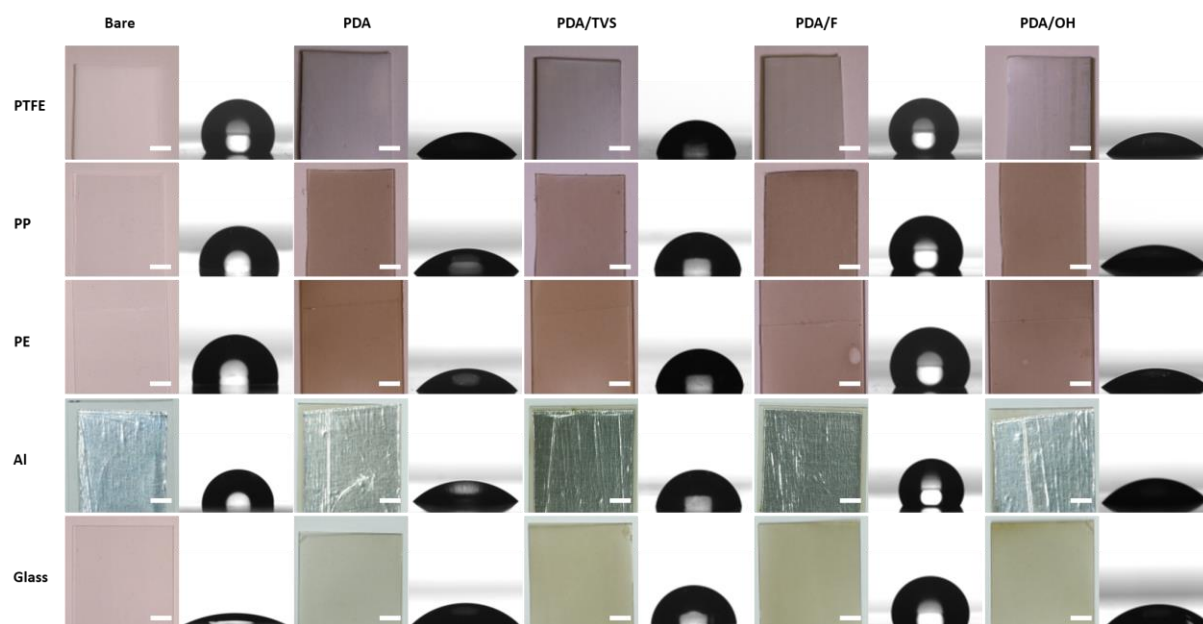


Figure 2.2 Digital photos of modified PE, PP, glass and Al slides and 2 μL water droplets on them. Bare: Bare substrates. PDA: PDA modified surface; PDA/TVS: PDA and TVS modified surface; PDA/F: 1H,1H,2H,2H-Perfluorodecanethiol (PFDT) click on PDA/TVS surface; PDA/OH: 2-Mercaptoethanol (ME) click on PDA/TVS surface. Copyright 2022, Wiley-VCH.

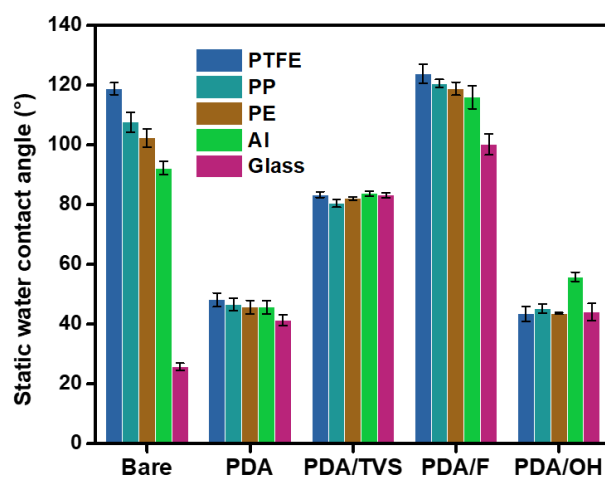


Figure 2.3 Static CA of bare substrates and surfaces with PDA coatings, followed by silanization (PDA/TVS), and thiol grafting (PDA/F and PDA/OH, respectively). Bare: bare substrates; PDA: PDA modified surface; PDA/TVS: PDA and TVS-modified surface; PDA/F: 1H,1H,2H,2H-Perfluorodecanethiol (PFDT) click on PDA/TVS surface; PDA/OH: 2-mercaptoethanol (ME) click on PDA/TVS surface. Copyright 2022, Wiley-VCH.

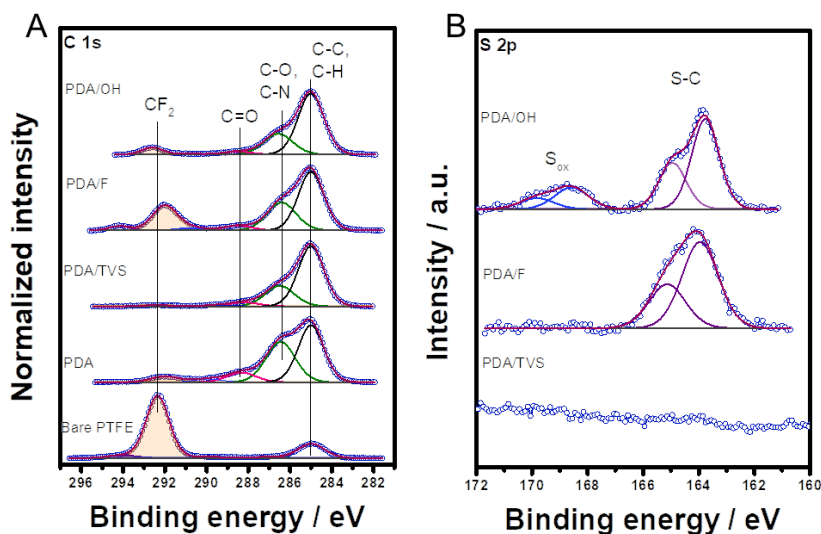


Figure 2.4 (A) C 1s XP spectra of different PTFE modification steps. (B) S 2p XP spectra of PDA/TVS, PDA/F and PDA/OH modified PTFE. Bare: bare substrates; PDA: PDA modified surface; PDA/TVS: PDA and TVS-modified surface; PDA/F: 1H,1H,2H,2H-Perfluorodecanethiol (PFDT) click on PDA/TVS surface; PDA/OH: 2-mercaptoethanol (ME) click on PDA/TVS surface. Copyright 2022, Wiley-VCH.

2.1.2.2 Silanization of polydopamine

After applying the PDA coating, we used trichlorovinylsilane (TVS) to secondary modify PDA coated substrates. The chlorosilane reacts with the amino and hydroxyl groups of the PDA coatings. Moisture from the surface and air further hydrolyzes the chlorosilane functionalities into silanol functional groups, which condensate to a polysiloxane network and increase the thickness of the coating to 42.3 ± 2.9 nm. The silanization resulted in an increase in the WCA on PTFE, PP, PE, Al and glass surfaces from $48 \pm 2^\circ$, $47 \pm 2^\circ$, $46 \pm 2^\circ$, $46 \pm 2^\circ$, and $41 \pm 2^\circ$, respectively, to $84 \pm 1^\circ$, $80 \pm 2^\circ$, $82 \pm 1^\circ$, $84 \pm 1^\circ$, and $83 \pm 1^\circ$, respectively (Figure 2.3), demonstrating successful surface modification independent of the substrate used. In the XPS characterization, the Si 2p_{3/2} peak at 102.8 eV in the PTFE/PDA/TVS (the material names are given as “Substrate material/first coating/secondary modification”) sample also confirmed successful silanization (Figure 2.5). The R_q value of the PDA/TVS-modified silicon wafer increased to 3.69 ± 0.43 nm, showing that TVS forms aggregates on the surface of the PDA (Figure 2.1C). The thickness of the PDA/TVS layer on the silicon wafer

was 42.3 ± 2.9 nm, which was almost three times that of the PDA coating. In addition, we used trichloro(1*H*,1*H*,2*H*,2*H*-perfluorooctyl)silane and trichloroethylsilane to test the reactivity of other chlorosilanes with PDA coatings. As shown in Figure 2.6, the static WCA increased from 45° to 80° and 90° , respectively, after the silanization. In the case of trichloro(1*H*,1*H*,2*H*,2*H*-perfluorooctyl)silane, the WCA was not as high as expected probably because its low vapor pressure reducing the density of functional groups after deposition.¹⁷⁹

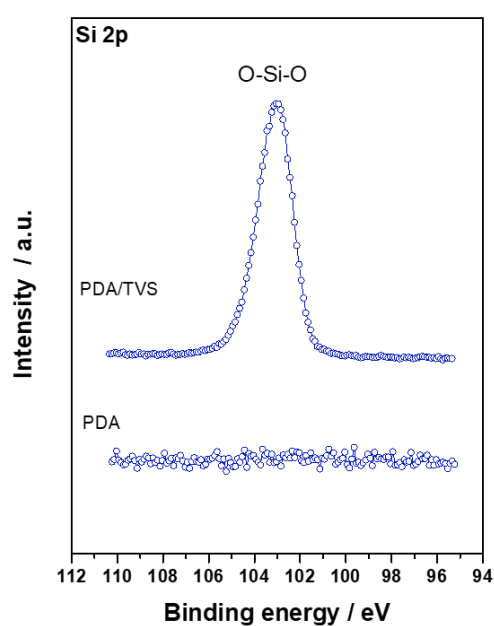


Figure 2.5 Si 2p XP spectra of PDA and TVS silanized PDA on PTFE. Copyright 2022, Wiley-VCH.

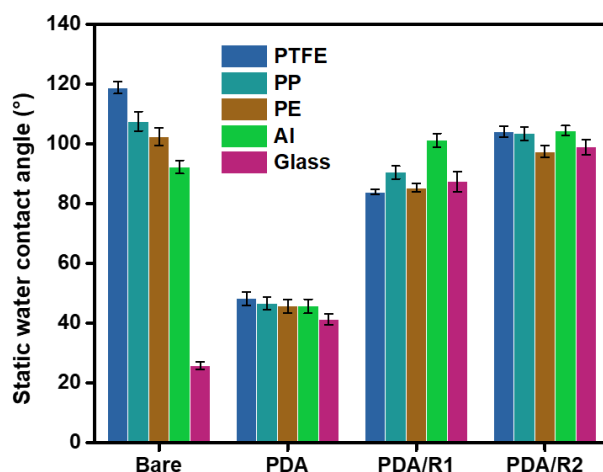


Figure 2.6 Static water contact angle of surfaces. Bare: bare substrates; PDA: PDA modified surfaces; PDA/R1: PDA and trichloro(1H,1H,2H,2H-perfluorooctyl)silane modified surfaces; PDA/R2: PDA and ethyl trichlorosilane modified surfaces. Copyright 2022, Wiley-VCH.

2.1.2.3 UV-induced thiol-ene reaction

Substrates modified with TVS were then functionalized using the photoclick thiol-ene reaction. Different materials were covered with a 1H,1H,2H,2H-perfluorodecanethiol (PFDT) solution and irradiated with 265 nm UV light (3.0 mW cm^{-2}) for 1 min through a quartz slide. The static WCA on PTFE, PP, PE, Al and glass surfaces changed from $84 \pm 1^\circ$, $80 \pm 2^\circ$, $82 \pm 1^\circ$, $84 \pm 1^\circ$, and $83 \pm 1^\circ$, respectively, to $124 \pm 1^\circ$, $121 \pm 1^\circ$, $119 \pm 2^\circ$, $116 \pm 4^\circ$, and $100 \pm 4^\circ$, respectively (Figure 2.3), thus confirming the success of the photoclick thiol-ene reaction. Compared with the PTFE/PDA/TVS sample, additional peaks (C 1s peak from CF_3 at 294.2 eV and C 1s peak from CF_2 at 292.0 eV) stemming from PFDT appeared in the XP spectra of the PTFE/PDA/F sample, confirming the successful modification with PFDT (Figure 2.4). The corresponding F 1s peak at 689.1 eV, typical of a covalently bound fluorine, was also observed (Figure 2.7). To demonstrate universality of the photoclick thiol-ene reaction on the PDA/TVS coating, we functionalized the vinyl-bearing surfaces with hydrophilic thiol 2-mercaptoethanol (ME) in the same way. The static WCA on PTFE, PP, PE, Al and glass surfaces changed from $84 \pm 1^\circ$, $80 \pm 2^\circ$, $82 \pm 1^\circ$, $84 \pm 1^\circ$, and $83 \pm 1^\circ$, respectively, to $43 \pm 3^\circ$, $45 \pm 2^\circ$, $44 \pm 1^\circ$, $56 \pm 2^\circ$, and $44 \pm 3^\circ$, respectively, indicating successful completion of the reaction and substrate independency (Figure 2.3). At the same time, the S $2p_{3/2}$ peak at 163.9 eV

appeared in both the PTFE/PDA/F and PTFE/PDA/OH samples, indicating that both PFDT and 2-mercaptoethanol (ME) had clicked to the siloxane surface successfully (Figure 2.4B). PDA coatings can also react with thiols,⁵⁵ here, we reacted PFDT and ME with PDA coatings directly and characterized them by XPS as a comparison of our method. As shown in Figure 2.8, the fluorine content measured by XPS increased from 5.7 atomic% (at%) to 12.9 at% after reacting PFDT directly with the PDA layer. However, the difference was much less marked than that achieved with the thiol-ene reaction (from PDA/TVS 0.9 at% to PDA/TVS/F 27.1 at%). As a marker of the PDA layer, the nitrogen signal was also followed in parallel with these reaction steps. The nitrogen concentration did not decrease significantly after the reaction of PDA with either PFDT or ME, whereas a non-negligible decrease in the nitrogen fraction was observed after the thiol-ene click reaction (Figure 2.8), indicating that the PDA-thiol reaction is much slower than the thiol-ene click reaction. In addition, the secondary modification of the PDA coating became reversible through the fluoride-induced desilylation (*vide infra*).

Chlorosilanes are commonly used as surface modification reagents; therefore, we compared direct modifications based on bare substrates using our PDA-based approach. We silanized bare substrates, performed photoclick thiol-ene reactions, and then measured the WCAs of the resulting surfaces (Figure 2.9). While the glass sample showed a significant change as expected, the WCAs of the PTFE and Al samples hardly changed after both the TVS treatment and the photoclick thiol-ene reaction. TVS reacts with hydroxyl group on glass, thus TVS aggregates attach readily to the glass surface.¹⁸⁰ Due to the absence or low density of OH groups on the surfaces of bare PTFE or Al, modification of these surfaces by TVS was not possible. For bare PP and PE, small amount of TVS aggregates attached to the surface, causing small changes in the WCA and WCA hysteresis after the photoclick thiol-ene reaction with PFDT and ME (Figure 2.3, 2.9 and Table 2.1). This showed that the PDA layer effectively changed the surface properties of the substrates, facilitating their subsequent modification. Thus, the introduction of PDA drastically improves the substrates compatibility with chlorosilanes.

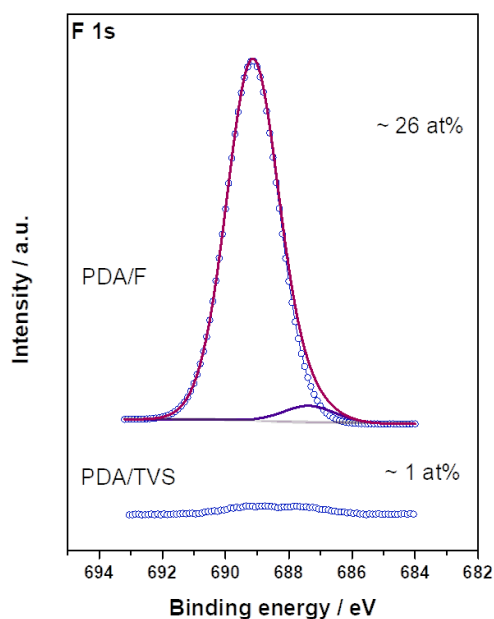


Figure 2.7 F 1s XP spectra of PFDT clicked TVS silanized PDA on PTFE. Copyright 2022, Wiley-VCH.

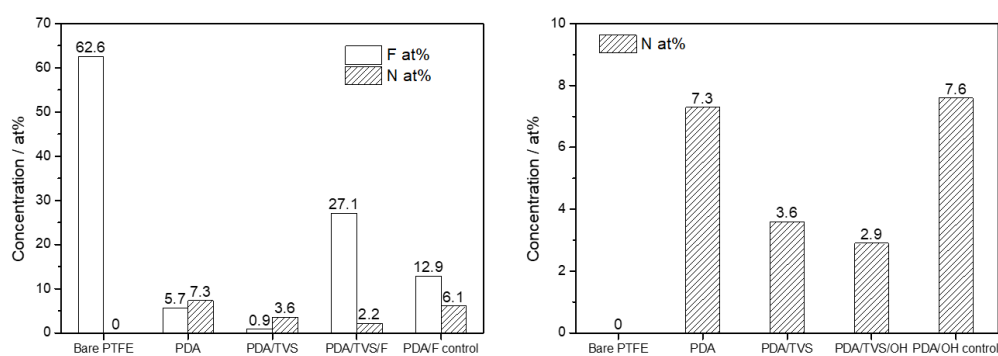


Figure 2.8 Fluorine and nitrogen surface concentrations (atomic %) based on XPS along substrate modification. PDA: PDA coated PTFE; PDA/TVS: TVS modified PTFE with PDA coating; PDA/TVS/F: PFDT clicked PDA/TVS; PDA/F control: PFDT react directly with PDA layer; PDA/TVS/OH: ME clicked PDA/TVS; PDA/OH control: ME react directly with PDA layer. Copyright 2022, Wiley-VCH.

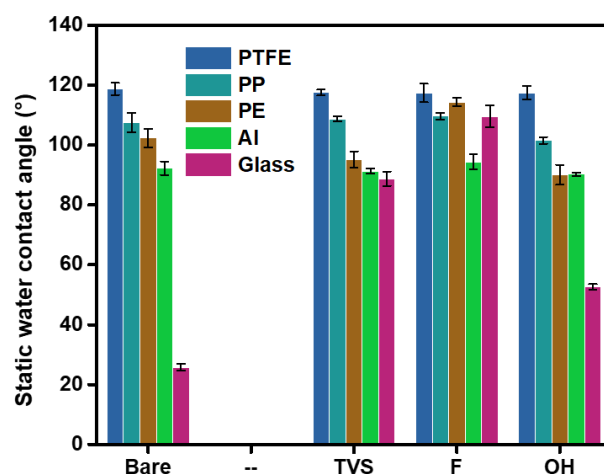


Figure 2.9 Static water contact angle of surface without polydopamine. Bare: bare substrates; TVS: TVS modified bare surface; F: 1H,1H,2H,2H-Perfluorodecanethiol (PFDT) click on TVS surface; OH: 2-Mercaptoethanol (ME) click on TVS surface. Copyright 2022, Wiley-VCH.

Table 2.1 Water contact angel hysteresis of modified PTFE, PP, PE, Al and glass. Bare: bare substrates; PDA: PDA modified surface; PDA/TVS: PDA and TVS modified surface; PDA/F: 1H,1H,2H,2H-Perfluorodecanethiol (PFDT) click on PDA/TVS surface; PDA/OH: 2-Mercaptoethanol (ME) click on PDA/TVS surface; TVS: TVS modified bare surface; F: 1H,1H,2H,2H-Perfluorodecanethiol (PFDT) click on TVS surface; OH: 2-Mercaptoethanol (ME) click on TVS surface. Copyright 2022, Wiley-VCH.

CA hysteresis (°)	Bare	PDA	PDA/TVS	PDA/F	PDA/OH	TVS	F	OH
PTFE	23	50	32	36	52	22	24	25
PP	20	52	29	34	53	22	23	24
PE	26	49	27	31	49	28	29	30
Al	25	53	22	31	59	25	28	30
glass	28	44	28	32	41	57	33	40

2.1.2.4 Stability of modified surfaces

The hydrolytic stability of the PDA/TVS layer and thiol click layers was investigated by

monitoring the static WCA at different times after immersing the substrates in a 1:1 ethanol/water mixture for 72 h (Figure 2.10). In the first 24 h, the static WCA of the PDA/TVS layer on all substrates decreased by several degrees. With the exception of glass, the static WCA of all substrates remained constant after immersion for more than 24 h (Figure 2.10A). After 72 h, the static WCA of all substrates was higher than 70° and the large difference compared with the static WCA of PDA was retained (Table 2.2). After click reaction with PFDT, all coatings were much more stable and the static WCA did not change significantly after 72 h. The hydrophilic thiol modified layer on PTFE, PE and Al remained hydrophilic after 72 h (Figure 2.10B). In addition to the broad applicability on several substrate materials, the stability of the PDA/TVS layer and the thiol-ene post-modifications is of great significance to their practical applications.

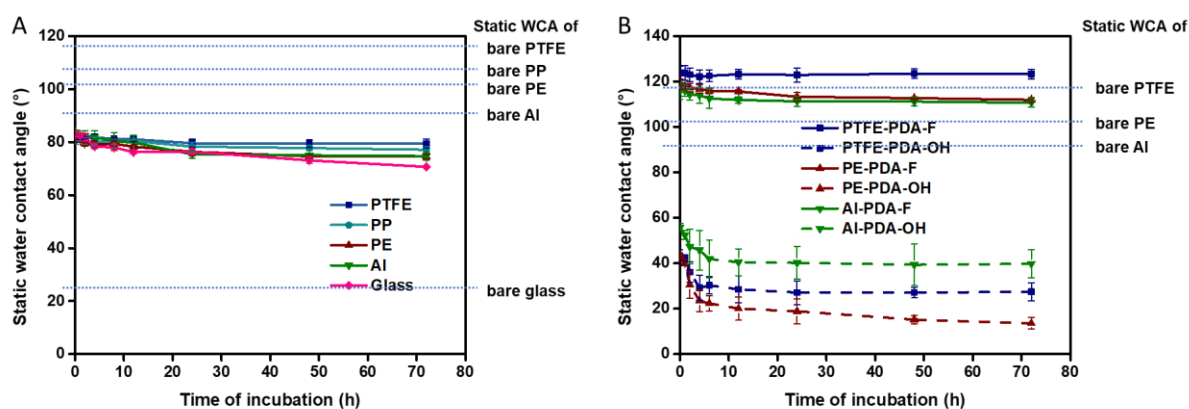


Figure 2.10 (A) Stability of polydopamine and trichlorovinylsilane (PDA/TVS) coating in ethanol/water=1:1 mixed solvent. (B) Stability of PFDT and ME click surface in ethanol/water=1:1 mixed solvent. Copyright 2022, Wiley-VCH.

Table 2.2 SCA, ACA and RCA of modified PTFE, PP, PE, Al, glass after immersing in ethanol/water mixed solvent. Copyright 2022, Wiley-VCH.

Unit °	0h			72h		
	SCA	ACA	RCA	SCA	ACA	RCA
PTFE-PDA/TVS	83.3±1.0	89.5±0.8	57.6±1.1	79.4±1.6	88.7±0.8	58.3±0.5
PP-PDA/TVS	80.4±1.3	92.4±0.6	63.9±0.3	77.1±1.2	92.0±0.3	60.0±0.6

PE-PDA/TVS	82.0±0.5	88.8±1.7	62.2±0.2	74.5±0.9	86.5±0.1	57.9±0.2
Al-PDA/TVS	83.7±0.7	85.2±0.6	63.5±0.1	74.7±1.5	77.6±0.4	0
Glass-PDA/TVS	83.1±0.8	91.5±1.2	63.5±0.1	70.7±0.4	77.3±0.6	56.7±0.4

2.1.2.5 Patterning on different materials

The advantage of this method is that PDA coating is substrate independent, thus allowing us to pattern various materials using essentially the same protocol. To demonstrate this universality, we reacted PDA/TVS-modified substrates with PFDT by UV irradiation for 1 min through a photomask (Figure 2.11) to generate hydrophobic pattern. After washing with acetone and reaction with hydrophilic ME under UV for a further 1 min, the region of the surface that did not react with PFDT in the previous step was rendered hydrophilic (Figure 2.12A). ToF-SIMS imaging of OH⁻ and CF₃⁻ secondary ions showed the patterning of ME and PFDT on PP, PE, and PTFE coated with PDA (Figure 2.12C, Figure 2.13). The pattern fidelities at the edge of the obtained 1-mm squares were below 100 μm (approximately 20 μm on PP and PE, and approximately 80 μm on PTFE). These results showed that TVS modification of PDA coating can be used to achieve accurate spatial programming of the surface of various materials. Different types of hydrophilic-hydrophobic patterns were created on PTFE, PP, Al and glass. Water flowed across the microscopic PFDT-ME-patterned surface of PP, with spontaneous dewetting of the PFDT areas to form an array of separated droplets located on ME-modified areas. A precise and continuous winding route pattern with a path width of 350 μm was obtained on PP. For large-scale patterns on PTFE, Al and glass, water was added by pipetting to form a pattern on the hydrophilic area (Figure 2.12B).

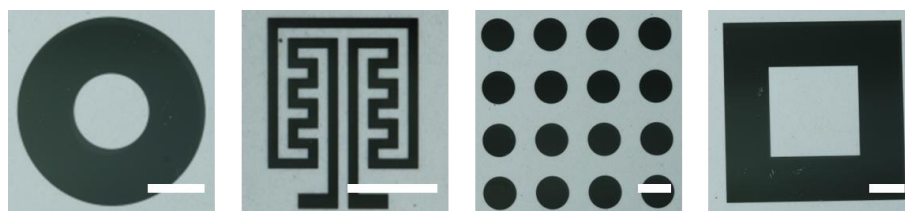


Figure 2.11 Photomasks used for UV-induced thiol-ene photo-click reaction on PTFE, PP, Al and glass. Scale bar: 3 mm. Copyright 2022, Wiley-VCH.

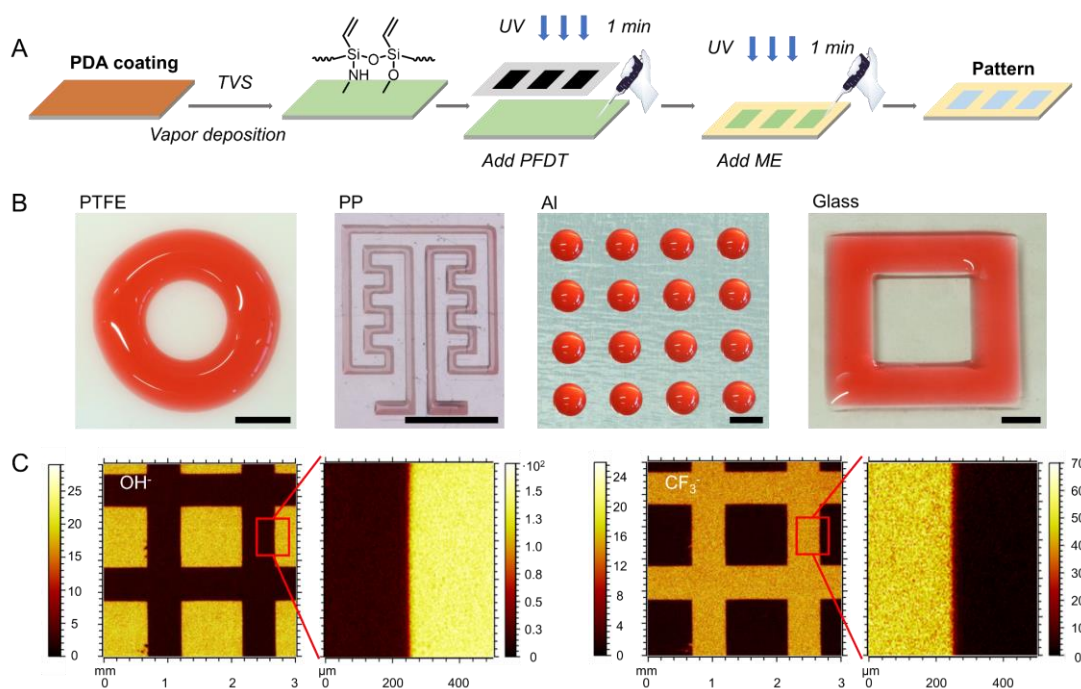


Figure 2.12 Substrate-independent patterning of TVS modified PDA-coated surfaces via UV-induced thiol-ene click reaction. (A) Schematic representation of the silanization reaction and UV-induced thiol-ene photoclick reactions used to create hydrophilic-hydrophobic patterns on PDA coated substrates. (B) Water pattern on hydrophilic-hydrophobic pattern produced on various substrates: PTFE, PP, Al and glass. Water containing a food dye. Scale bar: 3 mm. (C) ToF-SIMS 2D images of negative OH⁻ and CF₃⁻ secondary ions, showing the patterning of ME and PFDT on PP coated with PDA, respectively. Copyright 2022, Wiley-VCH.

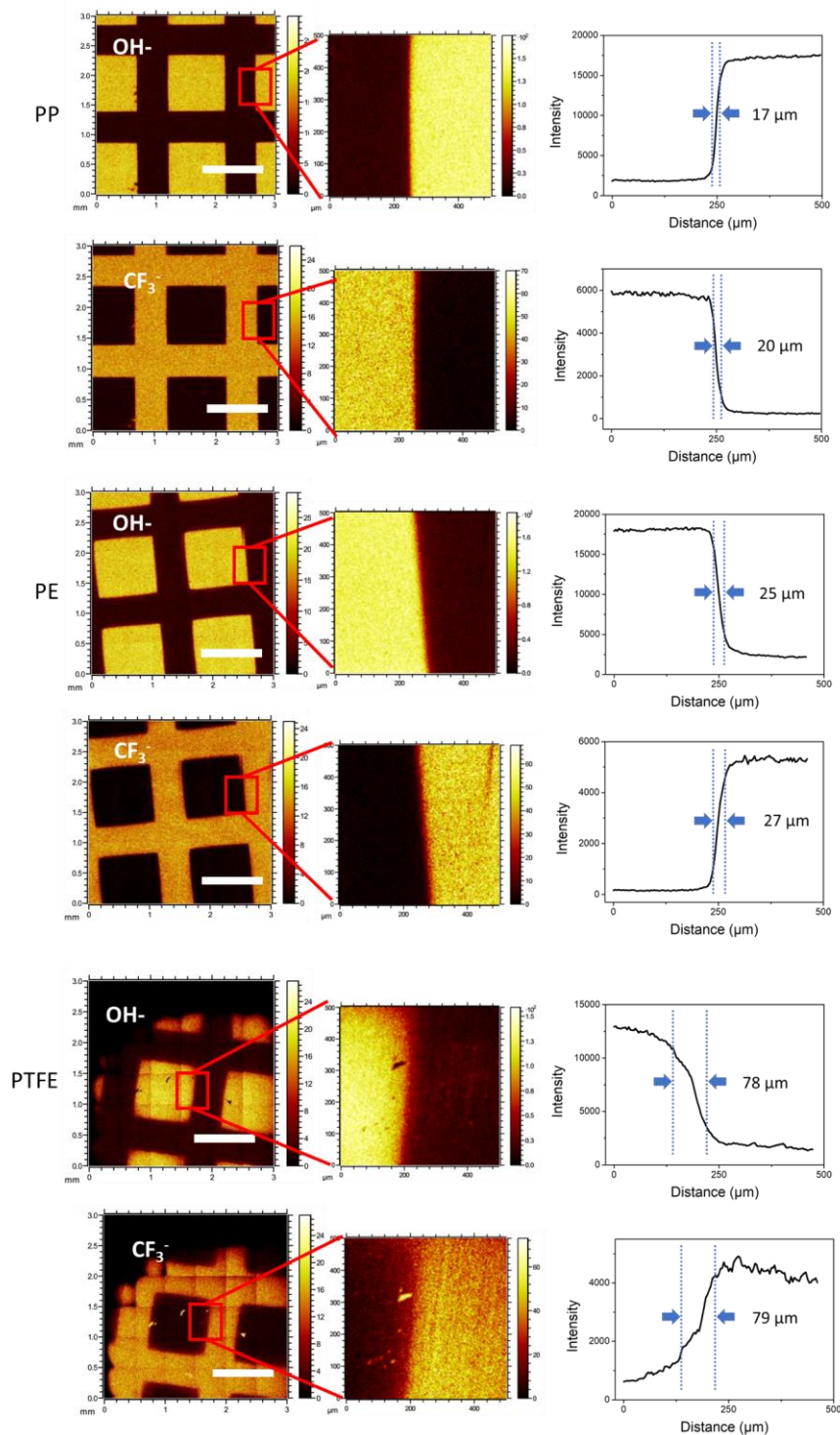


Figure 2.13 ToF-SIMS 2D graphs of negative OH^- and CF_3^- secondary ions, showing the patterning of ME and PFDT on PP, PE, PTFE coated with PDA, respectively. The pattern resolution at the square spot edge is around $20\ \mu\text{m}$ on PP, $25\ \mu\text{m}$ on PE and $80\ \mu\text{m}$ on PTFE (intensity of secondary ions from 16% to 84%). Scale bar: 1 mm. Copyright 2022, Wiley-VCH.

2.1.2.6 Re-writable process via silanization and desilanization

Recently, we demonstrated the use of silanization and desilanization for creating, erasing and re-writing the surface wettability patterns on polymer and silicon substrates. Reversible and versatile control of surface wettability was achieved by modifying the hydrophilic surface with fluorinated alkyl silane, followed by removing the functionalization by fluoride anions.¹¹² This dynamic and reversible process is of great significance for the recovery and reuse of substrates. To demonstrate the desilanization process on PDA coatings, TVS silanized PDA pre-coated substrates were treated with TBAF solution for 10 min. AFM images showed that the surface became smoother after TBAF treatment, with a similar R_q value 0.84 ± 0.13 nm to that of the unmodified PDA coating on silicon wafers (0.90 ± 0.04 nm, Figure 2.14B). The static WCA of surfaces treated with TBAF on different substrates ranged from 40° to 50° , which is almost the same as that of the original PDA coating (Figure 2.14C). After re-silanization of the TBAF treated surfaces with TVS, the static WCA was restored to 80° . Repeatability of the process was demonstrated by multiple cycles of desilanization and silanization (Figure 2.14C). After three cycles, the original hydrophilicity of PTFE, PP, PE, Al and glass with PDA coating was maintained, with static WCA ranging from 40° to 50° (Figure 2.14C). Silanization and desilanization was correlated with the presence and absence of the Si 2p doublet (with Si 2p_{3/2} at 102.8 eV), respectively (Figure 2.14D). Finally, we demonstrated that the reversible process was successful after the TVS layer was reacted with thiols. After PFDT was clicked under UV, the static WCA on different substrates increased to more than 100° . After treatment with TBAF solution in the same way as the TVS-modified substrates, the hydrophilicity of the surfaces was restored and the static WCA dropped to 40° (Figure 2.15). This reversible process was shown to be repeated successfully in multiple cycles. Thus, combining PDA coating and silanization allows rapid and accurate definition of the properties of a variety of substrates. Furthermore, repeated patterning of surfaces can be achieved by TBAF desilanization to restore hydrophilicity of the original PDA coating. Following this process, a new pattern can be generated on the same substrate by silanization and the UV-induced thiol-ene click reaction (Figure 2.16A). As shown in Figure 2.16B, hydrophilic pattern filled with water was created on PTFE and the entire surface was rendered hydrophilic by TBAF treatment. The surface was then silanized and clicked with PFDT and ME to create a new circular water pattern on the PTFE. Square pattern was also removed, and a new semicircle pattern created on glass with PDA coating (Figure 2.16C).

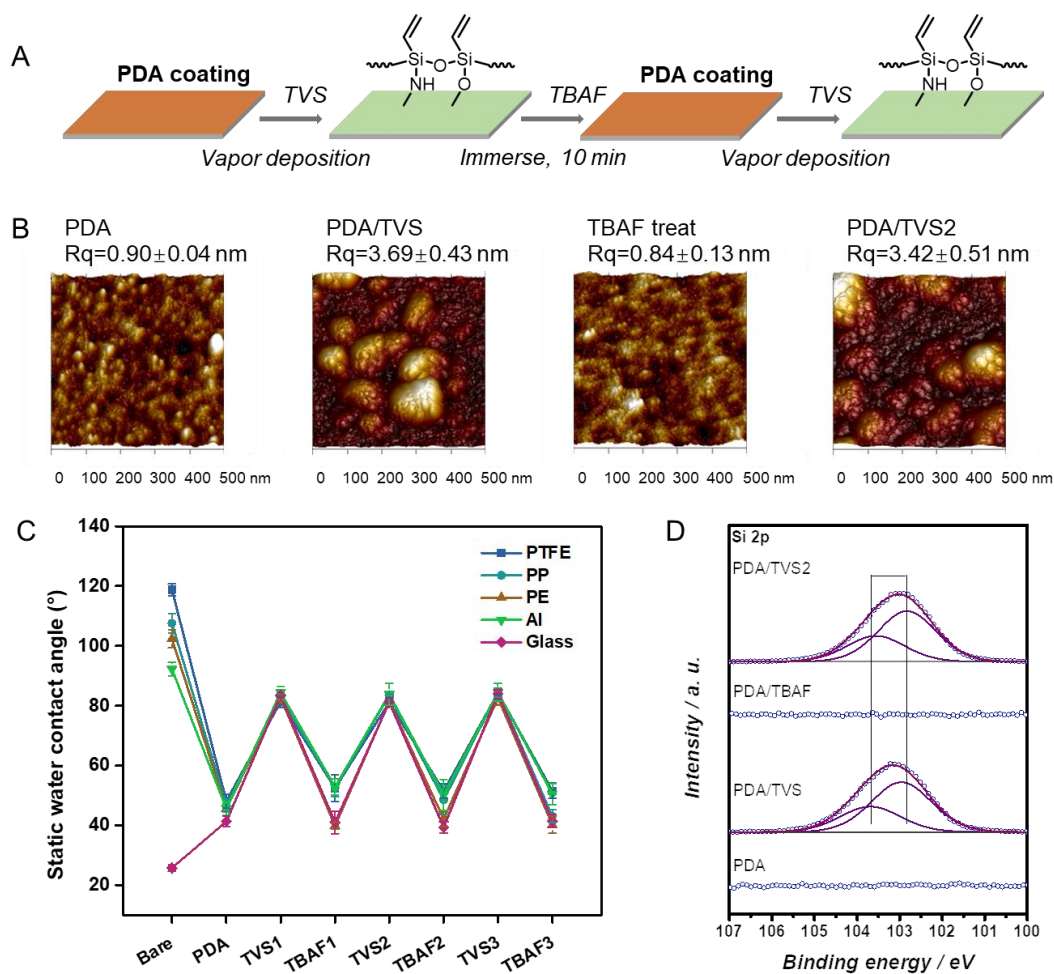


Figure 2.14 Reversible silanization process on PDA-coated substrates. (A) Schematic representation of the process to reverse the TVS-modified PDA coating. (B) AFM images of PDA, PDA/TVS, PDA/TBAF and PDA/TVS2 modified silicon wafers. (C) Static WCA changes of PDA-coated PTFE, PP, PE, Al and glass treated with TVS and TBAF. (D) Si 2p XP spectra of PDA, PDA/TVS, PDA/TBAF and PDA/TVS2 modified PP. Bare: bare substrates; PDA: PDA modified surface; PDA/TVS: PDA and TVS-modified surface; PDA/TBAF: TBAF treated PDA/TVS surface; PDA/TVS2: TVS silanization on PDA/TBAF. Copyright 2022, Wiley-VCH.

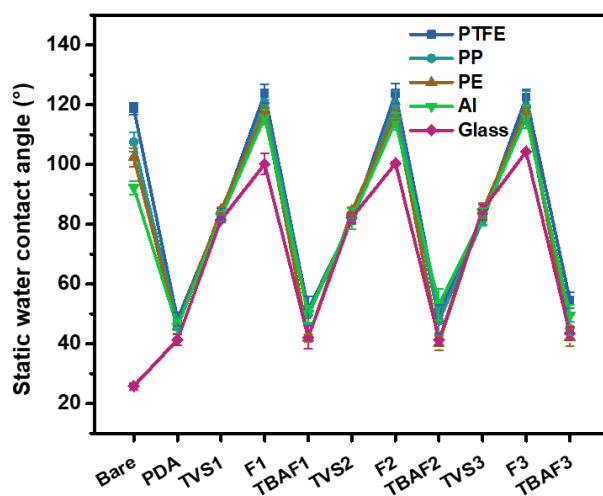


Figure 2.15 SCA change of PDA coated PTFE, PP, PE, Al and glass treated with TVS, PFDT click and TBAF. Copyright 2022, Wiley-VCH.

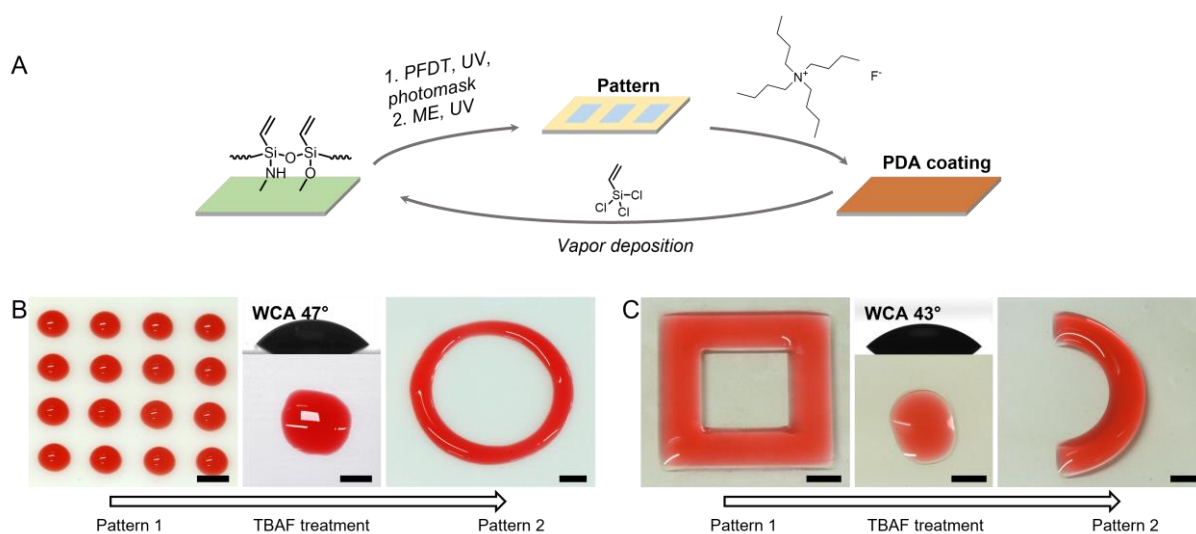


Figure 2.16 Writing, erasing and re-writing patterns on PDA-coated materials using TBAF treatment. (A) Schematic representation of the process to erase and re-write patterns on PDA coating using the TBAF treatment. (B) Examples of the possibility to reversibly create functional chemical patterns on PTFE substrates with PDA coating. Left: round hydrophilic spots (patterned with ME) show the water droplet array on PTFE (pattern 1); middle: pattern 1 erased by TBAF treatment; right: new pattern prepared on PDA coated PTFE substrates. (C) Pattern reversibility on PDA coated glass substrates. Left: hydrophilic square on glass filled with water (pattern 1); middle: pattern 1 erased by TBAF treatment; right: new pattern prepared on the TBAF treated area. Scale

bar: 3 mm. Copyright 2022, Wiley-VCH.

2.1.2.7 Application of the PDA/TVS modification strategy

PDA-based surface coating method offers the advantage of substrate-independency and simplicity. In addition, the dip-coating method allows modification of large objects with complex shapes in a single step process. As our patterning method is based on the use of PDA coating as the first layer, the method benefits from these same advantages. To demonstrate the feasibility of functionalization and patterning of complex large-scale objects, we performed modification and patterning on various objects (soft adhesive PE tape, a plant leaf, a plastic flabellum and a metal spoon). After PDA coating, TVS modification, and patterning (hydrophobic PFDT and hydrophilic ME reacted by thiol-ene click reaction), hydrophilic-hydrophobic patterns formed on the objects and could be visualized by water patterns confined by the hydrophobic regions (Figure 2.17 and 2.18). Thus, the method allows to create chemical patterns on flexible, natural, curved and large substrates in only three steps.

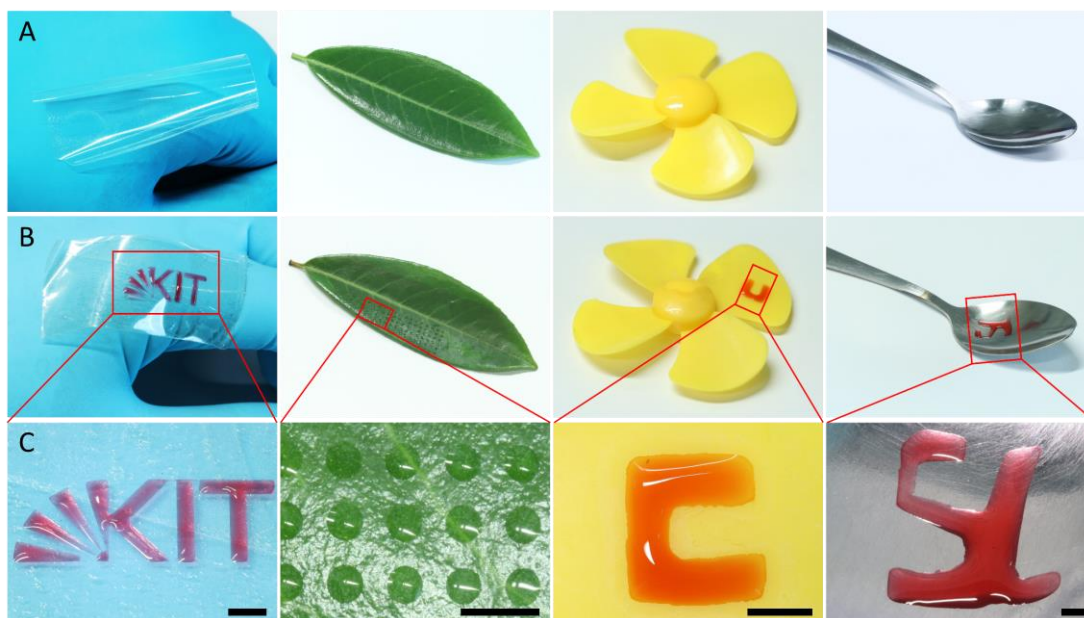


Figure 2.17 Application of the PDA/TVS modification strategy on complex-shaped large objects: soft adhesive PE tape, a plant leaf, a plastic flabellum and a metal spoon. Digital images of objects before (A) and after (B) modification. (C) Water pattern on objects (red patterns contain food dye). From left to right: Pattern on soft adhesive PE tape; array of round hydrophilic spots on a fluorinated plant leaf; letter “C” on a plastic flabellum; letter “SL” on a metal spoon. Scale bar: 3

mm. Copyright 2022, Wiley-VCH.

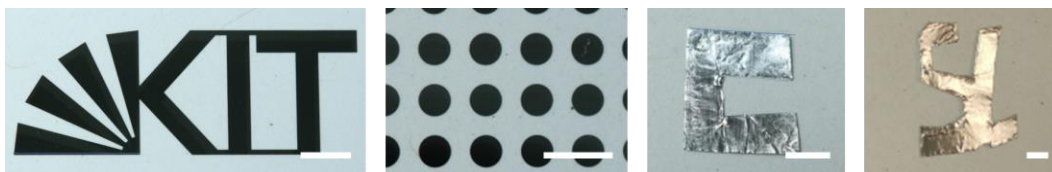


Figure 2.18 Photomasks used for UV-induced thiol-ene photo-click reaction on complex objects. Scale bar: 3 mm. Copyright 2022, Wiley-VCH.

2.1.3 Summary

In summary, I have established a rapid, facile and substrate-independent strategy for reversible surface modification and patterning. This strategy is based on three steps: polydopamine coating, functionalization of polydopamine using trichlorovinylsilane, and UV-induced modification or patterning using thiol-ene reaction. We have demonstrated that this method can be extended to a variety of substrates, including polytetrafluoroethylene, polypropylene, polyethylene, aluminum and glass, using essentially the same procedure for all substrates. We further investigated reversibility of the silanization step and re-usability of patterned substrates to create new patterns on the same surface in multiple cycles of silanization and desilanization. This is important for the reuse of surfaces and for achieving higher flexibility in applications of PDA-coated surfaces. Finally, we demonstrated that the versatility of polydopamine coatings allows modification and patterning of complex large-scale objects, such as soft adhesive polyethylene tape, plant leaves, plastic flabellum and metal objects. Thus, our universal and simple approach for substrate independent surface modification and patterning will help in the development of novel functional materials, surfaces and devices, which can be useful in myriads of applications.

2.1.4 Experimental Details

2.1.4.1 Chemicals and materials

3-Hydroxytyramine hydrochloride (99%) and tetrabutylammonium fluoride hydrate (99%) were purchased from Acros Organics (Geel, Belgium). Isopropanol, ethanol and acetone were obtained

from Merck (Darmstadt, Germany). All other chemicals were purchased from Sigma-Aldrich (Darmstadt, Germany) and used without further purification. PTFE plates, PP plates, PE adhesive tape and aluminum adhesive tape were purchased from RS Components GmbH (Frankfurt, Germany) and were cut to the desired size for use. NEXTERION B glass slides were obtained from Schott AG (Mainz, Germany) and silicon wafers (CZ-Si-wafer 50 mm) were obtained from Siegert Wafer (Aachen, Germany). Tris buffers were prepared at a 10 mM and adjusted to pH 8.5 using a Mettler Toledo digital pH meter (Shanghai, China).

2.1.4.2 Characterization

CA measurement

The static WCA (approximately 2 μL) on bare and modified substrates was measured using a DSA25S drop shape analyzer (Krüss, Hamburg, Germany). Advancing WCA values were obtained by measuring the WCA while the liquid was slowly added (at 0.2 $\mu\text{L s}^{-1}$) to increase the volume of droplet from approximately 5 μL to 15 μL in contact with the sample using a micrometer syringe. Receding WCA values were obtained by slowly retracting the liquid (0.2 $\mu\text{L s}^{-1}$) to decrease the volume of the droplet from 15 μL droplet to 5 μL .

Atomic force microscopy

AFM was performed on a Dimension Icon AFM (Bruker, Karlsruhe, Germany) in standard tapping mode under air (INT, KIT). Cantilevers (HQ/NSC15/AI BS; MikroMasch) were used with a nominal force constant of 40 N m^{-1} and a resonance frequency of 325 kHz.

Time-of-flight secondary ion mass spectrometry

ToF-SIMS analysis was performed using a TOF-SIMS.5 spectrometer (IONTOF GmbH, Münster, Germany) at IFG, KIT. A bunched primary beam of 25 keV Bi_3^+ ions was applied (10 kHz, 0.33 pA target current, approx. 1 ns pulse width). Mass scale calibration was based on C^- , CH^- , CF^- , C_2^- , and C_3^- signals. Large field of view images were obtained by rastering the primary ion beam and the sample stage, whereas $500 \times 500 \mu\text{m}^2$ images were obtained by rastering the primary beam alone (dose density 2×10^{11} ions cm^{-2} , 128×128 pixels). Charge compensation was achieved using an electron flood gun (21 eV) and time-of-flight analyzer tuning. Intensity traces were obtained by summing the signals of given secondary ions (devoid of detector saturation) from pixels parallel to

the pattern border (image de-rotating and summing) and calculating the spacing between 16% and 84% of the total signal step.

X-ray photoelectron spectroscopy

XPS analysis was performed using a K-Alpha+ XPS spectrometer (Thermo Fisher Scientific, East Grinstead, UK), IAM, KIT. Thermo Advantage software was used for data acquisition and processing. All surfaces were analyzed using a microfocused, monochromated Al K α X-ray source (400 μ m spot size). The K-Alpha+ charge compensation system was employed during analysis, using electrons of 8 eV energy, and low-energy argon ions to prevent any localized charge build-up. The spectra were fitted with one or more Voigt profiles (BE uncertainty: ± 0.2 eV) and Scofield sensitivity factors were applied for quantification.¹⁸¹ All spectra were referenced to the C 1s peak (C-C, C-H) at 285.0 eV binding energy controlled by means of the well-known photoelectron peaks of metallic Cu, Ag, and Au.

Digital photography

Digital photos were taken using a Canon EOS 80D digital camera.

2.1.4.3 Preparation of PDA coatings

PTFE, PP, PE and Al slides were cut to the desired size (usually 2.1 cm \times 7.6 cm). Glass slides were used as purchased (2.1 cm \times 7.6 cm). All slides were washed with isopropanol, ethanol and deionized (DI)-water, then immersed in 2 mg mL⁻¹ 3-hydroxytyramine hydrochloride tris solution (tris solution: 10 mM, pH 8.5) for 24 h. The slides were then rinsing thoroughly with DI water and dried.

2.1.4.4 Vapor deposition of vinylchlorosilane

PDA-coated substrates were placed in a desiccator containing an open vial with 0.5 mL trichlorovinylsilane (TVS). The desiccator was evacuated and left closed for 15 min. The reaction was performed in the gaseous phase at room temperature. Leave the samples in a fume hood for half an hour until the hydrochloric acid produced in the reaction has evaporated. All samples were then washed with ethanol and DI water and dried.

2.1.4.5 UV-induced thiol-ene photoclick

For fully reacted samples, TVS-modified substrates were wetted with acetone solution of 10 vol % of PFDT or ME, and irradiated with 3.0 mW cm^{-2} 265 nm UV light for 1 min. The samples were then washed several times with acetone and dried with airflow.

For patterning samples, substrates were wetted with a 10 vol % solution of PFDT in acetone, covered by a quartz photomask, and irradiated with an intensity of 3.0 mW cm^{-2} and a wavelength of 265 nm (UV) light for 1 min. The distance between substrates and photomasks were controlled by placing 200 μm polyimide spacers between them. Samples were then washed several times with acetone and dried with airflow. Next, substrates were wetted with a 10 vol % solution of ME in acetone and irradiated with an intensity of 3.0 mW cm^{-2} and a wavelength of 265 nm (UV) light for 1 min. The samples were washed several times with acetone and dried with airflow.

2.1.4.6 Degradation of siloxane layer with TBAF

TVS silanized substrates with PDA coating were immersed into 0.1 M TBAF ethanol solution. After 10 min treatment, the substrates were washed with ethanol and deionized water then dried.

2.2 Inherently UV Photodegradable Poly(meth)acrylate Gels*

*This chapter and associated sections were published previously. Figures and tables also have been published and reproduced for use in this chapter. Copyright has been acquired from the publisher.

Scheiger, J. M., Li, S., Brehm, M., Bartschat, A., Theato, P., & Levkin, P. A. (2021). *Advanced Functional Materials*, 31(49), 2105681.

This is a project in cooperation with Dr. Johannes Scheiger. Dr. Johannes Scheiger and Shuai Li contributed equally to this work. Dr. Johannes Scheiger proposed the original idea, performed and evaluated experiments. Shuai Li performed and evaluated experiments. This chapter only contains the experimental part completed by Shuai Li.

2.2.1 Introduction

Organogels (hydrophobic polymer gels) are three-dimensional networks swollen with organic liquids. These networks can be formed either via self-assembly of low-molecular weight gelators (LMOGs) or via polymerization reactions. Analogue to hydrogels, crosslinking is achieved chemically (covalent bonding,) or physically (cooperative interactions). However, the term organogel is controversial since there is no IUPAC definition, and some prefer to use the term only for non-covalent networks. In the scope of this work, the term organogel includes covalently crosslinked polymers. Applications of organogels include actuators,¹⁸² anti-biofouling,^{183,184} anti-waxing,¹⁸⁵ cosmetics,¹⁸⁶ drug and nutrition carriers,¹⁸⁷⁻¹⁹¹ encapsulants,¹⁹² freeze tolerant elastomers,¹⁹³ oil-water separation,^{194,195} solid edible oils,¹⁹⁶ and slippery and self-cleaning surfaces.¹⁹⁷⁻²⁰⁰ Control over the structure of organogels is mandatory for their applications or can enhance their functionality. For example, Zhang et al. demonstrated controlled water droplet sliding on a grooved organogel surface.²⁰¹ Moreover, the surface texture of organogels influences their wettability and optical properties.²⁰² However, fabrication of structured organogels is not trivial, since established methods for hydrogels cannot be employed readily. For example, the crosslinked polydimethylsiloxane (PDMS) molds utilized in soft-lithography swell in hydrophobic solvents and are thus prone to deformation.²⁰³⁻²⁰⁵ If the organogel has thermoreversible properties, micromolding can be used to create a defined structure.²⁰⁶ The fabrication of micro- or nano structured organogels can be controlled via supramolecular self-assembly.^{207,208} While this

approach does not require templates, it lacks variety and predictability of structures and is restricted to certain starting materials (e.g. LMOGs, block copolymers). The few reports available about photodegradable organogels suffer from long degradation times, require laborious synthesis of photolabile crosslinkers, or are too hydrophilic to serve in the applications mentioned above.²⁰⁹⁻²¹³ There has been no report about organogels that are readily synthesized, contain a large amount of hydrophobic solvent, and degrade fast under UV light. Thus, it is challenging to fabricate structured or patterned organogels. Recently, we reported the inherent photodegradability of poly(meth)acrylate hydrogels and demonstrated their use for biological applications.^{214,215} I hypothesized, that this approach could be extended beyond water infused hydrophilic networks to hydrophobic organogel networks. Since most (meth)acrylate monomers are hydrophobic, the monomer pool that can be addressed with our approach is naturally high. Herein, we report for the first time, the inherent photodegradation of poly(meth)acrylate organogels under UV light. Organogels were synthesized via free radical polymerization and their chemical composition and swelling properties were investigated. Structured organogels were fabricated via UV light irradiation and the solvent infusing the organogel was identified to be an influential factor for the photodegradation. The inherent photodegradability of poly(methacrylate) organogels reported herein is simple, cheap and was used to create a variety of structured organogels for application as an extractive fluid channel or positive photoresist.

2.2.2 Results and Discussion

2.2.2.1 Preparation and degradation of organogels

Organogels were synthesized via free radical polymerization using a 1:1 vol% mixture of *n*-butyl methacrylate (BMA) and lauryl methacrylate (LMA) as monomers and poly(propylene) glycol dimethacrylate (PPGDMA) as crosslinker in 1-nonanol as solvent (Figure 3.1A and B). The chemical composition and gel-like properties of the prepared organogels were confirmed with rheometry, infrared spectroscopy (IR), and UV-vis spectroscopy (Figure 3.2-3.4). When swollen in 1-butanol or 1-nonanol, the organogels showed inherent photodegradation properties under UV

light (Figure 3.1 C). Details about the UV lamp (i.e., power, emission spectrum) are provided in the supporting information (Figure 3.5).

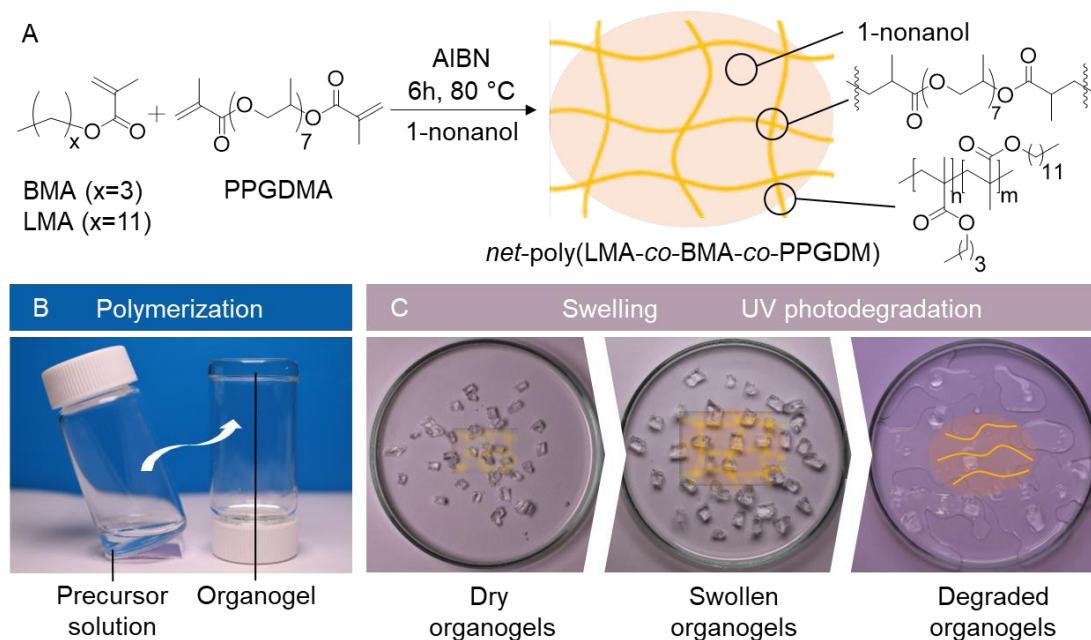


Figure 3.1 (A) Reaction equation for the synthesis of *net-poly(BMA-co-LMA-co-PPGDMA)* organogel from lauryl methacrylate (LMA) and butyl methacrylate (BMA) monomer with poly(propylene glycol) dimethacrylate (PPGDMA) as crosslinker. (B) Image of the organogel precursor solution and the as-prepared organogel in a vial. (C) Image and schematic molecular structure of organogel pieces without solvent, organogel pieces swollen in 1-nonanol and the swollen organogel pieces after 30 min of UV photodegradation. The diameter of the petri dish is 5 cm. Copyright 2022, Wiley-VCH.

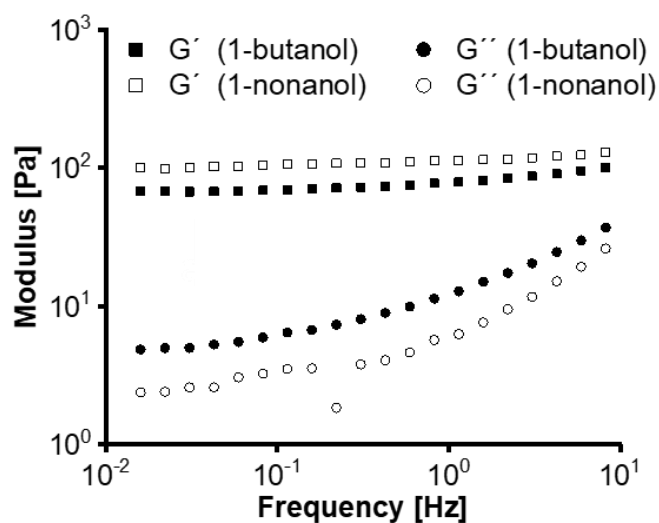


Figure 3.2 Rheometry of organogels swelled in the 1-butanol or 1-nonanol. The storage moduli (G') are independent of the frequency as expected for an elastic material. The observed increase of G'' with the frequency might be explained by pendent chains due to the low degree of cross-linking (0.5 vol% PPGDMA rel. to the monomers LMA+BMA). Copyright 2022, Wiley-VCH.

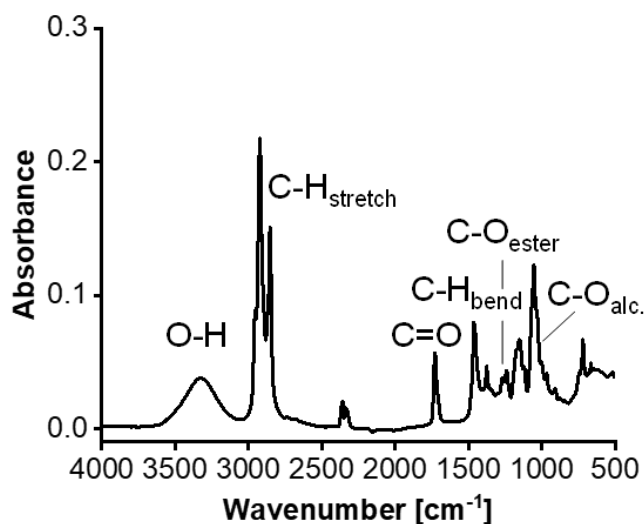


Figure 3.3 ATR-IR spectrum of an as-prepared organogel (1-nonanol). Position and width of relevant peaks: ν [cm^{-1}] = 3330 (b, s), 2957 (s), 2924 (vs), 2855 (vs), 1730 (m), 1466 (s), 1379 (m), 1242 (m), 1155 (m), 1057 (s), 721 (m). Copyright 2022, Wiley-VCH.

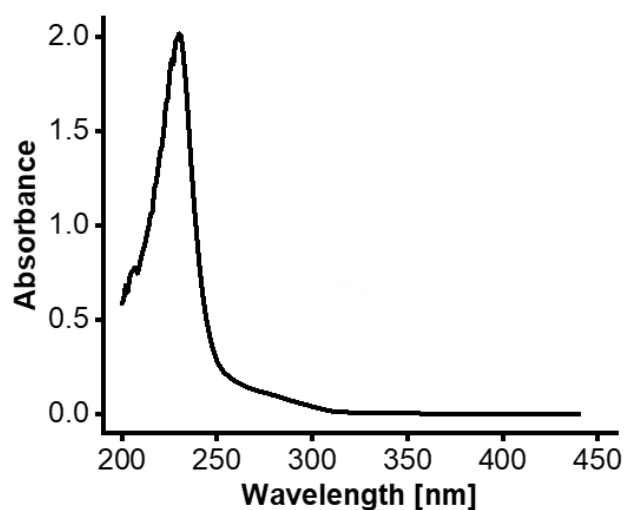


Figure 3.4 UV Vis spectrum of an as prepared organogel film (125 μm). The UV absorbance of the organogel starts from around 320 nm. The peak absorbance is at ca. 230 nm due to the ester functionalities in *net*-poly(LMA-*co*-BMA-*co*-PPGDMA). The contribution of 1-nonanol to the UV absorbance in the spectrum of the organogel is small, as evident by comparison with a UV-vis spectrum of pure 1-nonanol (Figure 3.8). Copyright 2022, Wiley-VCH.

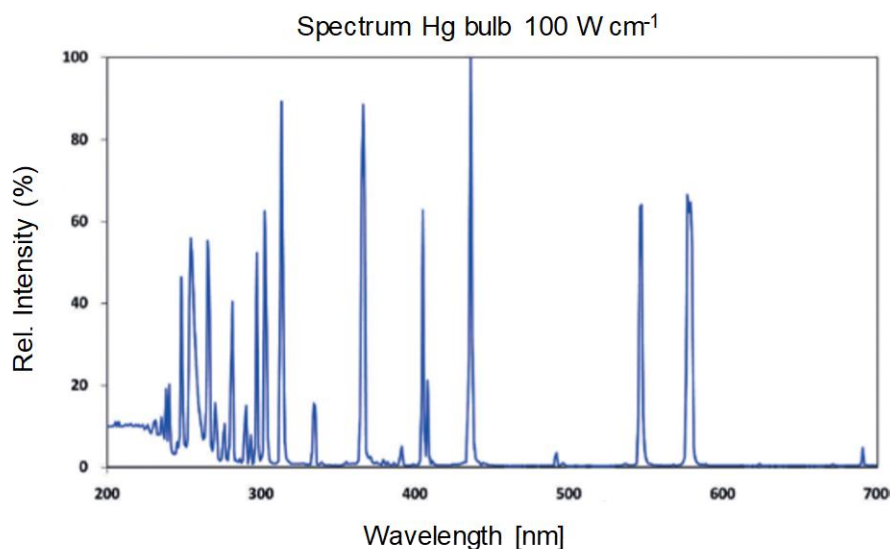


Figure 3.5 Emission spectrum of Hg bulbs used in the UVA cube 2000 from Dr. Hönle AG (Gräfelfing, Germany). The maximum power of the setup is 2000 W (100 W cm^{-1} , 20 cm bulb length). Spectrum taken from the product brochure of Dr. Hönle AG. For all experiments, the device was used at half power (1000 W). Copyright 2022, Wiley-VCH.

2.2.2.2 UV-induced degradation patterning

Increasing the UV irradiation time led to an increase in erosion depth (Figure 3.6A). Thus, the depth of degradation was controllable by the choice of irradiation time. Structured bulk organogels were prepared by exposing cuboid shaped organogels to UV light for 20 min using a photomask and were analyzed with optical profilometry (Figure 3.6B). The depth of erosion of a feature after 20 min UV irradiation was determined to be 1.185 ± 0.039 mm (SD, $n=3$) based on optical profilometry measurements at different positions of the pattern (Figure 3.7). Thin-film organogel patterns were analyzed with microscopy (Figure 3.6C). Round shapes or patterns with feature sizes as small as $100 \mu\text{m}$ were readily obtained. Organogels were transparent after all steps, i.e., synthesis, swelling, and degradation, indicating chemical homogeneity.

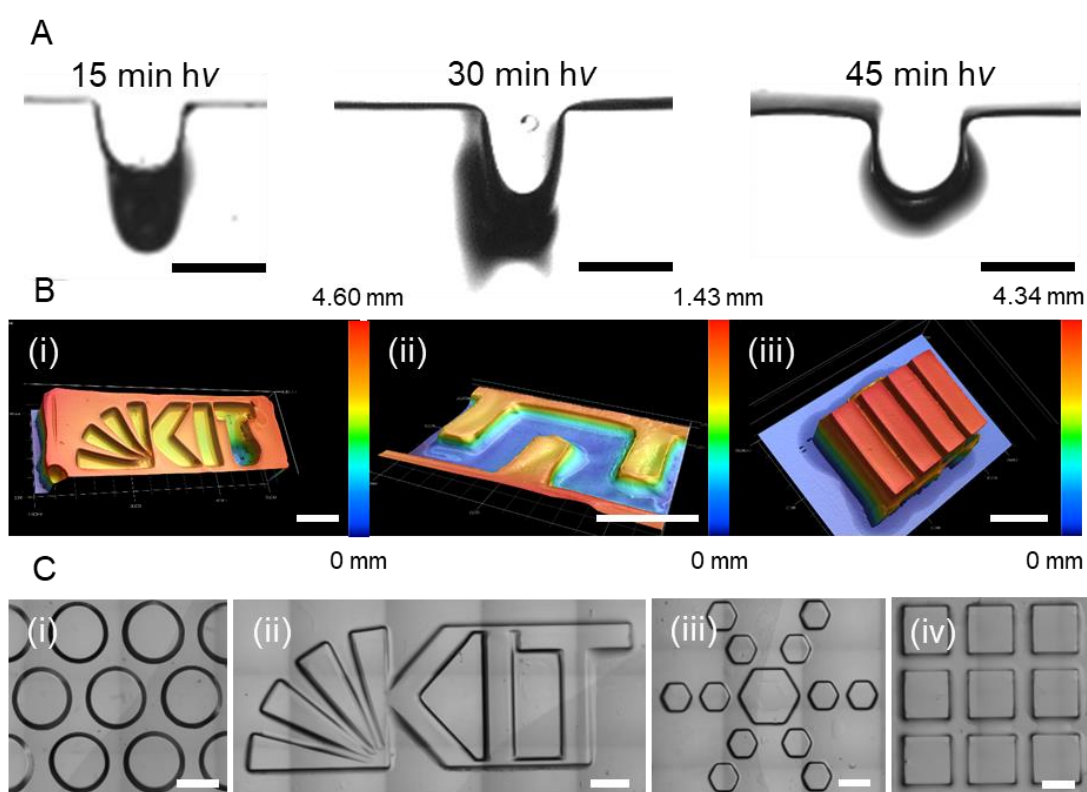


Figure 3.6 (A) Microscopy images of degradation profiles for different UV irradiation times. Scalebars are 1 mm. (B) 3D optical profilometry images of patterned bulk organogels such as (i) a geometrical pattern, (ii) a channel and (iii) a stripe pattern. Organogels were sprayed with chalk spray to enable optical profilometry measurements. The height of the organogels is 4 mm, the degradation depth is ca. 1.2 mm. Scalebars are 10 mm. (C) Brightfield microscope images of

different patterned organogel films such as (i) an array of circles, (ii) three letters, (iii) an array of hexagons, and (iv) an array of squares. The initial film thickness was 125 μm . Organogel films were exposed to UV light for 10 min using a photomask. Scalebars are 1 mm. Copyright 2022, Wiley-VCH.

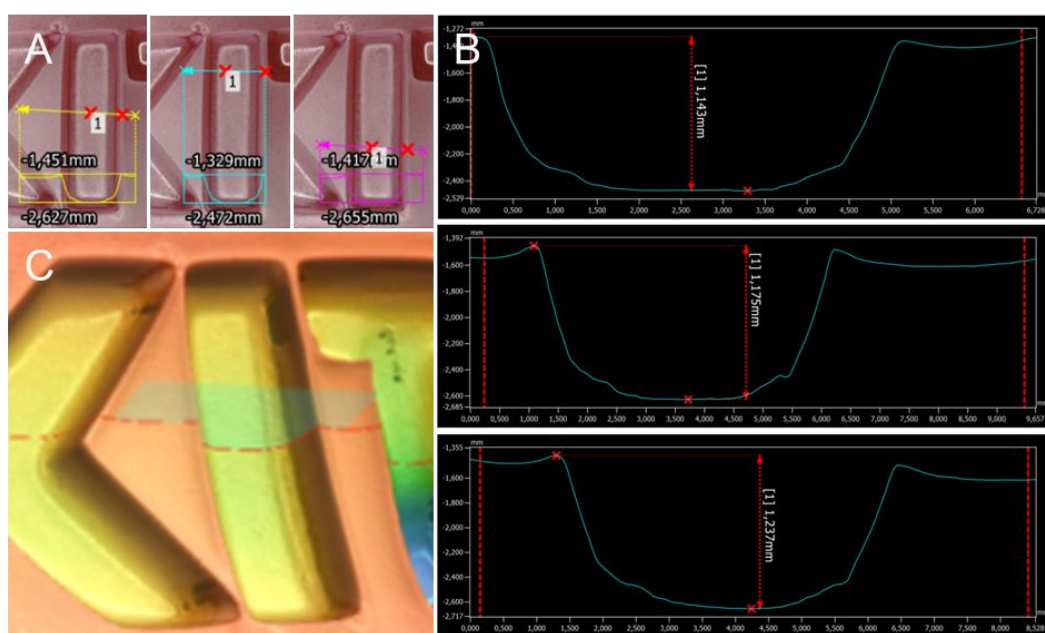


Figure 3.7 Optical profilometry measurements of a patterned organogel. The irradiation time was 20 min. (A) Profile measurements at three positions and (B) their respective height profiles. The average height with standard deviation was 1.185 ± 0.039 mm ($N=3$). (C) 3D image of the investigated cross section. Copyright 2022, Wiley-VCH.

2.2.2.3 Relationship between degradation and swelling solvent

The main difference between hydrogels and organogels is the polarity of the polymer network and thus the selection of solvents that can infuse the network. Hydrogels are inherently suitable for UV photochemistries, as water does not absorb significant amounts of UV light.²¹⁶ However, the choice of the solvent was found to be decisive for the photodegradation of organogels. We hypothesized, that this was due to two main factors: (i) the UV absorbance and (ii) swelling capability of the solvent. For a fast photodegradation process, the UV absorbance of the solvent should be low, and it should swell the organogel network strongly. A high UV absorbance of the solvent would reduce the effective light intensity available for the photodegradation, whereas insufficient swelling could

cause the gel network to undergo photocrosslinking, due to lower inter-chain distances within the polymer network.²¹⁵ To test our hypothesis, we measured UV-vis spectra of different solvents (Figure 3.8) and tested the swelling factor of selected solvents in our organogel networks. The swelling factor was defined as the mass of the swollen organogel (w_s) divided by the dry mass of the polymer network (w_d) (Table 3.1).

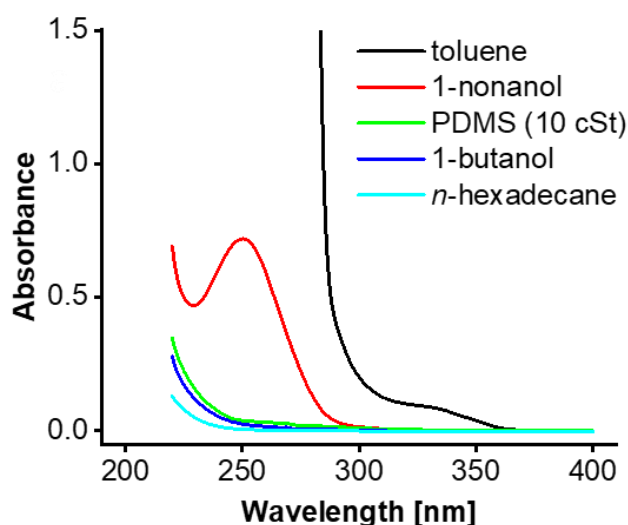


Figure 3.8 UV-Vis measurements for different organic solvents between 220 – 400 nm. The UV cutoff value, where the UV absorbance reaches 1, was found to be 290 nm for toluene. No UV cutoff was reached for the other solvents. 1-nonanol has an absorption band with a maximum at 250 nm, which is presumably an impurity with 1-nonanol in the commercial solvent.¹⁹² Copyright 2022, Wiley-VCH.

Table 3.1 Properties of solvents investigated for their influence on the photodegradation properties of organogels. Data are given as mean \pm SD ($n=3$). Copyright 2022, Wiley-VCH.

Solvent	1-Nonanol	1-Butanol	Toluene	PDMS
Swelling Factor ^a	3.78 ± 0.17	3.48 ± 0.07	15.88 ± 0.37	1.02 ± 0.01
UV Transmission ^b (%)	19	94	< 1	92
Boiling Point (°C)	214	118	111	-

^aDefined as w_s/w_d

^bDetermined at 250 nm

To first test the influence of the swelling on the photodegradation rate, as-prepared organogels were freed from 1-nonanol or swollen in excess 1-nonanol for different times (0, 6, and 48 h) to obtain organogels with a different content of 1-nonanol (0, 60.7, 67.5, and 76.3 wt%, respectively). The organogels were then exposed to UV light for different times and the mass fraction (m_t/m_0), defined as the mass of the organogels after irradiation (m_t) relative to their initial mass (m_0), was determined (Figure 3.9A). To ensure comparable results, the exposed surface area of the organogels was kept the same. The rate of photodegradation was found to increase with increasing 1-nonanol content. For example, after 30 min of irradiation 87 wt% of organogels swollen for 0 h (60.7 wt% 1-nonanol) remained, whereas organogels swollen for 48 h (76.3 wt% of 1 nonanol) were fully degraded into a polymer solution, i.e., a liquefied organogel. For dry organogels (0 wt% of 1-nonanol), no loss of mass was detected. GPC measurements of organogels irradiated for different times revealed monomodal molecular weight distributions. The molecular weight averages (M_N , M_W) and the dispersity (\mathcal{D}) decreased with increasing irradiation time (Figure 3.10 and Table 3.2). The photodegradation products were separated from 1-nonanol by precipitation in cold methanol and their chemical composition was analyzed with IR, UV-vis, and NMR spectroscopy (Figure 3.11-13). ^1H and ^{13}C NMR spectra of degraded polymers did not differ significantly for different irradiation times and closely resembled those of pure poly(butyl methacrylate) or poly(lauryl methacrylate), whereas UV-vis spectroscopy and IR spectroscopy showed indications of photooxidation. To clarify the influence of the UV absorbance and swelling factor of the solvent on the speed of photodegradation, organogels immersed into an excess of toluene, 1 butanol, or PDMS (10 cSt) for 48 h, respectively, were irradiated with UV light for 10 min (Figure 3.9B). Toluene and PDMS were chosen as model solvents to represent a low transmission but high swelling solvent (toluene) and a high transmission but low swelling solvent (PDMS).

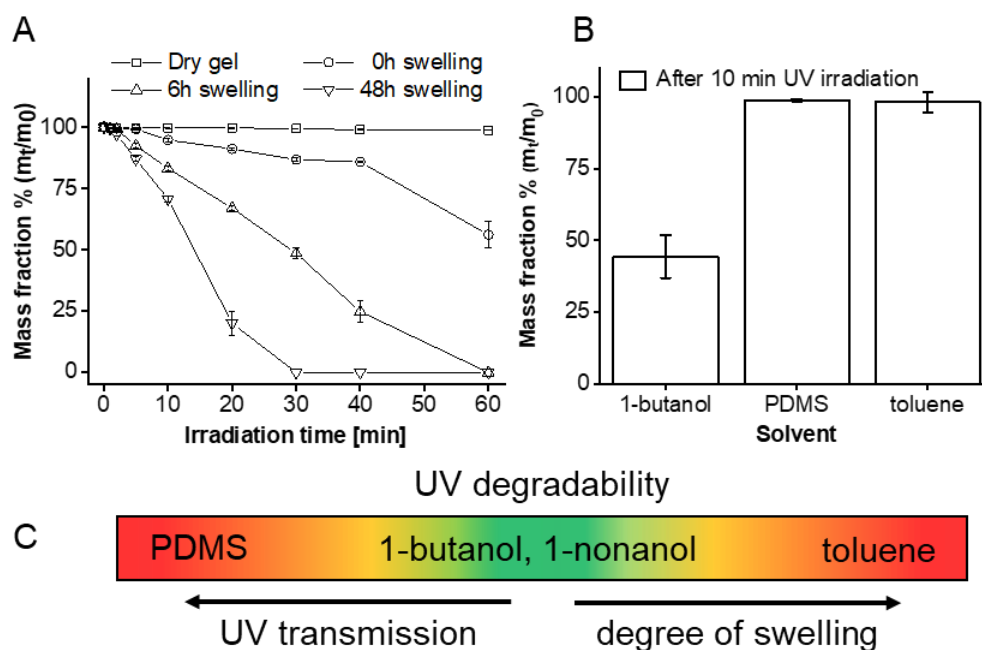


Figure 3.9 (A) Photodegradation speed of dry and as-prepared organogels swollen in 1-nonanol for 0, 6, and 48 h. The resulting 1-nonanol content of the organogels was 0, 60.7, 67.5, and 76.3 wt%, respectively. Data are given as mean \pm SD (n=4) (B) Photodegradation of organogels swollen in 1-butanol, PDMS, and toluene after 10 min of UV light irradiation. (C) Scheme summarizing how the solvent properties affected the photodegradation of organogel. Solvents with low UV light transmission or swelling capability inhibited the photodegradation of organogels (red), whereas highly swelling, UV-transmitting solvents such as 1-butanol or 1-nonanol enabled the photodegradation of organogels (green). Copyright 2022, Wiley-VCH.

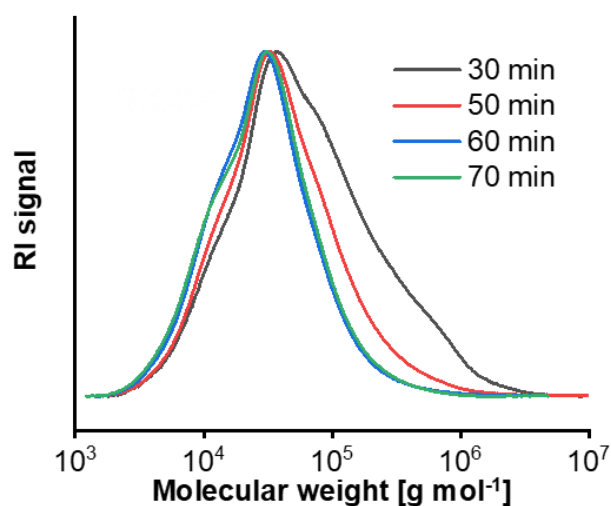


Figure 3.10 GPC traces of a photodegraded gel irradiated for 30, 50, 60, and 70 min. The number average molecular weight (M_N) and the weight average molecular weight (M_W) decreased with increasing irradiation time. Interestingly, the molecular weight distribution became narrower with increasing irradiation time as observed from the steady decrease of the dispersity (\mathcal{D}) from 30 min ($\mathcal{D} = 4.84$) to 70 min ($\mathcal{D} = 2.51$). These results indicate a random chain cleavage mechanism since long polymer chains are statistically more likely to be cleaved somewhere in the middle of the chain rather than on the sides. Such an effect could also explain the initial strong decrease of the molecular weight observed between 30 min and 50 min irradiation, which is mainly caused by the disappearance of the high molecular weight shoulder. The same effect was previously described by our group for the UV photodegradation of poly(meth)acrylate hydrogels.^{193,194} Copyright 2022, Wiley-VCH.

Table 3.2 GPC data of gels for different irradiation times. Copyright 2022, Wiley-VCH.

Irradiation time [min]	M_N [kg mol ⁻¹]	M_W [kg mol ⁻¹]	\mathcal{D}
30	30.7	148.8	4.84
50	23.7	78.4	3.31
60	19.1	48.7	2.55
70	18.8	47.3	2.51

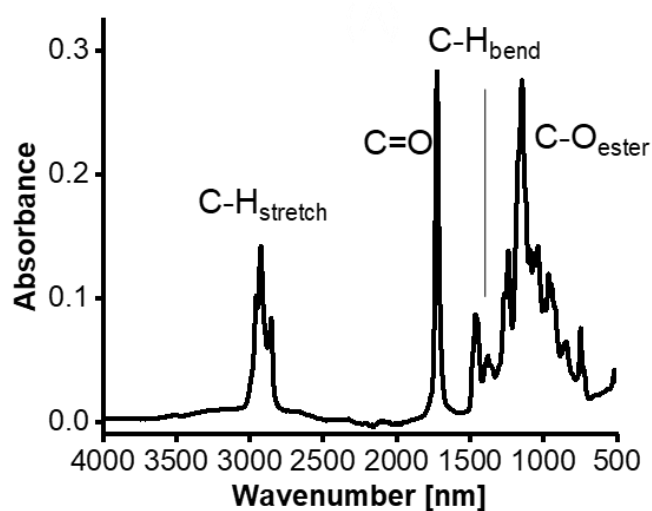


Figure 3.11 ATR FT-IR spectrum of an organogel photodegraded for 30 min. Position and width of relevant peaks: ν [cm^{-1}] = 2958 (m), 2925 (s), 2855 (m), 1726 (vs), 1464 (m), 1381 (w), 1240 (s), 1147 (vs), 966 (s), 748 (m). Copyright 2022, Wiley-VCH.

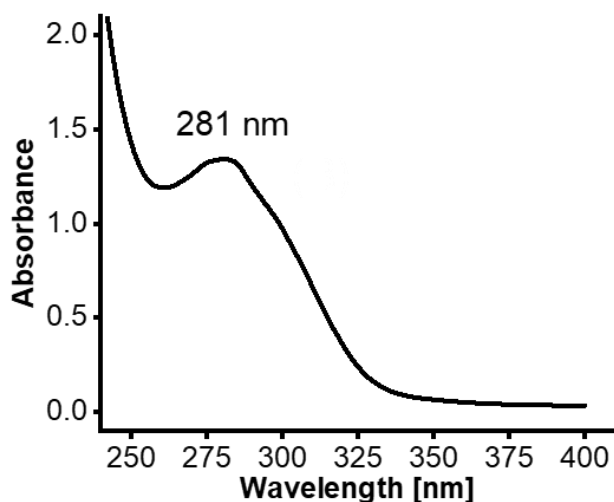


Figure 3.12 UV-vis spectrum of an organogel photodegraded for 30 min. The degraded organogel was diluted with MeCN. In contrast to the unirradiated organogel, an absorbance maximum at 281 nm was found. This indicated the formation of functional groups such as aldehydes or ketones (esters of formic acid) as by-products of the photodegradation. This finding hinted towards involvement of molecular oxygen from air. Such photooxidation processes were reported for poly(alkyl methacrylate) polymers (including poly(butyl methacrylate)) before.^{187,188} Copyright 2022, Wiley-VCH.

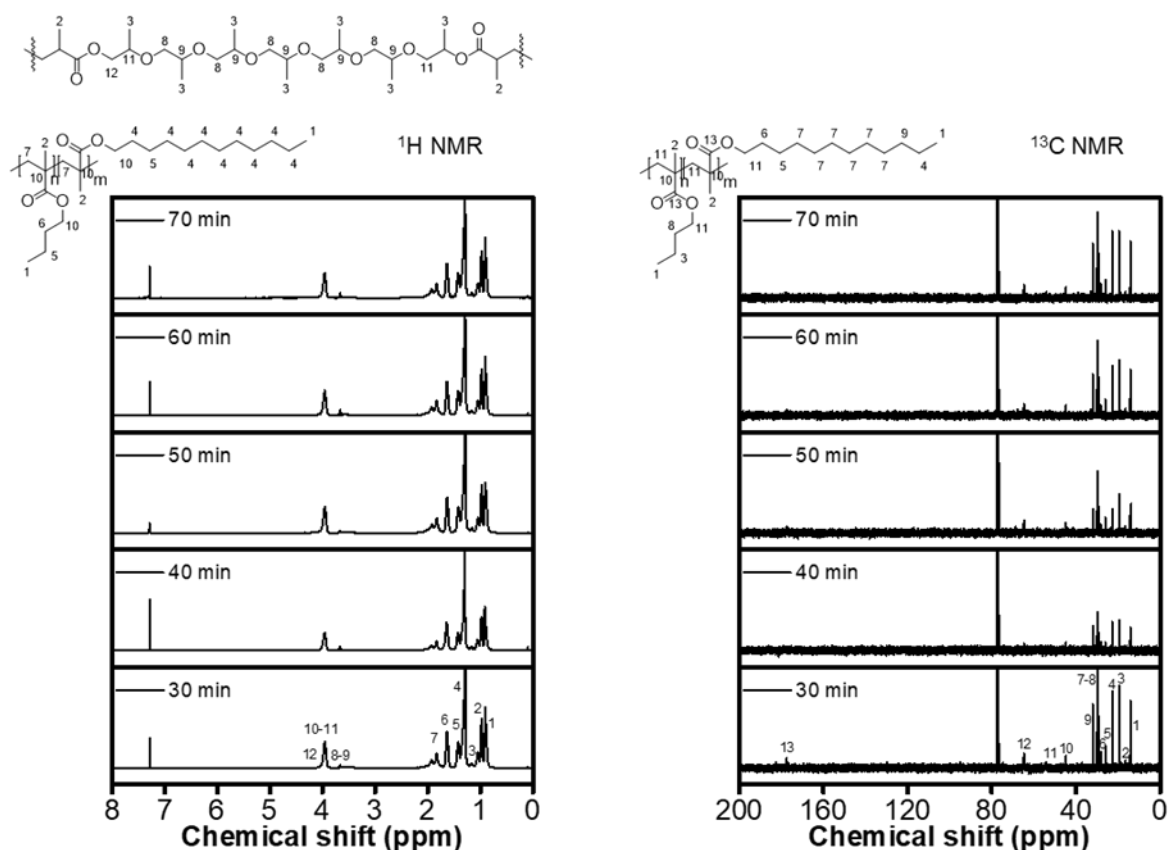


Figure 3.13 ^1H NMR and ^{13}C NMR spectra of gels irradiated for 30, 40, 50, 60, and 70 min. After photodegradation, polymers were precipitated in cold methanol and dried in an oven. The polymer was then dissolved in CDCl_3 . Both ^1H and ^{13}C NMR spectra of polymer solutions irradiated for different times did not change significantly. This is presumably because the number of functional groups introduced by UV cleavage reactions is very small relative to the number of repeating units. Thus, the spectra look like those of unirradiated poly(butyl methacrylate) and poly(lauryl methacrylate). The signals corresponding to the crosslinker (PPGMDA) could be detected only in the ^1H spectra. Copyright 2022, Wiley-VCH.

Toluene had the highest swelling factor (15.88 ± 0.37) but does not transmit UV light below 280 nm, whereas PDMS possesses a negligible UV absorbance but a very low swelling factor (1.02 ± 0.01). Interestingly, neither the toluene infused organogel nor the PDMS infused organogel showed significant photodegradation after 10 min irradiation time. In contrast, organogels infused with 1-butanol showed an even faster photodegradation than those infused with 1-nonanol, which we attributed to the lower UV absorbance of 1-butanol compared to 1-nonanol. In conclusion, an ideal solvent for the photodegradation of organogels can swell the organogel network strongly whilst

being transparent for UV light. If only one of these conditions was fulfilled, it could not compensate the other requirement, as shown by the incapability of organogels swollen in toluene or PDMS to degrade under UV light (Figure 3.9C). It is expected that all *n*-alcohols between 1-butanol and 1-nonanol (C₅-C₈) are suitable as solvents for the photodegradation of organogels due to their hydrophobicity, low UV absorbance, and high boiling point. For this study, 1-nonanol was preferable over 1-butanol due its higher boiling point, lower hazard potential, and more pleasant smell (Figure 3.14).

	1-butanol	1-nonanol
Hazard (GHS)		
	Danger	Attention
LD 50 (rat)	> 790 mg/kg	> 5000 mg/kg
Vapor pressure	0.5 kPa at 20 °C	0.17 kPa at 104 °C

Figure 3.14 Comparison of the safety hazards of 1-butanol and 1-nonanol. The low vapor pressure and low hazards of 1-nonanol eased handling of organogels. Copyright 2022, Wiley-VCH.

2.2.2.4 Investigation of slippery properties

To investigate the application of inherently photodegradable organogels as slippery lubricant infused porous (SLIP) materials, we investigated whether the wettability properties of bulk organogels infused with 1-nonanol could be altered via UV light irradiation (Table 3.3). For 30 s and 60 s of irradiation we could not detect an effect on the water contact angle hysteresis ($\Delta\theta$) before and after degradation outside the frame of errors. For 120 s of UV irradiation, $\Delta\theta$ decreased by 2.1 ° between the pristine and irradiated state, which could be attributed to a surface erosion induced release of 1-nonanol. For all irradiation times, a decrease in the advancing (θ_a) and receding (θ_r) water contact angles was observed. In conclusion, the organogels' slippery properties were slightly more pronounced after photodegradation, which we attributed to the formation of an excess layer of 1-nonanol serving as lubricant. The low contact angle hysteresis of water droplets

suggested that the critical sliding angle of 1-nonanol infused organogels should be low, which is a relevant property for substrates in microfluidics applications.

Table 3.3 Wettability of organogels before and after UV irradiation. Data is given as mean \pm SD (n=5). Copyright 2022, Wiley-VCH.

Before UV irradiation			UV exposure [s]	After UV irradiation		
θ_a [°]	θ_r [°]	$\Delta\theta$ [°]		θ_a [°]	θ_r [°]	$\Delta\theta$ [°]
49.1 \pm 2.2	45.4 \pm 0.8	3.9 \pm 0.8	30	45.7 \pm 0.8	43.9 \pm 1.1	3.1 \pm 1.2
49.7 \pm 1.1	44.6 \pm 0.7	6.5 \pm 1.0	60	46.6 \pm 0.9	40.0 \pm 0.7	7.7 \pm 0.7
50.6 \pm 1.4	44.6 \pm 0.7	7.7 \pm 0.5	120	47.2 \pm 1.8	41.6 \pm 0.7	5.6 \pm 0.8

2.2.2.5 Organogel-based photoresists

The transfer of light-induced structures onto substrates that are not photodegradable themselves is the key principle of photoresist technology. To date, no positive gel-based photoresists have been demonstrated, even though gels offer advantages over established procedures using linear polymers such as PMMA.²¹⁸ First, no designated step is required to remove irradiated polymer fragments from the copper surface using a solvent (“developer”), since the degraded organogel dissolves into the solvent released upon gel degradation. Second, the inherently photodegradable organogels can be removed with affordable UV lamps, whereas PMMA typically requires x-ray or electron beams to degrade efficiently.²¹⁸ To test the suitability of inherently photodegradable organogels as a photoresist, we coated a copper circuit board with a thin film of organogel (200 μm). The organogel film was then spatially degraded with UV light for 10 min using a photomask and immersed into 0.5 M aq. FeCl_3 solution for two hours. Unprotected copper was etched by the FeCl_3 , whereas copper covered by the organogel remained (Figure 3.15A).

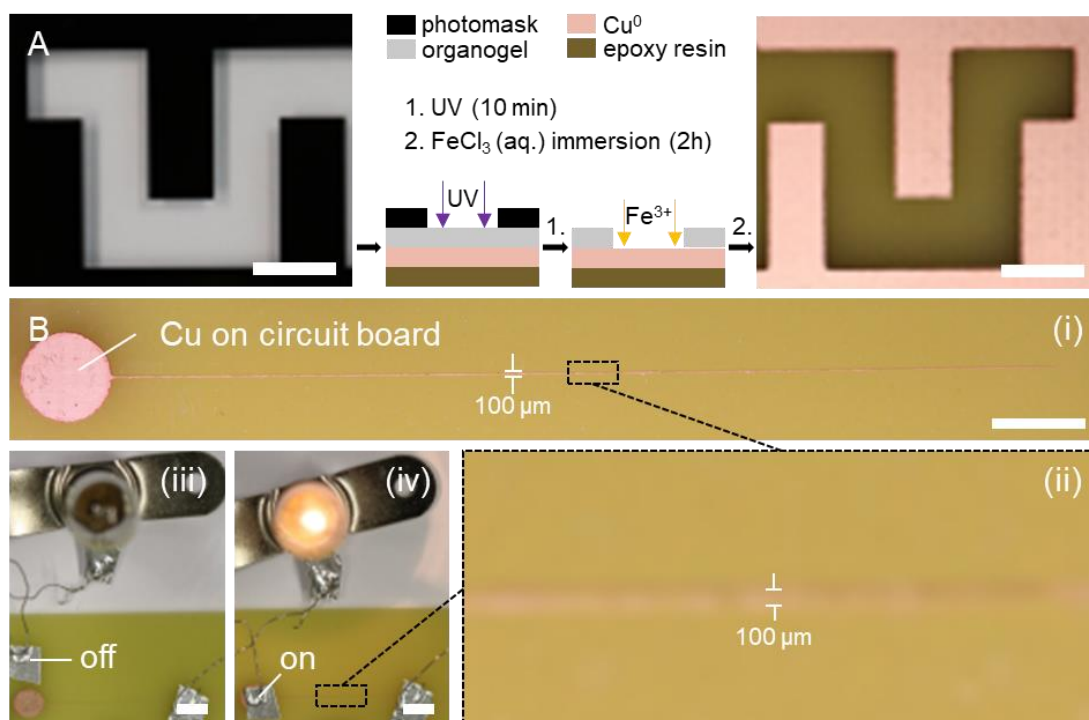


Figure 3.15 (A) Preparation of a copper pattern on an epoxy resin circuit board. (B) Image (i) and magnification (ii) of a thin ($100\ \mu\text{m}$) and long ($50\ \text{mm}$) Cu^0 stripe on a circuit board. The stripe conducted the electric current, as apparent by a light bulb turning on upon connecting a battery and a bulb along the copper stripe (iii, iv). Scalebars are $5\ \text{mm}$. Copyright 2022, Wiley-VCH.

To test whether thin conducting features can be obtained, we used a photomask with a slit length of $50\ \text{mm}$ and a slit width of $100\ \mu\text{m}$ together with the organogel photoresist. The respective copper pattern conducted the electric current (Figure 3.15B). This method could offer a cheap and simple alternative to fabricate circuit boards for labs and businesses without access to expensive x-ray and electron beam setups. Photopatterned organogels could further be used as stamps for contact printing. The resolution of the stamped patterns, however, was rather low due to the soft nature of the organogels (Figure 3.16).

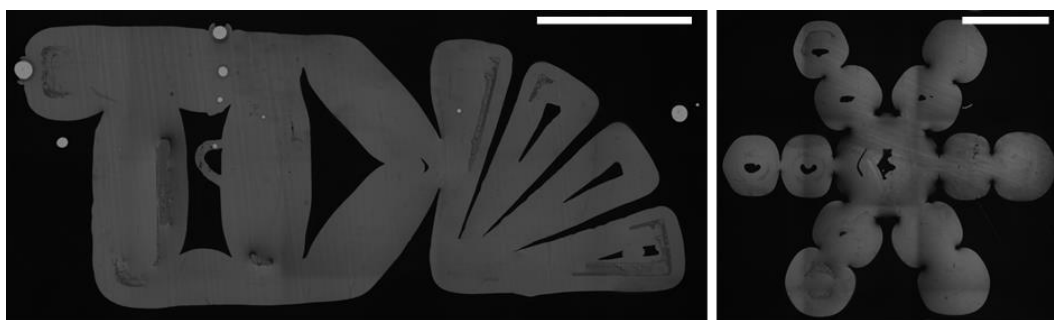


Figure 3.16 Microscopy images of surface patterns produced via organogel stamping. Structured organogel films were loaded with tetrabutylammonium fluoride (TBAF) and pressed on a surface coated with 1H,1H,2H,2H-trichloroperfluorooctylsilane (TCPOS), according to a procedure published recently.¹¹² The surface areas exposed to the TBAF loaded organogel were de-silanzed and turned hydrophilic, whereas the surrounding surface remained hydrophobic. Water could then be confined on the hydrophilic spots. Upon contact with water, the surfaces became transparent in the hydrophilic areas (bright), whereas the hydrophobic areas did not transmit light due to their high porosity (dark). Scale bars are 10 mm. Copyright 2022, Wiley-VCH.

2.2.3 Summary

Organogels with customized 3D or surface structure can improve the performance of organogels in applications such as oil-water separation, drug delivery, or as slippery-, anti-waxing, anti-bacterial or self-healing surfaces. In this chapter, inherently photodegradable poly(methacrylate) organogels offer a simple and versatile way to fabricate structured organogels without the need for additional photolabile crosslinks. The UV transmission and swelling ability of the infusing organic solvent were identified as the key factors influencing the photodegradability of organogels, which will presumably hold true for other photoresponsive or photoreactive organogels in the future. Moreover, the first ever use of a gel as a positive photoresist has been demonstrated, which is interesting for photolithographic fabrication processes in the electronics industry. Since the solvent (developer) for the polymer is already incorporated in the organogel network, the degraded polymer does not need to undergo a dissolution step but can be rinsed off immediately. Since organogels are hydrophobic soft-materials, inherently photodegradable organogels could serve as an alternative to the frequently used soft-lithography.

2.2.4 Experimental Details

2.2.4.1 Chemicals and materials

All chemicals were purchased from Merck (Darmstadt, Germany) and used as delivered. Inhibitors were removed from the monomer and crosslinker by filtration through basic alumina.

2.2.4.2 Characterization

ATR FT-IR (Attenuated total reflection Fourier transform infrared)

ATR FT-IR spectra were recorded with a Bruker Tensor 27 spectrometer from Bruker Optic (Ettlingen, Germany). A 45° geometry with a diamond crystal (single reflection) was used. As prepared organogels were pressed on the ATR crystal to ensure contact. Photodegraded organogels were precipitated in cold methanol and extracted by centrifugation for 5 min at 1000 rpm in a 15 mL Falcon tube. The precipitate was dissolved in THF and then drop casted onto a glass plate. THF was removed in an oven at 80 °C overnight. This was repeated several times until a thick polymer layer had formed on the glass. The polymer layer was then tightly pressed onto the ATR crystal.

GPC (Gel permeation chromatography)

Organogel pieces were photodegraded for 30, 50, 60, and 70 min. The resulting polymer solution was precipitated in cold methanol. The suspension was centrifuged for 5 min at 1000 rpm in a 15 mL Falcon Tube, and the precipitate was collected by filtration. The precipitate was dissolved in THF (ca. 2 mg mL⁻¹), filtered through 0.43 µm PTFE filters and injected in a Tosoh EcoSEC GPC system from Tosoh (Tokio, Japan) equipped with a SDV 5 µm bead size guard column (50 × 8 mm) followed by three SDV 5 µm columns (300 × 7.5 mm, subsequently 100, 1000, and 105 Å pore size, PSS), and a differential refractive index (DRI) detector. THF was used as eluent at 35 °C with a flow rate of 1.0 mL min⁻¹. The SEC system was calibrated using linear poly(methyl methacrylate) standards ranging from 800 to 1.82 × 10⁶ g mol⁻¹.

Microscopy

Images were recorded on a Keyence BZ 9000 from Keyence (Osaka, Japan).

NMR

^1H and ^{13}C NMR spectra were recorded on a 500 MHz spectrometer from Bruker (Rheinstetten, Germany) using CDCl_3 (99.8 atom% D) from Merck (Darmstadt, Germany) as a solvent. For the ^1H and ^{13}C spectrum 16 and 256 scans were collected, respectively. Data were analyzed using MestReNova 14.1.0 from Mestrelab Research S.L. (Santiago de Compostela, Spain).

Optical Profilometer

For profilometry measurements, a 3D-Profilometer VR-5200 from Keyence (Osaka, Japan) was used. Organogels were treated with chalk spray to generate a thin, non-transparent surface prior to the measurements.

Rheometry

Rheological measurements were carried out on an ARES G2 rotational rheometer from TA Instruments (obtained from Waters GmbH, Eschborn, Germany) equipped with a parallel plate Invar geometry (13 mm diameter) at a gap of 3 mm. Organogel discs were prepared using 2 mL precursor solution in a round 20 mL vial and were swelled in excess 1-nonanol for 48 h. An amplitude sweep was carried out to confirm that the measurements were performed within the linear viscoelastic regime. Oscillatory frequency sweeps were conducted at 25 °C with a constant strain of 1% in the frequency range of 100-0.1 rad s^{-1} .

UV lamp

Photodegradation experiments were performed using a UVA cube 2000 from Dr. Hönle AG (Gräfelfing, Germany) with 20 cm Hg bulbs and a power of 100 W cm^{-1} .

UV-Vis

Spectra were recorded with a PerkinElmer Lambda 35 UV/VIS spectrometer from PerkinElmer Ink. (Waltham, USA). Organogel films (125 μm) were measured on a quartz glass slide using air as background. Photodegraded organogels were diluted with acetonitrile and were measured in a quartz glass cuvette using acetonitrile (HPLC grade) as background.

Water contact angle

Measurements were performed with a DSA 25 contact angle goniometer from Krüss (Hamburg, Germany) using the sessile drop technique. Advancing contact angles were determined by measuring the contact angle while the droplet volume was increased from 5 μL to 15 μL at a rate of 0.2 $\mu\text{L s}^{-1}$. Receding contact angles were obtained in the reverse process. For tilting experiments,

the device was programmed to tilt the surface to 0-5° before depositing a droplet with a volume of 5 μ L. All experiments were repeated five times to form an average.

2.2.4.3 Synthesis of *net*-poly(LMA-*co*-BMA-*co*-PPGDM) organogel films and bulk materials

Precursor solutions were prepared from 2 mL (1.73 g) lauryl methacrylate (LMA), 2 mL (1.79 g) butyl methacrylate (BMA) and 8 mL (6.58 g) 1-nonanol or 1-butanol, respectively. As initiator, 40 mg of 2,2'-Azobis(2-methylpropionitril) (AIBN) and 110 mg of poly(propylene glycol) dimethacrylate (PPGDMA) crosslinker were added and the resulting mixture was warmed to ca. 30 °C and agitated to ensure quantitative dissolution of AIBN. The resulting polymerization solution was distributed into different reactions vessels. Reactions were carried out at 80 °C in an oven for 6h. Depending on the targeted shape of the organogel, the polymerization was carried out in 20 mL vials for disc shaped gels or in a Teflon mold covered with glass for cuboid gels. The largest organogel was prepared in a petridish (d = 5 cm) using 10 mL of organogel precursor solution. After swelling, the diameter increased to 7 cm. Organogel films were prepared by pipetting 200 μ L of organogel precursor solution in between polyimide spacers on a glass slide. The glass slide was then covered with another glass slide and they were clamped together.

2.2.4.4 Photolithography of organogels

Gels were placed onto a glass plate and (optionally) a chromium photomask (quartz glass) was placed on top of the organogel. The gels were then exposed to UV irradiation for defined times using a timer. The light intensity was kept constant and was monitored using a UVA and a UVC sensor from Dr. Hönle AG (Gräfelfing, Germany). After irradiation, organogels were briefly rinsed with water, methanol, or ethanol and then carefully blow dried to remove excess solvent.

2.2.4.5 Swelling properties

As prepared organogels were swelled in excess *n*-hexanes overnight. Excess liquid was removed by filtration. This was repeated three times. Then, *n*-hexanes was removed from the polymeric network by drying the organogel in a fume hood for 1 h and then in an oven at 80 °C overnight.

Organogels were then immersed into an excess of solvent for 48 h and their respective swelling constants were determined as *swelling constant* = $\frac{w_{swelled}}{w_{dry}}$.

2.3 Pampers to Paints and Pressure Sensitive Adhesives: Recycling of Superabsorbers via UV Degradation

2.3.1 Introduction

Nowadays, plastic products have become a necessity of human life. However, 76% of plastic products are discarded after single using, resulting in a huge waste of non-renewable petroleum resources.²¹⁹ At the same time, these waste plastics are seriously damaging the natural environment.²²⁰⁻²²² Recycling and reusing of waste plastic can not only reduce the pressure on environment, but also ensure an efficient use of the limited resources of petroleum.

In recent decades, various techniques for recycling plastic products have been developed.²²³⁻²²⁶ These recycling processes are generally grouped into the following four recycling types: primary recycling, secondary (melting) recycling, tertiary (chemical) recycling, and energy recovery.^{223,227} Primary recycling is a simple process but can only be applied to a small percentage of discarded plastics and the quality of recycled product is usually reduced.²²⁸⁻²³⁰ Melting recycling is suitable for linear polymer but cannot be used for cross-linked polymers.²³¹⁻²³³ Chemical recycling is applicable to a wide range of plastics, but usually requires more time and resources such as energy or chemicals.²³⁴⁻²³⁷ Energy recycling is the final strategy in the recycling of plastic products in which the polymer is irreversibly destroyed, potentially usually producing harmful gases and residues.²³⁸ Polymer networks made from superabsorbent sodium polyacrylate as used in disposable pampers and hygiene products are covalently cross-linked polymers that are hard to recycle by mechanical recycling since they do not melt but rather decompose at 300 °C.²³⁹ Most of the discarded superabsorbent products are directly landfilled or incinerated. In recent years, researchers turned their attention to such difficult-to-recycle polymers.²⁴⁰⁻²⁴⁴ For example, the recycled superabsorbent materials are directly used for soil moisturization.^{240,241} In 2021, McNeil and co-workers proposed a strategy for the tertiary (chemical) recycling of sodium polyacrylate pampers based on the acid or base catalyzed hydrolysis of ester bonds.²⁴⁴ The authors demonstrated the clean conversion of a sodium polyacrylate network into linear sodium polyacrylate followed by an esterification to quantitative conversion, which were useful as pressure sensitive adhesives. However, the initial step of hydrolysis required very long reaction times (16 h), the use of an acid

(H₂SO₄) or base (NaOH), and heating (80 °C). Inspired by this work and our previous experience with the UV photodegradation of poly(meth)acrylate hydrogels,¹⁷⁵ we hypothesized that the time, energy, and chemicals consuming process of hydrolysis could be replaced by a rapid UV photodegradation of the sodium polyacrylate networks in a swollen hydrogel state. Herein, we demonstrate the inherent rapid photodegradation of sodium polyacrylate hydrogels and their conversion into polybutylacrylate (PBA) and poly 2-ethylhexylacrylate (PEHA) for lackquers and as pressure sensitive adhesives (PSA). In our research, we take advantage of the inherent photodegradability of sodium polyacrylates in superabsorbent polymers, degrading cross-linked sodium polyacrylates to water-soluble linear polymers within minutes under UV irradiation. These degraded polymers can be directly used in waterborne pigment additives or further esterified to synthesize pressure sensitive adhesives. Synthesized esters have potential as removable and general-purpose pressure sensitive adhesives. The recycling and reuse of superabsorbent materials is an important contribution to reduce the pollution of the environment and a sustainable use of polymers.

2.3.2 Results and Discussion

2.3.2.1 Swelling and degradation of superabsorbent materials

In this study an UVAcube 2000 from Dr. Hönle AG (Gräfelfing, Germany) using a 2000 W Hg bulb was utilized for UV irradiation. The lamp was calibrated to 15.0 mW/cm² (use 1000W power) at 265 nm with the OAI 306 UV power meter. The light source at 265 nm (15.0 mW/cm²) was used for UV irradiation unless otherwise specified. The crosslinked sodium polyacrylate was extracted from commercially available pampers produced by Proctor and Gamble (P&G). From published patents it is known that these superabsorbent polymer are sodium poly(acrylate) crosslinked with ~0.05 mol% poly(ethylene glycol) diacrylate.²⁴⁵ Powdered poly acrylate superabsorber (PAS) transformed into a hydrogel infusing it with water, 100 times of its weight, i.e., resulting in a hydrogel consisting of 1 wt% PAS and 99 wt% water. After UV irradiation for only 5 min the solid hydrogel transformed into a clear solution due to the degradation of the crosslinked polymer network into a linear polymer (Figure 4.1A). Compared to the degradation via the hydrolysis of

superabsorbent polymers, the UV degradation process did not require additional reagents and shortens the degradation time from hours to minutes (Figure 4.1B).²⁴⁴ To monitor the degradation process, the changes in complex viscosity of the CSPA gel-solution after different UV degradation times were measured by rheometer. A substantial drop of 99.5 % of the complex viscosity from 84.5 ± 1.6 to 0.4 ± 0.0 Pa s was observed after 2 minutes of UV irradiation, at a frequency of 1 rad s^{-1} , and reached a value of $2.8 \pm 1.2 \times 10^{-2}$ Pa s after 5 min, which is very close to the complex viscosity of water (Figure 4.1C, Figure 4.2). This indicates that the degradation of the sodium polyacrylate hydrogel occurred rapidly in the first 2 minutes and was completely degraded to a linear polymer after only 5 minutes. The molecular weight of the degraded polymer chains could be controlled by the UV irradiation time. With increasing UV irradiation time, the molecular weight of the polymer chains continued to decrease as determined with water-based size exclusion chromatography (Figure 4.1D, Table 4.1). The hydrodynamic radius of polymer chain in aqueous solution decreased with the increase of UV irradiation time as determined with dynamic light scattering (Figure 4.1E). The determination of the hydrodynamic radius and the molecular weight demonstrate that UV irradiation can not only be used to rapidly de-crosslink or break the crosslinked PAS in but also that it can be used to alter the molecular properties of the linear sodium polyacrylate (NaPA) polymer.

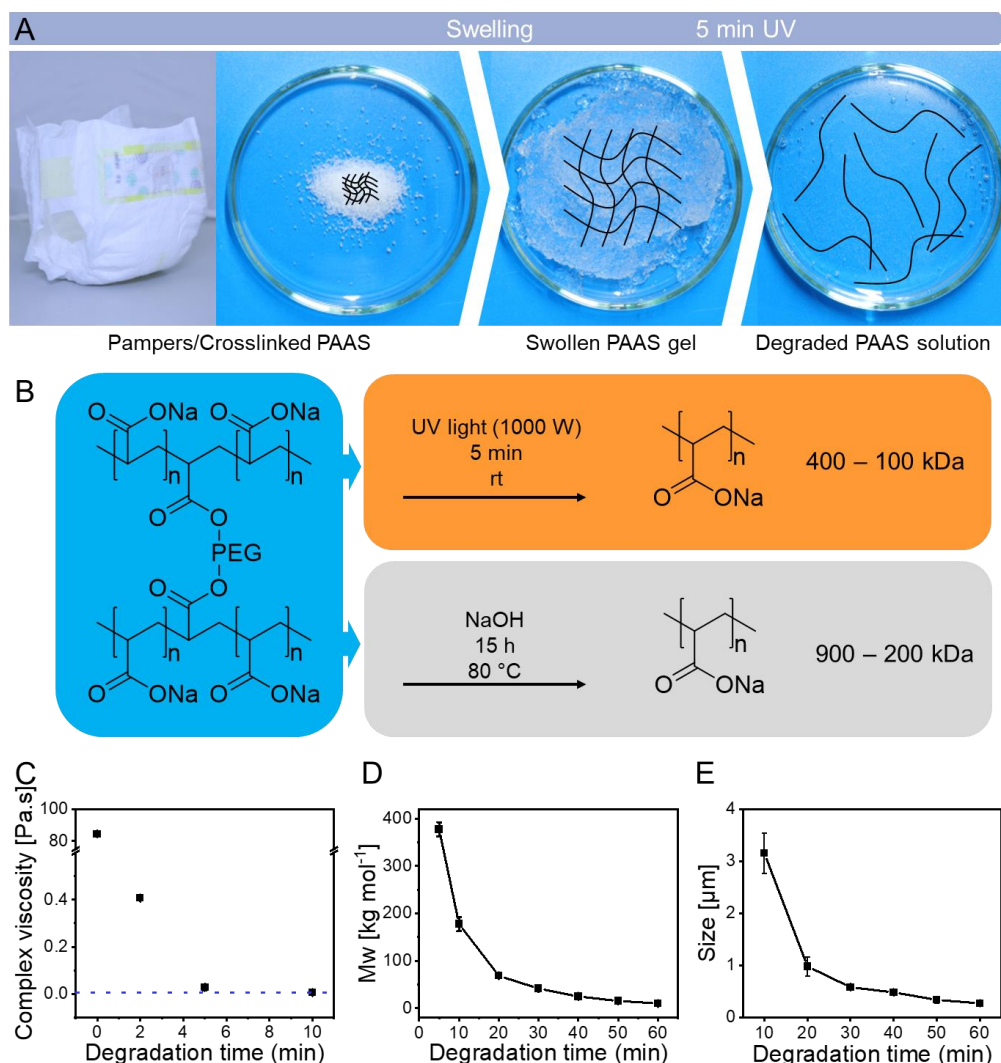


Figure 4.1 (A) Image of pampers and powdered superabsorbent cross-linked sodium polyacrylate (PAS), sodium polyacrylate hydrogel and degraded sodium polyacrylate solution after 5 min of UV photodegradation (15 mW cm^{-2}). The diameter of the petri dish is 5 cm. (B) Degradation process cross-linked sodium polyacrylate. Blue box: molecular structure of cross-linked sodium polyacrylate; Orange box: UV degradation process in this study; Grey box: hydrolysis degradation process in previous study.²⁴⁴ (C) Changes of the complex viscosity of PAS gel after different UV degradation times as determined by rheometry. Oscillatory frequency sweeps were conducted at 25°C with a constant strain of 2% at a frequency of 1 rad s^{-1} . Blue dotted line: The complex viscosity of water at 25°C ($8.9 \times 10^{-4} \text{ Pa}\cdot\text{s}$). (D) Weight average molecular weight (Mw) of NaPA after different UV photodegradation times as measured by SEC. (E) Hydrodynamic size of NaPA after different times UV photodegradation times as determined by dynamic light scattering (DLS).

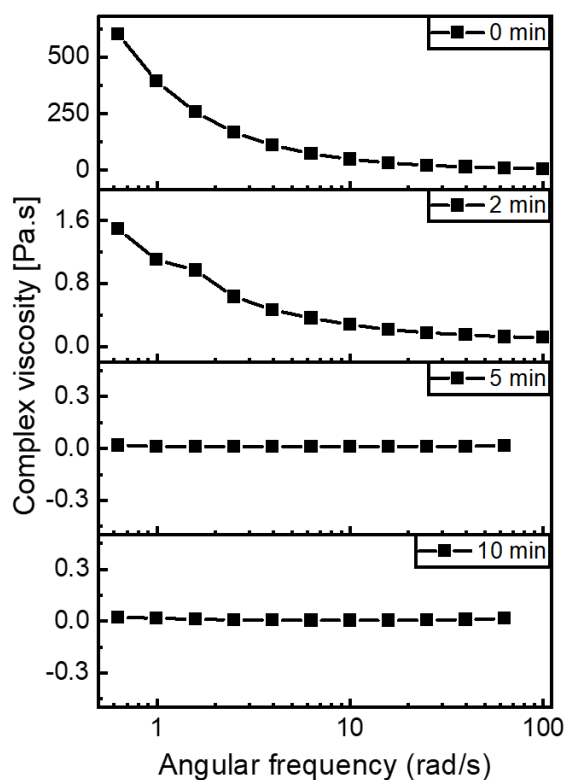


Figure 4.2 Complex viscosity change of PAS gel-solution after different UV degradation time measured by rheometer, oscillatory frequency sweeps were conducted at 25°C with a constant strain of 2% in the frequency range of 100-0.1 rad s⁻¹.

Table 4.1 GPC data of gels for different irradiation times.

Irradiation time [min]	M _N [kg mol ⁻¹]	M _w [kg mol ⁻¹]	Đ
5	90.3	362.6	4.0
10	58.2	192.9	3.3
20	14.8	71.3	4.8
30	9.3	41.0	4.4
40	5.6	25.5	4.6
50	3.5	15.4	4.4
60	2.9	10.2	3.5

2.3.2.2 Continuous preparation of photodegradation solution

The UV degradation of crosslinked PAS is a surface erosion process, i.e., the top layer will degrade first and turn from a gel to an aqueous solution. Since the degradation of the linear polymer chains continues in aqueous solution, this would lead to a gradient in the degree of degradation from the top to the bottom of the PAS hydrogel. To compensate for influence of the depth of light penetration and to ensure the use of the minimum dosage of UV light, the degradation was conducted in a Buchner filter equipped with a cellulose filter (Figure 4.3A). The thickness of the gel in device is ~5mm unless otherwise specified. The degraded polymer solution can flow into a collection flask and is protected from further degradation while the gel is held back from the cellulose filter and the Buchner filter. The aqueous solution from the degraded PAS hydrogel was collected and dried by rotary evaporation at 60 °C (4 h) to obtain linear sodium polyacrylate as a solid, which was then ground into a powder. In our previous studies, we found that the rate of degradation of the cross-linked poly(meth)acrylate network was closely related to its degree of swelling.^{175,246} Here, the degradation efficiency of crosslinked PAS superabsorbent polymers with different degrees of swelling were evaluated. The degradation-time curves were calculated by the weight of the obtained degradation solution at different time points. Cross-linked PAS extracted from Pampers (Figure 4.3B, D) and as purchased from Sigma-Aldrich (Figure 4.3C, E) were compared. In agreement with our previous findings, the rate of degradation decreased significantly with an increasing polymer mass fraction in the gel. Gels with a polymer mass fraction of 0.5 wt.% gels were degraded within 4-5 minutes while 2 wt.% gels took 14-18 minutes to be completely degraded (Figure 4.3B, C). At the same time, the molecular weight of polymer degradation products from high polymer mass fractions were slightly larger than from low polymer mass fractions (Figure 4.3D, E). It indicated that the UV-induced degradation rate of superabsorbent crosslinked PAS is also affected by the swelling degree, degradation rate of the polymer network is faster while the swelling degree is higher. 1 wt.% PAS from Sigma-Aldrich was used in subsequent experiments due to the uncertainty about potential additives in commercial Pampers, the possible contamination of the PAS with cellulose fibers, and for the purpose of convenience.

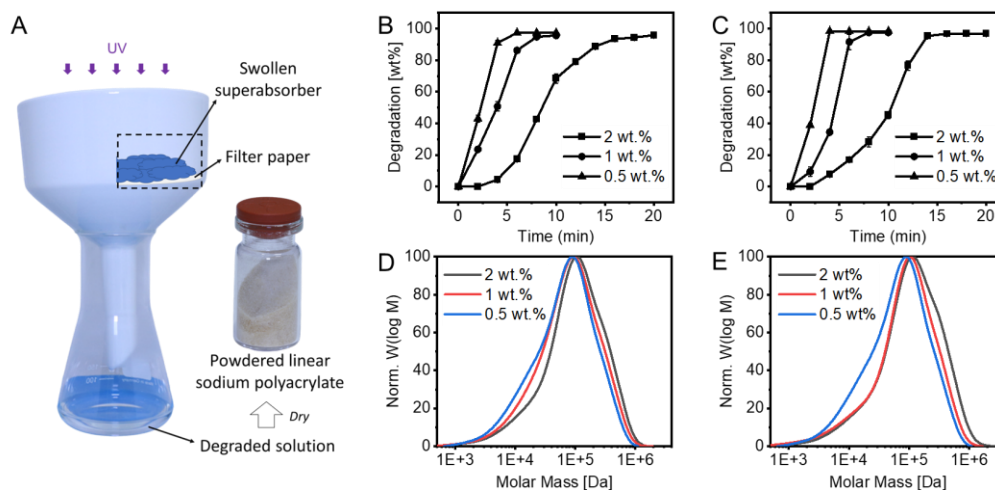


Figure 4.3 (A) Schematic diagram of rapid and continuous preparation of PAS hydrogel photodegradation solution in Buchner funnel. (B), (C) Kinetics of photodegradation as quantified by the mass percentage of the NaPA photodegradation product for different swelling ratios. (D), (E) Molecular weight of degraded NaPA as determined by with aqueous gel permeation chromatography (GPC), UV degradation time of 2 wt.%, 1 wt.% and 0.5 wt.% samples are 20 min, 10 min and 5 min, respectively. (B, D: cross-linked PAS from P&G pampers; C, E: cross-linked PAS from Sigma-Aldrich. 2 wt.%, 1 wt.%, 0.5 wt.%; mass percentage of cross-linked PAS in swollen gel.)

2.3.2.3 Characterization of soluble NaPA

The process of degradation was investigated with $^1\text{H-NMR}$ and $^{13}\text{C-NMR}$ in D_2O (Figure 4.4A, B). In the cross-linked PAS, peaks of hydrogens on the main chain of PAS were very broad in the $^1\text{H-NMR}$ spectrum. Hydrogen peaks of the methylene and methine groups on the backbone became fairly sharp after 10 min UV irradiation (Figure 4.4A). At the same time, peaks of the methine carbon were visible in the $^{13}\text{C-NMR}$ spectrum of the starting crosslinked PAS, whereas no peaks of methylene and carbonyl carbons could be observed. Peaks of methylene carbon and carbonyl carbon appeared in the degradation products, and the peak of methine carbon became more pronounced (Figure 4.4B). The cross-linking distorted the relaxation of the polymer chains, $^1\text{H-NMR}$ and $^{13}\text{C-NMR}$ results indicated that UV irradiation degraded the cross-linked PAS to a linear soluble polymer. In the ATR-IR spectra, no significant difference between NaPA before and after UV degradation could be observed, indicating that 10 minutes of UV initiation did not cause

excessive photooxidation (Figure 4.4C). However, the formation of species absorbing UV light ($\lambda_{\text{max}} = 275 \text{ nm}$) is detectable already after 10 min UV-vis spectroscopy (Figure 4.4D). The UV absorbance increased with increasing UV degradation time and increasingly absorbs blue light, causing a macroscopic faint yellow color. Yellowing is indicative for the formation of oxydized moieties, such as aldehydes, ketones, or more. The mechanism of photodegradation of PAS is thus likely to involve known photooxidative pathways, namely the formation of peroxy radicals (R-O-O•), hydroperoxyls (R-O-OH), oxyl radicals (R-O•), and peroxides (R-O-O-R).²⁴⁷

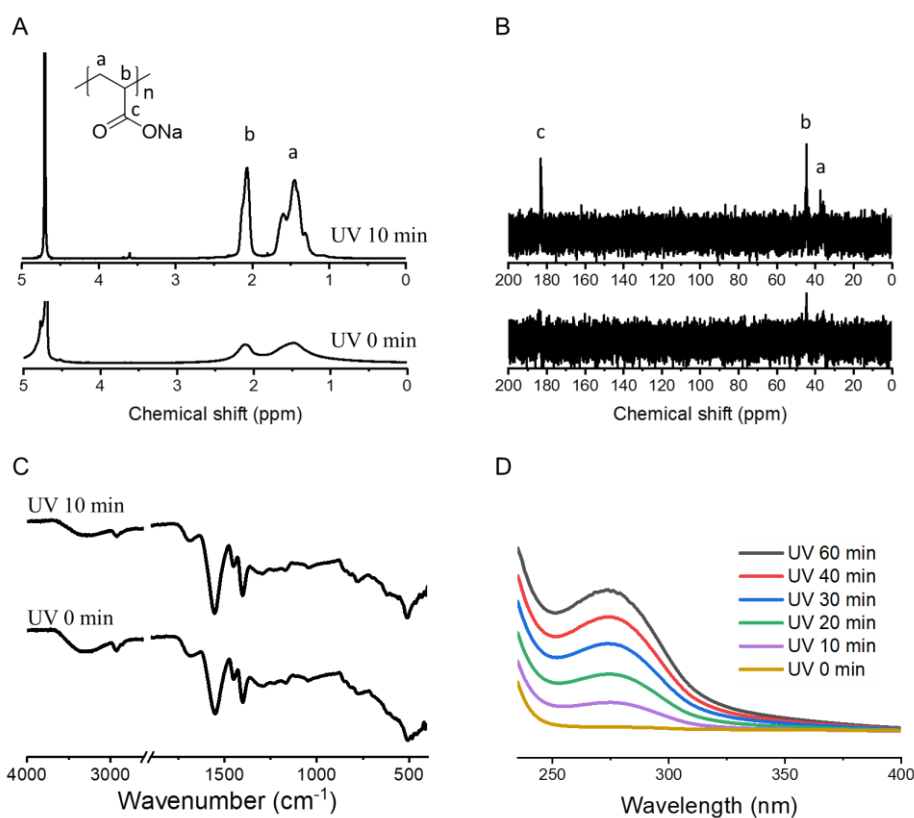


Figure 4.4 (A, B) ^1H NMR and ^{13}C NMR spectra of crosslinked PAS before and after UV irradiation for 10 min. The polymer was dissolved in D_2O . (C) ATR FT-IR spectrum of cross-linked PAS and 10 min's UV degraded PAS. (D) UV-vis spectra of a PAS gel (solution) after different UV degradation time. Concentration of PAS in water is 10 mg mL^{-1} (~1 wt.%).

2.3.2.4 Esterification of NaPA

To demonstrate that UV photodegraded PAS gels are suitable as a resource for applications as laquers and as pressure sensitive adhesives, photodegraded sodium polyacrylate (NaPA) was

esterified with *n*-butanol and 2-ethylhexanol. Inexpensive alcohols are commonly used in the chemical industry to convert acrylic acid to the respective acrylates.²⁴⁸ Here, *n*-butanol and 2-ethylhexanol, were used to esterify the photodegraded NaPA (Figure 4.5A). The synthesis procedures followed the procedure as described by McNeil et al,²⁴⁴ and here added excess sulfuric acid (1.00 instead of 0.25 equivalent) to acidify sodium polyacrylate. ¹H-NMR and ¹³C-NMR measurements confirmed the successful synthesis of both poly butyl acrylate (PBA) and 2-ethylhexyl polyacrylate (PEHA) (Figure 4.5B, C). The peak integral ratio between peak b and peak c in the ¹H NMR spectrum of methine and methylene hydrogen on the main chain is 1 to 2, indicating an efficiency of esterification close to 100%. In the ATR FT-IR spectrum, peak of methyl and methylene appeared at 2865 cm⁻¹, 2964 cm⁻¹, peak of C-O-C appeared at 1162 cm⁻¹, further confirmed the successful synthesis of PBA and PEHA (Figure 4.5D). At the same time, the peak of the carbonyl group in the products at 1560 cm⁻¹ completely disappeared and reappeared at 1730 cm⁻¹ indicated that all carboxylates were converted to esters. The molecular weight of NaPA increased from 140 kg mol⁻¹ to 220 kg mol⁻¹ (PBA) and to 180 kg mol⁻¹ (PEHA), respectively (Figure 4.5E). The isolated yields of PBA and PEHA were 78.7% and 86.4%, respectively.

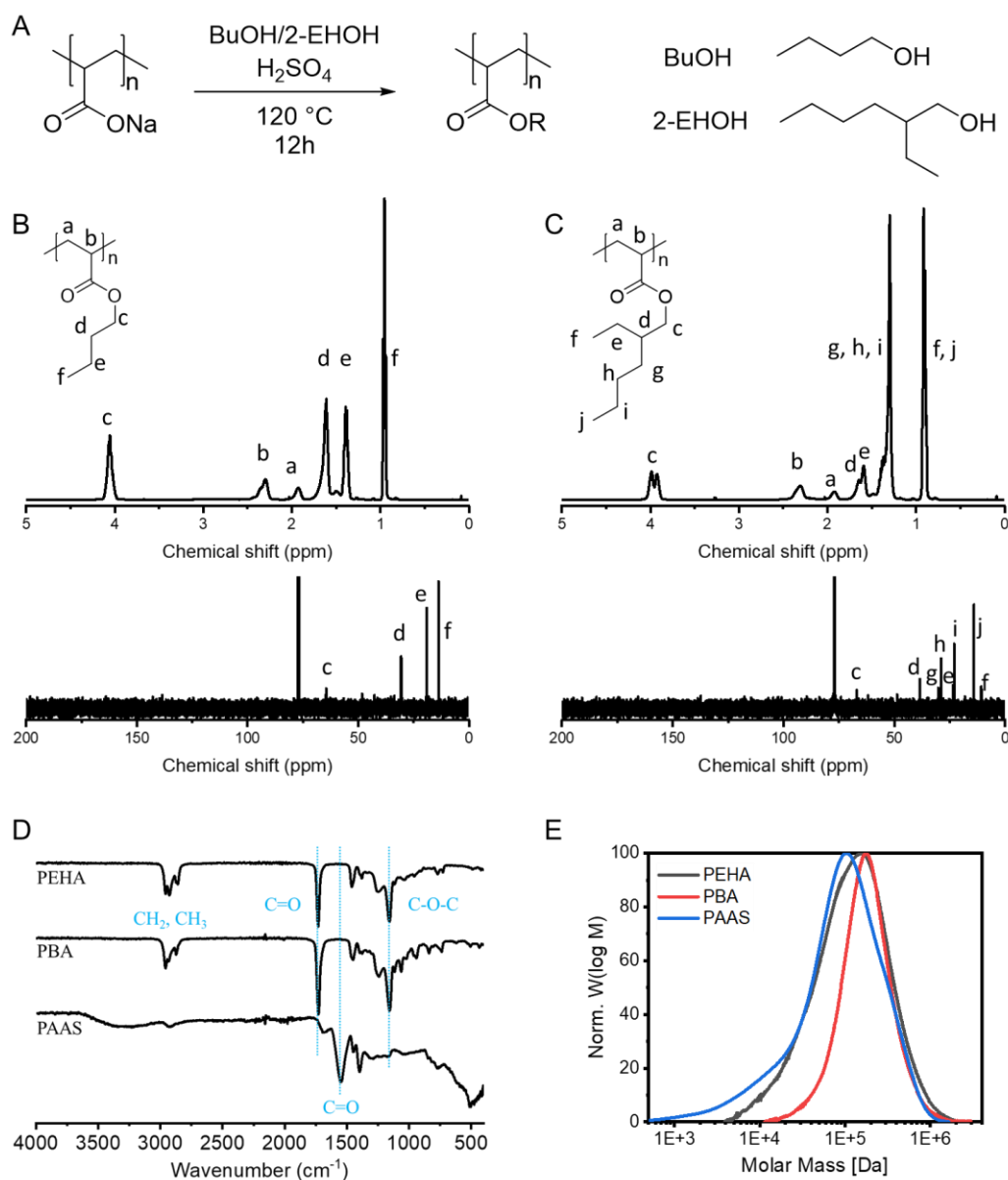


Figure 4.5 (A) Reaction equation of the esterification of degraded NaPA with *n*-butanol and 2-ethylhexanol. B, C) $^1\text{H NMR}$ and $^{13}\text{C NMR}$ spectra of poly butyl acrylate (PBA) and poly 2-ethylhexyl acrylate (PEHA) in CDCl_3 . (D) ATR FT-IR spectrum of 10 min's UV degraded NaPA and the esterification products PBA, PEHA. (E) Molecular weight of 10 min's UV degraded NaPA measured by aqueous gel permeation chromatography and esterification product PBA, PEHA measured by tetrahydrofuran gel permeation chromatography.

2.3.2.5 Application of NaPA, PBA and PEHA

Linear sodium polyacrylate (NaPA) is commercially used as a thickener for food or aqueous paints, and as water-retention agent for paints. Through UV degradation, linear NaPA free of other

chemicals could be obtained from crosslinked superabsorbent PAS. Recycled linear NaPA could be used directly as paint thickeners. The viscosity of methylene blue aqueous solution with and without degraded linear NaPA were measured by rheology (Figure 4.6A). After adding linear NaPA to the aqueous paint solution consisting of methylene blue in water, the viscosity of the solution increased significantly. Digital photographs and optical microscope images showed that the paints with NaPA paint exhibit a higher gloss and could form a stable film on surface of the paper instead of being soaked into it (Figure 4.6B). PBA and PEHA obtained by esterification have potential as pressure-sensitive adhesives. Here, the storage and loss moduli of PBA and PEHA were determined via rheology (Figure 4.6C, D). Chang's viscoelastic window (VW) was used to evaluate their performance as pressure-sensitive adhesives (Figure 4.6E). To determine Chang's viscoelastic window, the storage (G') and loss (G'') moduli must be determined at the bonding and debonding frequencies of 0.01 and 100 rad s^{-1} , respectively. The VW of PSA is defined by these four moduli. In Chang's VW, the existing pressure sensitive adhesives were divided into five categories, high modulus-low loss classic adhesive (quadrant 1), high modulus-high loss high shear PSA (quadrant 2), low modulus-low loss removable PSA (quadrant 3), low modulus-high loss cold temperature PSA (quadrant 4) and medium modulus-medium loss general purpose PSA (central).²⁴⁹ Molecular weight of PBA and PEHA used here were 220 kg mol^{-1} and 180 kg mol^{-1} , they were low molecular weight pressure sensitive adhesive. The storage modulus and loss modulus of PBA were located between 10^3 and 10^5 Pa, indicating that it could be used as removable and general-purpose PSA. This is also illustrated by the fact that PBA mainly fell within the central area and 3 quadrants in VW. The storage modulus and loss modulus of PEHA at low frequency were too low, indicating that it would flow easily when standing still and tended to residue when peeled off. This might affect its use in some application scenarios, but could still be used as removable PSA. It mainly fell within in the 3 quadrants in VW and went beyond the lowest modulus range of the 3 quadrants also indicated that its application was restricted. This limitation could be improved by increasing the molecular weight of degraded NaPA.

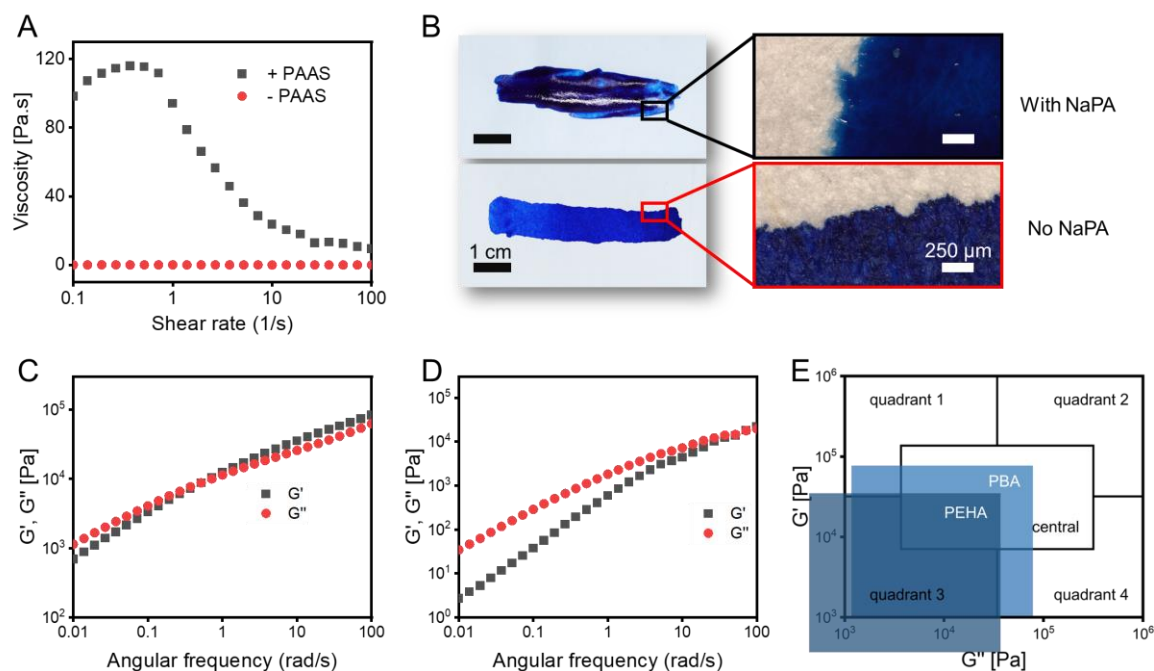


Figure 4.6 (A) Viscosity of methylene blue aqueous solution (10 mg mL^{-1}) with and without degraded NaPA (0.5 g mL^{-1}) measured by rheometer, sweeps were conducted at 25°C . (B) Drawings on paper using an aqueous solution of methylene blue with and without degraded NaPA. (C, D) Storage and loss modulus of PBA and PEHA measured by rheometer. Frequency sweeps were conducted at 25°C with a constant strain of 1% in frequency of 1 rad s^{-1} . (E) Plots of storage (G') versus loss (G'') moduli for PBA and PEHA, including visualization of Chang's viscoelastic window.

2.3.3 Summary

A rapid approach to recycle crosslinked sodium polyacrylate is presented. The recycling process is based on the inherent UV induced degradability of sodium polyacrylate, which thus does not require additional chemical reagents during the whole process and recycle rate is close to 100%. The recycled linear sodium polyacrylate can be used directly as a thickener for aqueous paints and can be esterified for applications as a pressure sensitive adhesive. The esterification process uses common industrial methods, which is also simple and efficient. PBA and PEHA synthesized from recycled NaPA have potential as removable and general-purpose pressure sensitive adhesives. The

recycling and reuse of superabsorbent materials is of great significance for reducing environmental pollution and sustainable development.

2.3.4 Experimental Details

2.3.4.1 Chemicals and materials

The superabsorbent polymer obtained from commercial pampers (P&G) is a sodium poly(acrylate) crosslinked via $\sim 0.05\text{mol}\%$ poly(ethylene glycol) diacrylate co-monomer.²⁴⁵ Another superabsorbent polymer is a sodium poly(acrylate) partly crosslinked via poly(ethylene oxide) purchased from Sigma-Aldrich. Isopropanol, ethanol and acetone were obtained from Merck (Darmstadt, Germany). All other chemicals were purchased from Sigma-Aldrich (Darmstadt, Germany) and used without further purification. PTFE plates, PP plates and aluminum plates were purchased from RS Components GmbH (Frankfurt, Germany) and were cut to the desired size for use. NEXTERION B glass slides were obtained from Schott AG (Mainz, Germany).

2.3.4.2 Characterization

UV lamps

In this study an UVAcube 2000 from Dr. Hönle AG (Gräfelfing, Germany) using a 2000 W Hg bulb was utilized for UV irradiation. The lamp was calibrated to 15 mW cm^{-2} at 260 nm with the OAI 306 UV power meter. The light source at 260 nm (15 mW cm^{-2}) was used for UV irradiation unless otherwise specified.

Aqueous size-exclusion chromatography (SEC)

SEC measurements were performed on a SECcurity GPC System - Polymer Standards Service GmbH, Mainz - Agilent Technologies 1260 Infinity, comprising an autosampler, a Suprema $5\text{ }\mu\text{m}$ bead-size guard column (8 x 50 mm, PSS) followed by two Suprema $5\text{ }\mu\text{m}$ columns (8 x 300 mm, subsequently mixed-bed S and mixed-bed M, PSS), and a differential refractive index (RI) detector and a UV detector. The measurements were performed using disodium hydrogen phosphate 0.07M in water as the eluent at room temperature with a flow rate of $1\text{ mL}\cdot\text{min}^{-1}$. The SEC system was

calibrated using linear poly(acrylic acid) sodium salt standards (PSS) ranging from 1250 g·mol⁻¹ to 1 484 000 g·mol⁻¹

Size exclusion chromatography (SEC)

SEC measurements were performed on a TOSOH Eco-SEC HLC-8320 GPC System, comprising an autosampler, a SDV 5 µm bead-size guard column (50 × 8 mm, PSS) followed by three SDV 5 µm columns (300 × 7.5 mm, subsequently 100 Å, 1000 Å and 105 Å pore size, PSS), a differential refractive index (RI) detector using tetrahydrofuran (THF) as the eluent at 35 °C with a flow rate of 1 mL·min⁻¹.

The SEC system was calibrated using linear polymethylmethacrylate standards (PSS) ranging from 800 to 1.82·10⁶ g·mol⁻¹.

Rheometry

Rheological measurements were carried out on an ARES G2 rotational rheometer from TA Instruments (obtained from Waters GmbH, Eschborn, Germany) equipped with a parallel plate Invar geometry (13 mm diameter) at a gap of 3 mm.

Dynamic light scattering (DLS)

DLS measurements were conducted using a Zetasizer Nano ZS from Malvern (Kassel, Germany).

UV–vis spectroscopy

UV–vis spectroscopy was performed with an Infinite M200 Pro (Tecan Trading AG, Switzerland) plate reader.

NMR

NMR spectra were recorded on a Bruker Avance III 400 MHz spectrometer from Bruker (Karlsruhe, Germany).

Attenuated total reflection infrared spectroscopy (ATR-IR)

All IR measurements were performed on a Bruker Alpha II ATR-IR from 400–4000 cm⁻¹ at 25 °C.

Microscopy

Images were recorded on a Keyence AHX7000 from Keyence (Osaka, Japan).

Digital photography

Digital photos were taken using a Canon EOS 80D digital camera.

3 Conclusions and Outlook

This PhD thesis described three projects aimed at utilizing UV light to pattern surfaces, to structure bulk gels, and to recycle superabsorbers, i.e., (1) the photopatterning of polydopamine based surfaces, (2) the photodegradation and photopatterning of poly(meth)acrylate gels and gel films, and (3) the recycling of superabsorbers into soluble sodium polyacrylate, poly butyl acrylate, or poly 2-ethylhexyl acrylate.

In (1) the advantages of polydopamine coating were combined with those of silane chemistry and thiol-ene click chemistry, resulting in a substrate-independent and reversible surface patterning strategy. In the first part, a rapid, facile and substrate-independent strategy for reversible surface modification and patterning was developed. The strategy was consisted of three steps: a polydopamine coating, the functionalization of the polydopamine coating using trichlorovinylsilane, and the UV-induced modification or patterning of the vinylsiloxane functionalized polydopamine coating using a thiol-ene reaction. This method was extended to a variety of substrates, including polytetrafluoroethylene, polypropylene, polyethylene, aluminum, and glass. No pre-processing steps were required for any of the substrates. Through reversible silanization and desilanization, followed by thiol-ene click reaction, new patterns can be created repeatedly on the same surface, enabling the reuse of the substrate. Due to the universal applicability of polydopamine coatings, the developed strategy can be used to pattern objects with complex surfaces, such as plant leaves, toys, and soft tapes. This substrate-independent reversible surface patterning strategy has important implications for the development of novel functional materials and devices.

The focus of (2) is the UV photodegradation of poly(meth)acrylates to pattern poly(meth)acrylate organogels. Based on the inherent UV photodegradability of poly(meth)acrylates, a strategy was developed to rapidly pattern poly(meth)acrylate organogels without additional photosensitizers. The UV transmission and the swelling ability of the organic solvents infusing the organogel were identified as key factors affecting the photodegradability of the organogels, which is likely to be applicable to other light-responsive or photoreactive organogels in the future. In addition, the use of organogels as positive photoresist to manufacture copper circuit patterns is of great interest for

electronic industry manufacturing. Since the gel directly becomes a liquid polymer solution after the photodegradation, no dissolving step is required, and the polymer can be rinsed off conveniently. The developed technique to photodegrade organogels is a potential alternative to soft lithography. Finally, based on the inherent UV photodegradation of polyacrylates, a rapid and efficient strategy to recycle linear sodium polyacrylate from waste superabsorbent materials such as diapers was developed (3). No additional reagent was necessary for the recycling based on UV photodegradation, and the conversion of crosslinked sodium polyacrylate to linear sodium polyacrylate is close to 100%. Recycled linear sodium polyacrylate could be used as a thickener for water-based paints or can be esterified with *n*-butanol and 2-ethylhexanol to obtain poly butyl acrylate and poly 2-ethylhexyl acrylate for applications as pressure-sensitive adhesives. The esterification of linear sodium polyacrylate was conducted following procedures used in the chemical industry, which ensured the scalability of the strategy to recycle superabsorbers. The recycling of superabsorbent materials is of great significance for reducing environmental pollution and sustainable development.

However, there are still some meaningful research directions that can be further explored in these projects.

- (1) Polydopamine plays an important role in strategy due to its simple versatility. However, polydopamine coating is generally considered to be bonded physically to the surface of the substrate, resulting in a lower mechanical strength of the polydopamine coating than that of chemically bound coatings.²⁵⁰ Improving the mechanical strength of polydopamine on the surface of many substrates is a direction that can be further explored and improved in this project.
- (2) The use of UV-degradable poly(meth)acrylate as photoresist is an application with a large scope of applications in the electronics industry. However, so far organogels with only one component was studied in our project, poly(BMA-*co*-LMA-*co*-PPGDMA) organogel from lauryl methacrylate (LMA) and butyl methacrylate (BMA) monomer with poly(propylene glycol) dimethacrylate (PPGDMA) as crosslinker. The UV-induced degradation and patterning of poly(meth)acrylate organogels with a wider range of components need to be further explored and understood.

(3) Recycling and reusing waste polymers and functionalized materials not only maintains sustainable economic development, but also reduces environmental pollution. Based on the inherent UV photodegradation of polyacrylate gels, a strategy to rapidly obtain soluble sodium polyacrylate from waste superabsorbent materials was presented here. However, in the recycling process, the superabsorbent material needs to be swollen to a high degree. Isolating dilute aqueous solutions of sodium polyacrylate from water requires a lot of energy. Optimizing the degradation processes in terms of the demand for water and energy would be interesting for commercializing this strategy.

4 Appendix

4.1 Abbreviations

°C	degree celsius
AFM	atomic force microscopy
AIBN	2,2'-Azobis(2-methylpropionitril)
Al	aluminum
BMA	butyl methacrylate
CA	contact angle
CDCl ₃	chloroform, deuterated
δ	chemical shift
DCM	dichlormethane
DHI	3,4-dihydroxyindole
D ₂ O	deuterium oxide
DoG	Difference of Gaussian
DLS	dynamic light scattering
DMA	droplet microarray
eq.	equivalents
GPC	gel permeation chromatography
h	hour
Hz	hertz
IR	infrared
LMA	lauryl methacrylate
ME	2-mercaptoethanol
min	minutes
MNPs	metal nanoparticles
M _N	number-average Molecular Weight
M _w	weight average molecular weight

NaPA	sodium polyacrylate
nm	nanometer
NMR	nuclear magnetic resonance
PAS	polyacrylate superabsorber
PBA	poly butyl acrylate
PDA	polydopamine
PDMS	poly(dimethylsiloxane)
PE	polyethylene
PEG	poly(ethylene glycol)
PFDT	1H,1H,2H,2H-perfluorodecanethiol
PEHA	2-ethylhexyl polyacrylate
PMMA	polymethylmethacrylate
PP	polypropylene
PPGDMA	poly(propylene) glycol dimethacrylate
PTFE	polytetrafluoroethylene
rt	room temperature
SAMs	self-assembled monolayers
SEM	scanning electron microscope
SLIPS	slippery liquid-infused porous surfaces
TBAF	tetrabutylammonium fluoride
TCPOS	1H,1H,2H,2H-trichloroperfluorooctylsilane
THF	tetrahydrofuran
ToF-SIMS	time-of-flight secondary ion mass spectrometry
TVS	trichlorovinylsilane
UV	ultraviolet
μCP	microcontact printing
μm	micrometer
VW	viscoelastic window
XPS	X-ray photoelectron spectroscopy

4.2 Curriculum Vitae

Personal data

Name	Shuai Li
Date of birth	1993.10
Place of birth	Sichuan, China

Education

09.2018-present	PhD studies Karlsruhe Institute of Technology (KIT), Germany Institute of Biological and Chemical Systems-Functional Molecular Systems (IBCS-FMS) Supervisor: Prof. Dr. Pavel A. Levkin Research topic: Photo-induced surface modification and material recycle
09.2015-06.2018	Master studies Sichuan University (SCU), China Department of Polymer Science and Engineering Supervisor: Prof. Xianglin Luo Research topic: Anti-cancer drug delivery system
09.2011-06.2015	Bachelor studies Sichuan University (SCU), China Department of Polymer Science and Engineering
09.2008-06.2011	Secondary school Mianyang Nanshan Middle School, China

4.3 Publications

1. **Li, S.**, Scheiger, J. M., Wang, Z., Dong, Z., Welle, A., Trouillet, V., & Levkin, P. A. (2021). Substrate-Independent and Re-Writable Surface Patterning by Combining Polydopamine Coatings, Silanization, and Thiol-Ene Reaction. *Advanced Functional Materials*, 31(50), 2107716.
2. Scheiger, J. M.[#], **Li, S.**[#], Brehm, M., Bartschat, A., Theato, P., & Levkin, P. A. (2021). Inherently UV Photodegradable Poly (methacrylate) Gels. *Advanced Functional Materials*, 31(49), 2105681.
3. **Li, S.**, Scheiger, J. M., Wang, Z., & Levkin, P. A. Pampers to paints and pressure sensitive adhesives: Recycling of superabsorbers via UV degradation. (In preparation)
4. Behboodi-Sadabad, F., **Li, S.**, Lei, W., Liu, Y., Sommer, T., Friederich, P., ... & Levkin, P. A. (2021). High-throughput screening of multifunctional nanocoatings based on combinations of polyphenols and catecholamines. *Materials Today Bio*, 10, 100108.
5. Wang, Z., Cui, H., **Li, S.**, Feng, X., Aghassi-Hagmann, J., Azizian, S., & Levkin, P. A. (2021). Facile approach to conductive polymer microelectrodes for flexible electronics. *ACS Applied Materials & Interfaces*, 13(18), 21661-21668.

References

- ¹ Sun, T. *et al.*, Reversible Switching between Superhydrophilicity and Superhydrophobicity. *Angewandte Chemie International Edition* **43** 357 (2004).
- ² Seo, J., Lee, S., Lee, J. & Lee, T., Guided Transport of Water Droplets on Superhydrophobic – Hydrophilic Patterned Si Nanowires. *ACS APPL MATER INTER* **3** 4722 (2011).
- ³ Lee, S., Yim, C., Kim, W. & Jeon, S., Magnetorheological Elastomer Films with Tunable Wetting and Adhesion Properties. *ACS APPL MATER INTER* **7** 19853 (2015).
- ⁴ Wong, T. *et al.*, Bioinspired self-repairing slippery surfaces with pressure-stable omniphobicity. *NATURE* **477** 443 (2011).
- ⁵ Liu, J. *et al.*, Guided Self-Propelled Leaping of Droplets on a Micro-Anisotropic Superhydrophobic Surface. *Angewandte Chemie International Edition* **55** 4265 (2016).
- ⁶ Liu, H. *et al.*, Bioinspired surfaces with superamphiphobic properties: concepts, synthesis, and applications. *ADV FUNCT MATER* **28** 1707415 (2018).
- ⁷ Kota, A. K., Kwon, G. & Tuteja, A., The design and applications of superomniphobic surfaces. *NPG ASIA MATER* **6** e109 (2014).
- ⁸ Ademovic, Z., Gonera, A., Mischnick, P. & Klee, D., Biocompatible Surface Preparation Using Amino-Functionalized Amylose. *BIOMACROMOLECULES* **7** 1429 (2006).
- ⁹ Weinhart, M. *et al.*, Linear Poly(methyl glycerol) and Linear Polyglycerol as Potent Protein and Cell Resistant Alternatives to Poly(ethylene glycol). *Chemistry - An Asian Journal* **5** 1992 (2010).
- ¹⁰ Kumawat, M. *et al.*, Surface Engineered Peroxidase-Mimicking Gold Nanoparticles to Subside Cell Inflammation. *LANGMUIR* **38** 1877 (2022).
- ¹¹ Yang, H. *et al.*, Smart Antibacterial Surface Made by Photopolymerization. *ACS APPL MATER INTER* **8** 28047 (2016).
- ¹² Zhao, Z. *et al.*, Universal Antibacterial Surfaces Fabricated from Quaternary Ammonium Salt-Based PNIPAM Microgels. *ACS APPL MATER INTER* **12** 19268 (2020).
- ¹³ Zhang, F. *et al.*, Phosphorylcholine- and cation-bearing copolymer coating with superior antibiofilm and antithrombotic properties for blood-contacting devices. *J MATER CHEM B* **8** 8433 (2020).
- ¹⁴ Hancock, M. J., Sekeroglu, K. & Demirel, M. C., Bioinspired directional surfaces for adhesion, wetting, and transport. *ADV FUNCT MATER* **22** 2223 (2012).
- ¹⁵ Zheng, Y., Gao, X. & Jiang, L., Directional adhesion of superhydrophobic butterfly wings. *SOFT MATTER* **3** 178 (2007).
- ¹⁶ Rodrigues, S. N., Gonçalves, I. C., Martins, M. C. L., Barbosa, M. A. & Ratner, B. D., Fibrinogen adsorption, platelet adhesion and activation on mixed hydroxyl-/methyl-terminated self-assembled monolayers. *BIOMATERIALS* **27** 5357 (2006).
- ¹⁷ Huang, B., Wu, H., Kim, S. & Zare, R. N., Coating of poly(dimethylsiloxane) with n-dodecyl- β -D-maltoside to minimize nonspecific protein adsorption. *LAB CHIP* **5** 1005 (2005).
- ¹⁸ Sen Gupta, A. *et al.*, Glycocalyx-mimetic dextran-modified poly(vinyl amine) surfactant coating reduces platelet adhesion on medical-grade polycarbonate surface. *BIOMATERIALS* **27** 3084 (2006).
- ¹⁹ Heuberger, M., Drobek, T. & Spencer, N. D., Interaction Forces and Morphology of a Protein-Resistant Poly(ethylene glycol) Layer. *BIOPHYS J* **88** 495 (2005).
- ²⁰ Wang, B. *et al.*, Copolymer Brushes with Temperature-Triggered, Reversibly Switchable Bactericidal

- and Antifouling Properties for Biomaterial Surfaces. *ACS APPL MATER INTER* **8** 27207 (2016).
- ²¹ Huang, C. J., Brault, N. D., Li, Y., Yu, Q. & Jiang, S., Controlled hierarchical architecture in surface - initiated zwitterionic polymer brushes with structurally regulated functionalities. *ADV MATER* **24** 1834 (2012).
- ²² Xu, J. *et al.*, Stereochemical Strategy Advances Microbially Antiadhesive Cotton Textile in Safeguarding Skin Flora. *ADV HEALTHC MATER* **8** 1900232 (2019).
- ²³ Tian, D. *et al.*, Fast Responsive and Controllable Liquid Transport on a Magnetic Fluid/Nanoarray Composite Interface. *ACS NANO* **10** 6220 (2016).
- ²⁴ Ichimura, K., Oh, S. K. & Nakagawa, M., Light-driven motion of liquids on a photoresponsive surface. *SCIENCE* **288** 1624 (2000).
- ²⁵ Yao, X., Ju, J., Yang, S., Wang, J. & Jiang, L., Temperature - driven switching of water adhesion on organogel surface. *ADV MATER* **26** 1895 (2014).
- ²⁶ Prins, M. W., Welters, W. J. & Weekamp, J. W., Fluid control in multichannel structures by electrocapillary pressure. *SCIENCE* **291** 277 (2001).
- ²⁷ Liu, M., Nie, F., Wei, Z., Song, Y. & Jiang, L., In Situ Electrochemical Switching of Wetting State of Oil Droplet on Conducting Polymer Films. *LANGMUIR* **26** 3993 (2010).
- ²⁸ Wang, N., Xiong, D., Deng, Y., Shi, Y. & Wang, K., Mechanically Robust Superhydrophobic Steel Surface with Anti-Icing, UV-Durability, and Corrosion Resistance Properties. *ACS APPL MATER INTER* **7** 6260 (2015).
- ²⁹ Chen, J. *et al.*, Robust Prototypical Anti-icing Coatings with a Self-lubricating Liquid Water Layer between Ice and Substrate. *ACS APPL MATER INTER* **5** 4026 (2013).
- ³⁰ Ng, Y., Tay, S. & Hong, L., Formation of Icephobic Surface with Micron-Scaled Hydrophobic Heterogeneity on Polyurethane Aerospace Coating. *ACS APPL MATER INTER* **10** 37517 (2018).
- ³¹ Lv, J., Song, Y., Jiang, L. & Wang, J., Bio-Inspired Strategies for Anti-Icing. *ACS NANO* **8** 3152 (2014).
- ³² Sheikh, S., Sheng, J. C., Blaszykowski, C. & Thompson, M., New oligoethylene glycol linkers for the surface modification of an ultra-high frequency acoustic wave biosensor. *CHEM SCI* **1** 271 (2010).
- ³³ Bertolino, M. C. & Granados, A. M., Synthesis in situ of gold nanoparticles by a dialkynyl Fischer carbene complex anchored to glass surfaces. *APPL SURF SCI* **383** 375 (2016).
- ³⁴ Haensch, C., Hoepfener, S. & Schubert, U. S., Chemical modification of self-assembled silane based monolayers by surface reactions. *CHEM SOC REV* **39** 2323 (2010).
- ³⁵ Wang, L., Schubert, U. S. & Hoepfener, S., Surface chemical reactions on self-assembled silane based monolayers. *CHEM SOC REV* **5** 654 (2021).
- ³⁶ Hadjesfandiari, N., Weinhart, M., Kizhakkedathu, J. N., Haag, R. & Brooks, D. E., Development of Antifouling and Bactericidal Coatings for Platelet Storage Bags Using Dopamine Chemistry. *ADV HEALTHC MATER* **7** 1700839 (2018).
- ³⁷ Mao, S. *et al.*, Mussel-Inspired Polymeric Coatings to Realize Functions from Single and Dual to Multiple Antimicrobial Mechanisms. *ACS APPL MATER INTER* **13** 3089 (2021).
- ³⁸ Yu, B. *et al.*, Mussel-inspired polydopamine chemistry to modulate template synthesis of 1D metal - organic framework superstructures. *J MATER CHEM A* **6** 21567 (2018).
- ³⁹ Kolb, H. C., Finn, M. G. & Sharpless, K. B., Click Chemistry: Diverse Chemical Function from a Few Good Reactions. *Angewandte Chemie International Edition* **40** 2004 (2001).
- ⁴⁰ Rostovtsev, V. V., Green, L. G., Fokin, V. V. & Sharpless, K. B., A stepwise Huisgen cycloaddition process: copper (I) - catalyzed regioselective "ligation" of azides and terminal alkynes. *Angewandte Chemie* **114** 2708 (2002).

- ⁴¹ Zhang, Y., Chu, C., Ma, W. & Takahara, A., Functionalization of Metal Surface via Thiol – Ene Click Chemistry: Synthesis, Adsorption Behavior, and Postfunctionalization of a Catechol- and Allyl-Containing Copolymer. *ACS Omega* **5** 7488 (2020).
- ⁴² Binder, W. H. & Sachsenhofer, R., Polymersome/Silica Capsules by ‘Click’ -Chemistry. *MACROMOL RAPID COMM* **29** 1097 (2008).
- ⁴³ Zoppe, J. O. *et al.*, Surface-Initiated Controlled Radical Polymerization: State-of-the-Art, Opportunities, and Challenges in Surface and Interface Engineering with Polymer Brushes. *CHEM REV* **117** 1105 (2017).
- ⁴⁴ Nicosia, C. & Huskens, J., Reactive self-assembled monolayers: from surface functionalization to gradient formation. *MATER HORIZ* **1** 32 (2014).
- ⁴⁵ Pujari, S. P., Scheres, L., Marcelis, A. T. M. & Zuilhof, H., Covalent Surface Modification of Oxide Surfaces. *Angewandte Chemie International Edition* **53** 6322 (2014).
- ⁴⁶ Zhuravlev, L. T., Concentration of hydroxyl groups on the surface of amorphous silicas. *LANGMUIR* **3** 316 (1987).
- ⁴⁷ Formation of an Organized Monolayer by Solution Adsorption of Octadecyltrichlorosilane on Gold.
- ⁴⁸ Shen, Q., Liu, L. & Zhang, W., Fabrication of a Photocontrolled Surface with Switchable Wettability Based on Host – Guest Inclusion Complexation and Protein Resistance. *LANGMUIR* **30** 9361 (2014).
- ⁴⁹ Chen, C., Xu, P. & Li, X., Regioselective Patterning of Multiple SAMs and Applications in Surface-Guided Smart Microfluidics. *ACS APPL MATER INTER* **6** 21961 (2014).
- ⁵⁰ Carvalho, R. R. *et al.*, Local Light-Induced Modification of the Inside of Microfluidic Glass Chips. *LANGMUIR* **32** 2389 (2016).
- ⁵¹ Qin, G. *et al.*, Preparation, characterization, and protein-resistance of films derived from a series of α -oligo(ethylene glycol)- ω -alkenes on H – Si(111) surfaces. *RSC ADV* **7** 14466 (2017).
- ⁵² Vutti, S. *et al.*, Covalent and Stable CuAAC Modification of Silicon Surfaces for Control of Cell Adhesion. *CHEMBIOCHEM* **16** 782 (2015).
- ⁵³ Moore, E. *et al.*, Surface-Initiated Hyperbranched Polyglycerol as an Ultralow-Fouling Coating on Glass, Silicon, and Porous Silicon Substrates. *ACS APPL MATER INTER* **6** 15243 (2014).
- ⁵⁴ Li, Y. *et al.*, “Click” Immobilization on Alkylated Silicon Substrates: Model for the Study of Surface Bound Antimicrobial Peptides. *Chemistry - A European Journal* **17** 2656 (2011).
- ⁵⁵ Lee, H., Dellatore, S. M., Miller, W. M. & Messersmith, P. B., Mussel-inspired surface chemistry for multifunctional coatings. *SCIENCE* **318** 426 (2007).
- ⁵⁶ Yang, H. *et al.*, Dopamine: Just the Right Medicine for Membranes. *ADV FUNCT MATER* **28** 1705327 (2018).
- ⁵⁷ Hong, S. H. *et al.*, Sprayable Ultrafast Polydopamine Surface Modifications. *ADV MATER INTERFACES* **3** 1500857 (2016).
- ⁵⁸ Ryou, M., Lee, Y. M., Park, J. & Choi, J. W., Mussel-Inspired Polydopamine-Treated Polyethylene Separators for High-Power Li-Ion Batteries. *ADV MATER* **23** 3066 (2011).
- ⁵⁹ Ryu, J. H., Messersmith, P. B. & Lee, H., Polydopamine Surface Chemistry: A Decade of Discovery. *ACS APPL MATER INTER* **10** 7523 (2018).
- ⁶⁰ Wu, H., Wu, L., Zhou, X., Liu, B. & Zheng, B., Patterning Hydrophobic Surfaces by Negative Microcontact Printing and Its Applications. *SMALL* **14** 1802128 (2018).
- ⁶¹ Polymer Chemistry.
- ⁶² Du, X. *et al.*, UV-Triggered Dopamine Polymerization: Control of Polymerization, Surface Coating, and Photopatterning. *ADV MATER* **26** 8029 (2014).

- ⁶³ Ku, S. H., Ryu, J., Hong, S. K., Lee, H. & Park, C. B., General functionalization route for cell adhesion on non-wetting surfaces. *BIOMATERIALS* **31** 2535 (2010).
- ⁶⁴ Zhou, X. *et al.*, Three-Dimensional-Bioprinted Dopamine-Based Matrix for Promoting Neural Regeneration. *ACS APPL MATER INTER* **10** 8993 (2018).
- ⁶⁵ Cui, H. *et al.*, Assembly of Multi - Spheroid Cellular Architectures by Programmable Droplet Merging. *ADV MATER* **33** 2006434 (2021).
- ⁶⁶ Chang, C. *et al.*, Underwater Superoleophobic Surfaces Prepared from Polymer Zwitterion/Dopamine Composite Coatings. *ADV MATER INTERFACES* **3** 1500521 (2016).
- ⁶⁷ Zhang, L. *et al.*, Combination of Bioinspiration: A General Route to Superhydrophobic Particles. *J AM CHEM SOC* **134** 9879 (2012).
- ⁶⁸ Zhu, J. *et al.*, Elevated salt transport of antimicrobial loose nanofiltration membranes enabled by copper nanoparticles via fast bioinspired deposition. *J MATER CHEM A* **4** 13211 (2016).
- ⁶⁹ Lei, W. *et al.*, Polydopamine Nanocoating for Effective Photothermal Killing of Bacteria and Fungus upon Near-Infrared Irradiation. *ADV MATER INTERFACES* **3** 1600767 (2016).
- ⁷⁰ Wan, X. *et al.*, High-performance magnetic poly (arylene ether nitrile) nanocomposites: Co-modification of Fe₃O₄ via mussel inspired poly(dopamine) and amino functionalized silane KH550. *APPL SURF SCI* **425** 905 (2017).
- ⁷¹ Zhang, F., Fan, J. B. & Wang, S., Interfacial polymerization: From chemistry to functional materials. *Angewandte Chemie International Edition* **59** 21840 (2020).
- ⁷² Wan, X. *et al.*, A Wetting - Enabled - Transfer (WET) Strategy for Precise Surface Patterning of Organohydrogels. *ADV MATER* **33** 2008557 (2021).
- ⁷³ Lee, H. A., Park, E. & Lee, H., Polydopamine and Its Derivative Surface Chemistry in Material Science: A Focused Review for Studies at KAIST. *ADV MATER* **32** 1907505 (2020).
- ⁷⁴ Tran, T., Chen, X., Doshi, S., Stafford, C. M. & Lin, H., Grafting polysiloxane onto ultrafiltration membranes to optimize surface energy and mitigate fouling. *SOFT MATTER* **16** 5044 (2020).
- ⁷⁵ Yang, D. *et al.*, Improved electromechanical properties of NBR dielectric composites by poly (dopamine) and silane surface functionalized TiO₂ nanoparticles. *J MATER CHEM C* **4** 7724 (2016).
- ⁷⁶ Yang, D. *et al.*, Dopamine and silane functionalized barium titanate with improved electromechanical properties for silicone dielectric elastomers. *RSC ADV* **6** 9172 (2016).
- ⁷⁷ Liu, Z., Hu, Y., Liu, C. & Zhou, Z., Surface-independent one-pot chelation of copper ions onto filtration membranes to provide antibacterial properties. *CHEM COMMUN* **52** 12245 (2016).
- ⁷⁸ Lee, H. A., Park, E. & Lee, H., Polydopamine and its derivative surface chemistry in material science: a focused review for studies at KAIST. *ADV MATER* **32** 1907505 (2020).
- ⁷⁹ Hong, S. *et al.*, Non - covalent self - assembly and covalent polymerization co - contribute to polydopamine formation. *ADV FUNCT MATER* **22** 4711 (2012).
- ⁸⁰ Hong, S. *et al.*, Pyrogallol 2 - Aminoethane: A Plant Flavonoid - Inspired Molecule for Material - Independent Surface Chemistry. *ADV MATER INTERFACES* **1** 1400113 (2014).
- ⁸¹ Hong, S., Wang, Y., Park, S. Y. & Lee, H., Progressive fuzzy cation- π assembly of biological catecholamines. *SCI ADV* **4** t7457 (2018).
- ⁸² Collman, J. P., Devaraj, N. K. & Chidsey, C. E. D., “Clicking” Functionality onto Electrode Surfaces. *LANGMUIR* **20** 1051 (2004).
- ⁸³ Collman, J. P., Devaraj, N. K., Eberspacher, T. P. A. & Chidsey, C. E. D., Mixed Azide-Terminated Monolayers: A Platform for Modifying Electrode Surfaces. *LANGMUIR* **22** 2457 (2006).
- ⁸⁴ Gupta, N. *et al.*, A versatile approach to high-throughput microarrays using thiol-ene chemistry. *NAT*

CHEM **2** 138 (2010).

⁸⁵ Tan, K. Y., Ramstedt, M., Colak, B., Huck, W. T. S. & Gautrot, J. E., Study of thiol – ene chemistry on polymer brushes and application to surface patterning and protein adsorption. *POLYM CHEM-UK* **7** 979 (2016).

⁸⁶ Dübner, M., Gevrek, T. N., Sanyal, A., Spencer, N. D. & Padeste, C., Fabrication of Thiol – Ene “Clickable” Copolymer-Brush Nanostructures on Polymeric Substrates via Extreme Ultraviolet Interference Lithography. *ACS APPL MATER INTER* **7** 11337 (2015).

⁸⁷ Meng, X. *et al.*, Thermoresponsive Arrays Patterned via Photoclick Chemistry: Smart MALDI Plate for Protein Digest Enrichment, Desalting, and Direct MS Analysis. *ACS APPL MATER INTER* **10** 1324 (2018).

⁸⁸ Cengiz, N., Gevrek, T. N., Sanyal, R. & Sanyal, A., Orthogonal thiol – ene ‘click’ reactions: a powerful combination for fabrication and functionalization of patterned hydrogels. *CHEM COMMUN* **53** 8894 (2017).

⁸⁹ Amato, D. V., Lee, H., Werner, J. G., Weitz, D. A. & Patton, D. L., Functional Microcapsules via Thiol – Ene Photopolymerization in Droplet-Based Microfluidics. *ACS APPL MATER INTER* **9** 3288 (2017).

⁹⁰ Feng, W. *et al.*, Surface patterning via thiol – yne click chemistry: an extremely fast and versatile approach to superhydrophilic – superhydrophobic micropatterns. *ADV MATER INTERFACES* **1** 1400269 (2014).

⁹¹ Dietrich, M. *et al.*, Photoclickable surfaces for profluorescent covalent polymer coatings. *ADV FUNCT MATER* **22** 304 (2012).

⁹² Tischer, T. *et al.*, Photo – patterning of non – fouling polymers and biomolecules on paper. *ADV MATER* **26** 4087 (2014).

⁹³ Blasco, E. *et al.*, Photochemical generation of light responsive surfaces. *ADV FUNCT MATER* **23** 4011 (2013).

⁹⁴ Sun, X., Stabler, C. L., Cazalis, C. S. & Chaikof, E. L., Carbohydrate and Protein Immobilization onto Solid Surfaces by Sequential Diels – Alder and Azide – Alkyne Cycloadditions. *BIOCONJUGATE CHEM* **17** 52 (2006).

⁹⁵ Lee, K. Y. J., Wang, Y. & Nie, S., In vitro study of a pH-sensitive multifunctional doxorubicin-gold nanoparticle system: therapeutic effect and surface enhanced Raman scattering. *RSC ADV* **5** 65651 (2015).

⁹⁶ Wedler-Jasinski, N. *et al.*, Recodable surfaces based on switchable hydrogen bonds. *CHEM COMMUN* **52** 8753 (2016).

⁹⁷ Young, J. F. *et al.*, Strong and Reversible Monovalent Supramolecular Protein Immobilization. *CHEMBIOCHEM* **11** 180 (2010).

⁹⁸ Haensch, C. *et al.*, Reversible Supramolecular Functionalization of Surfaces: Terpyridine Ligands as Versatile Building Blocks for Noncovalent Architectures. *LANGMUIR* **24** 12981 (2008).

⁹⁹ Bilbao, N. *et al.*, The impact of grafted surface defects on the on-surface Schiff-base chemistry at the solid – liquid interface. *CHEM COMMUN* **54** 9905 (2018).

¹⁰⁰ Gandavarapu, N. R., Azagarsamy, M. A. & Anseth, K. S., Photo – click living strategy for controlled, reversible exchange of biochemical ligands. *ADV MATER* **26** 2521 (2014).

¹⁰¹ Palleau, E., Morales, D., Dickey, M. D. & Velev, O. D., Reversible patterning and actuation of hydrogels by electrically assisted ionoprinting. *NAT COMMUN* **4** (2013).

¹⁰² Xie, C. *et al.*, Reconfiguring surface functions using visible-light-controlled metal-ligand coordination.

NAT COMMUN **9** (2018).

¹⁰³ Grim, J. C. *et al.*, A Reversible and Repeatable Thiol – Ene Bioconjugation for Dynamic Patterning of Signaling Proteins in Hydrogels. *ACS CENTRAL SCI* **4** 909 (2018).

¹⁰⁴ Blinco, J. P. *et al.*, Dynamic covalent chemistry on surfaces employing highly reactive cyclopentadienyl moieties. *ADV MATER* **23** 4435 (2011).

¹⁰⁵ Preuss, C. M., Goldmann, A. S., Trouillet, V., Walther, A. & Barner-Kowollik, C., Biomimetic Dopamine-Diels-Alder Switches. *MACROMOL RAPID COMM* **34** 640 (2013).

¹⁰⁶ Nayab, S. *et al.*, Chemically reprogrammable metal organic frameworks (MOFs) based on Diels – Alder chemistry. *CHEM COMMUN* **53** 11461 (2017).

¹⁰⁷ Roling, O. *et al.*, Rewritable Polymer Brush Micropatterns Grafted by Triazolinedione Click Chemistry. *Angewandte Chemie International Edition* **54** 13126 (2015).

¹⁰⁸ Claus, T. K. *et al.*, Light-driven reversible surface functionalization with anthracenes: visible light writing and mild UV erasing. *CHEM COMMUN* **53** 1599 (2017).

¹⁰⁹ Kehrloesser, D., Baumann, R., Kim, H. & Hampp, N., Photochemistry of Coumarin-Functionalized SiO₂ Nanoparticles. *LANGMUIR* **27** 4149 (2011).

¹¹⁰ Zheng, Y. B. *et al.*, Surface-Enhanced Raman Spectroscopy To Probe Photoreaction Pathways and Kinetics of Isolated Reactants on Surfaces: Flat versus Curved Substrates. *NANO LETT* **12** 5362 (2012).

¹¹¹ Goldmann, A. S. *et al.*, Adaptable and reprogrammable surfaces. *ADV MATER* **31** 1902665 (2019).

¹¹² Brehm, M., Scheiger, J. M., Welle, A. & Levkin, P. A., Reversible Surface Wettability by Silanization. *ADV MATER INTERFACES* **7** 1902134 (2020).

¹¹³ Kathan, M. *et al.*, Control of Imine Exchange Kinetics with Photoswitches to Modulate Self-Healing in Polysiloxane Networks by Light Illumination. *Angewandte Chemie International Edition* **55** 13882 (2016).

¹¹⁴ Du, X. *et al.*, Reversible and rewritable surface functionalization and patterning via photodynamic disulfide exchange. *ADV MATER* **27** 4997 (2015).

¹¹⁵ Shen, L. *et al.*, Surface Micropatterning of Uniaxially Oriented Polyethylene Films Using Interference Holography for Strain Sensors. *LANGMUIR* **33** 14592 (2017).

¹¹⁶ Yu, Q. *et al.*, Porous Pure MXene Fibrous Network for Highly Sensitive Pressure Sensors. *LANGMUIR* **38** 5494 (2022).

¹¹⁷ Wang, Z. *et al.*, Facile Approach to Conductive Polymer Microelectrodes for Flexible Electronics. *ACS APPL MATER INTER* **13** 21661 (2021).

¹¹⁸ Pardo, L., Wilson, W. C. & Boland, T., Characterization of Patterned Self-Assembled Monolayers and Protein Arrays Generated by the Ink-Jet Method. *LANGMUIR* **19** 1462 (2003).

¹¹⁹ Arrabito, G. *et al.*, On the Relationship between Jetted Inks and Printed Biopatterns: Molecular-Thin Functional Microarrays of Glucose Oxidase. *LANGMUIR* **25** 6312 (2009).

¹²⁰ Zhang, F. *et al.*, Direct Adsorption and Detection of Proteins, Including Ferritin, onto Microlens Array Patterned Bioarrays. *J AM CHEM SOC* **129** 9252 (2007).

¹²¹ Xu, M., Zhou, Z., Wang, Z. & Lu, H., Self-Assembled Microlens Array with Controllable Focal Length Formed on a Selective Wetting Surface. *ACS APPL MATER INTER* **12** 7826 (2020).

¹²² Xu, Q. *et al.*, Fabrication of polymer microlens array with controllable focal length by modifying surface wettability. *OPT EXPRESS* **26** 4172 (2018).

¹²³ Yang, X., Zhuang, K., Lu, Y. & Wang, X., Creation of Topological Ultraslippery Surfaces for Droplet Motion Control. *ACS NANO* **15** 2589 (2021).

¹²⁴ Alqurashi, T. *et al.*, Laser Inscription of Microfluidic Devices for Biological Assays. *ACS APPL*

MATER INTER **11** 12253 (2019).

¹²⁵ Paulssen, D., Hardt, S. & Levkin, P. A., Droplet Sorting and Manipulation on Patterned Two-Phase Slippery Lubricant-Infused Surface. *ACS APPL MATER INTER* **11** 16130 (2019).

¹²⁶ Kwak, M. K., Jeong, H. E. & Suh, K. Y., Rational design and enhanced biocompatibility of a dry adhesive medical skin patch. *ADV MATER* **23** 3949 (2011).

¹²⁷ Mihailescu, M. *et al.*, Laser-assisted fabrication and non-invasive imaging of 3D cell-seeding constructs for bone tissue engineering. *J MATER SCI* **51** 4262 (2016).

¹²⁸ Jun, I. *et al.*, Creating Hierarchical Topographies on Fibrous Platforms Using Femtosecond Laser Ablation for Directing Myoblasts Behavior. *ACS APPL MATER INTER* **8** 3407 (2016).

¹²⁹ Garcia, R., Knoll, A. W. & Riedo, E., Advanced scanning probe lithography. *NAT NANOTECHNOL* **9** 577 (2014).

¹³⁰ Szoszkiewicz, R. *et al.*, High-Speed, Sub-15 nm Feature Size Thermochemical Nanolithography. *NANO LETT* **7** 1064 (2007).

¹³¹ Gotsmann, B., Duerig, U., Frommer, J. & Hawker, C. J., Exploiting chemical switching in a Diels - Alder polymer for nanoscale probe lithography and data storage. *ADV FUNCT MATER* **16** 1499 (2006).

¹³² Song, J., Michas, C., Chen, C. S., White, A. E. & Grinstaff, M. W., Controlled Cell Alignment Using Two - Photon Direct Laser Writing - Patterned Hydrogels in 2D and 3D. *MACROMOL BIOSCI* **21** 2100051 (2021).

¹³³ Lee, S., Moon, J. J. & West, J. L., Three-dimensional micropatterning of bioactive hydrogels via two-photon laser scanning photolithography for guided 3D cell migration. *BIOMATERIALS* **29** 2962 (2008).

¹³⁴ Han, S. T. *et al.*, Microcontact printing of ultrahigh density gold nanoparticle monolayer for flexible flash memories. *ADV MATER* **24** 3556 (2012).

¹³⁵ Schmaltz, T., Sforazzini, G., Reichert, T. & Frauenrath, H., Self - assembled monolayers as patterning tool for organic electronic devices. *ADV MATER* **29** 1605286 (2017).

¹³⁶ Singh, M., Haverinen, H. M., Dhagat, P. & Jabbour, G. E., Inkjet printing—process and its applications. *ADV MATER* **22** 673 (2010).

¹³⁷ Liang, S. *et al.*, Microfluidic Patterning of Metal Structures for Flexible Conductors by In Situ Polymer-Assisted Electroless Deposition. *ADV SCI* **4** 1600313 (2017).

¹³⁸ Feng, W., Li, L., Du, X., Welle, A. & Levkin, P. A., Single - Step Fabrication of High - Density Microdroplet Arrays of Low - Surface - Tension Liquids. *ADV MATER* **28** 3202 (2016).

¹³⁹ Nuzzo, R. G. & Allara, D. L., Adsorption of bifunctional organic disulfides on gold surfaces. *J AM CHEM SOC* **105** 4481 (1983).

¹⁴⁰ Bain, C. D. & Whitesides, G. M., Molecular-Level Control over Surface Order in Self-Assembled Monolayer Films of Thiols on Gold. *SCIENCE* **240** 62 (1988).

¹⁴¹ Perl, A., Reinhoudt, D. N. & Huskens, J., Microcontact printing: limitations and achievements. *ADV MATER* **21** 2257 (2009).

¹⁴² Krämer, S., Fuierer, R. R. & Gorman, C. B., Scanning Probe Lithography Using Self-Assembled Monolayers. *CHEM REV* **103** 4367 (2003).

¹⁴³ Nicosia, C. & Huskens, J., Reactive self-assembled monolayers: from surface functionalization to gradient formation. *MATER HORIZ* **1** 32 (2014).

¹⁴⁴ Zhou, Z., Yu, P., Geller, H. M. & Ober, C. K., Biomimetic Polymer Brushes Containing Tethered Acetylcholine Analogs for Protein and Hippocampal Neuronal Cell Patterning. *BIOMACROMOLECULES* **14** 529 (2013).

¹⁴⁵ Wong, A. M. *et al.*, Controlled-Height Brush Polymer Patterns via Surface-Initiated Thiol-

- Methacrylate Photopolymerizations. *ACS MACRO LETT* **8** 1474 (2019).
- ¹⁴⁶ Jia, X., Jiang, X., Liu, R. & Yin, J., Facile Approach to Patterned Binary Polymer Brush through Photolithography and Surface-Initiated Photopolymerization. *ACS APPL MATER INTER* **2** 1200 (2010).
- ¹⁴⁷ Li, Y. *et al.*, Hierarchical Polymer Brush Nanoarrays: A Versatile Way to Prepare Multiscale Patterns of Proteins. *ACS APPL MATER INTER* **5** 2126 (2013).
- ¹⁴⁸ Li, L. *et al.*, Direct UV-Induced Functionalization of Surface Hydroxy Groups by Thiol-OI Chemistry. *Angewandte Chemie International Edition* **53** 3835 (2014).
- ¹⁴⁹ Du, X. *et al.*, UV - triggered dopamine polymerization: control of polymerization, surface coating, and photopatterning. *ADV MATER* **26** 8029 (2014).
- ¹⁵⁰ Zhang, C. *et al.*, CuSO₄ /H₂ O₂ -Induced Rapid Deposition of Polydopamine Coatings with High Uniformity and Enhanced Stability. *Angewandte Chemie* **128** 3106 (2016).
- ¹⁵¹ Zeng, Y. *et al.*, UV - Triggered Polydopamine Secondary Modification: Fast Deposition and Removal of Metal Nanoparticles. *ADV FUNCT MATER* **29** 1901875 (2019).
- ¹⁵² Behboodi-Sadabad, F., Trouillet, V., Welle, A., Messersmith, P. B. & Levkin, P. A., Surface Functionalization and Patterning by Multifunctional Resorcinarenes. *ACS APPL MATER INTER* **10** 39268 (2018).
- ¹⁵³ Zheng, Z. G. *et al.*, Light - patterned crystallographic direction of a self - organized 3d soft photonic crystal. *ADV MATER* **29** 1703165 (2017).
- ¹⁵⁴ Liu, C., Fan, Z., Tan, Y., Fan, F. & Xu, H., Tunable structural color patterns based on the visible - light - responsive dynamic diselenide metathesis. *ADV MATER* **32** 1907569 (2020).
- ¹⁵⁵ Liu, Y. *et al.*, Fabrication of anticounterfeiting nanocomposites with multiple security features via integration of a photoresponsive polymer and upconverting nanoparticles. *ADV FUNCT MATER* **31** 2103908 (2021).
- ¹⁵⁶ Zhao, X., Khandoker, M. A. R. & Golovin, K., Non-Fluorinated Omniphobic Paper with Ultralow Contact Angle Hysteresis. *ACS APPL MATER INTER* **12** 15748 (2020).
- ¹⁵⁷ Wolfe, D. B. *et al.*, Customization of Poly(dimethylsiloxane) Stamps by Micromachining Using a Femtosecond-Pulsed Laser. *ADV MATER* **15** 62 (2003).
- ¹⁵⁸ Shin, J. *et al.*, Monolithic digital patterning of polydimethylsiloxane with successive laser pyrolysis. *NAT MATER* **20** 100 (2021).
- ¹⁵⁹ Li, L. *et al.*, Inherent Photodegradability of Polymethacrylate Hydrogels: Straightforward Access to Biocompatible Soft Microstructures. *ADV FUNCT MATER* **29** 1902906 (2019).
- ¹⁶⁰ Xia, Y. & Whitesides, G. M., Soft Lithography. *Angewandte Chemie International Edition* **37** 550 (1998).
- ¹⁶¹ Wong, D. Y., Griffin, D. R., Reed, J. & Kasko, A. M., Photodegradable Hydrogels to Generate Positive and Negative Features over Multiple Length Scales. *MACROMOLECULES* **43** 2824 (2010).
- ¹⁶² Tibbitt, M. W., Kloxin, A. M., Dyamenahalli, K. U. & Anseth, K. S., Controlled two-photon photodegradation of PEG hydrogels to study and manipulate subcellular interactions on soft materials. *SOFT MATTER* **6** 5100 (2010).
- ¹⁶³ Azagarsamy, M. A., McKinnon, D. D., Alge, D. L. & Anseth, K. S., Coumarin-Based Photodegradable Hydrogel: Design, Synthesis, Gelation, and Degradation Kinetics. *ACS MACRO LETT* **3** 515 (2014).
- ¹⁶⁴ Fairbanks, B. D., Singh, S. P., Bowman, C. N. & Anseth, K. S., Photodegradable, Photoadaptable Hydrogels via Radical-Mediated Disulfide Fragmentation Reaction. *MACROMOLECULES* **44** 2444 (2011).
- ¹⁶⁵ Lunzer, M. *et al.*, A disulfide-based linker for thiol - norbornene conjugation: formation and cleavage

- of hydrogels by the use of light. *POLYM CHEM-UK* **13** 1158 (2022).
- ¹⁶⁶ Rapp, T. L., Highley, C. B., Manor, B. C., Burdick, J. A. & Dmochowski, I. J., Ruthenium - Crosslinked Hydrogels with Rapid, Visible - Light Degradation. *Chemistry - A European Journal* **24** 2328 (2018).
- ¹⁶⁷ Liu, C., Tan, Y., He, C., Ji, S. & Xu, H., Unconstrained 3D Shape Programming with Light - Induced Stress Gradient. *ADV MATER* **33** 2105194 (2021).
- ¹⁶⁸ Mitsuoka, T., Torikai, A. & Fueki, K., Wavelength sensitivity of the photodegradation of poly (methyl methacrylate). *J APPL POLYM SCI* **47** 1027 (1993).
- ¹⁶⁹ Yan, M., Choi, S., Subramanian, K. & Adesida, I., The effects of molecular weight on the exposure characteristics of poly (methylmethacrylate) developed at low temperatures. *Journal of Vacuum Science & Technology B: Microelectronics and Nanometer Structures Processing, Measurement, and Phenomena* **26** 2306 (2008).
- ¹⁷⁰ Torikai, A., Ohno, M. & Fueki, K., Photodegradation of poly (methyl methacrylate) by monochromatic light: Quantum yield, effect of wavelengths, and light intensity. *J APPL POLYM SCI* **41** 1023 (1990).
- ¹⁷¹ Torikai, A., Hiraga, S. & Fueki, K., Photodegradation of blends of poly (methyl methacrylate) and poly (styrene-co-methyl methacrylate). *POLYM DEGRAD STABIL* **37** 73 (1992).
- ¹⁷² Soeriyadi, A. H. *et al.*, A detailed surface analytical study of degradation processes in (meth)acrylic polymers. *Journal of Polymer Science Part A: Polymer Chemistry* **50** 1801 (2012).
- ¹⁷³ Chiantore, O., Trossarelli, L. & Lazzari, M., Photooxidative degradation of acrylic and methacrylic polymers. *POLYMER* **41** 1657 (2000).
- ¹⁷⁴ Kaczmarek, H., Kamińska, A. & van Herk, A., Photooxidative degradation of poly (alkyl methacrylate) s. *EUR POLYM J* **36** 767 (2000).
- ¹⁷⁵ Scheiger, J. M. *et al.*, Inherently UV Photodegradable Poly (methacrylate) Gels. *ADV FUNCT MATER* **31** 2105681 (2021).
- ¹⁷⁶ Shanti, R. *et al.*, Degradation of ultra-high molecular weight poly(methyl methacrylate-co-butyl acrylate-co-acrylic acid) under ultra violet irradiation. *RSC ADV* **7** 112 (2017).
- ¹⁷⁷ Grassie, N., Photodegradation of methacrylate/acrylate copolymers. *PURE APPL CHEM* **34** 247 (1973).
- ¹⁷⁸ Du, X. *et al.*, Bio-inspired strategy for controlled dopamine polymerization in basic solutions. *POLYM CHEM-UK* **8** 2145 (2017).
- ¹⁷⁹ Psarski, M. *et al.*, Vapor phase deposition of fluoroalkyl trichlorosilanes on silicon and glass: Influence of deposition conditions and chain length on wettability and adhesion forces. *MATER CHEM PHYS* **204** 305 (2018).
- ¹⁸⁰ Fadeev, A. Y. & McCarthy, T. J., Self-Assembly Is Not the Only Reaction Possible between Alkyltrichlorosilanes and Surfaces: Monomolecular and Oligomeric Covalently Attached Layers of Dichloro- and Trichloroalkylsilanes on Silicon. *LANGMUIR* **16** 7268 (2000).
- ¹⁸¹ Scofield, J. H., Hartree-Slater subshell photoionization cross-sections at 1254 and 1487 eV. *J ELECTRON SPECTROSC* **8** 129 (1976).
- ¹⁸² Zhang, F. *et al.*, A monolithic hydro/organo macro copolymer actuator synthesized via interfacial copolymerization. *NPG ASIA MATER* **9** e380 (2017).
- ¹⁸³ Zhang, H., Wang, P. & Zhang, D., Designing a transparent organogel layer with self-repairing property for the inhibition of marine biofouling. *Colloids and Surfaces A: Physicochemical and Engineering Aspects* **538** 140 (2018).
- ¹⁸⁴ Wang, Y. *et al.*, Bioinspired Solid Organogel Materials with a Regenerable Sacrificial Alkane Surface

Layer. *ADV MATER* **29** 1700865 (2017).

¹⁸⁵ Yao, X. *et al.*, Self-Replenishable Anti-Waxing Organogel Materials. *Angewandte Chemie International Edition* **54** 8975 (2015).

¹⁸⁶ Kirilov, P. *et al.*, Aqueous dispersions of organogel nanoparticles – potential systems for cosmetic and dermo-cosmetic applications. *INT J COSMETIC SCI* **36** 336 (2014).

¹⁸⁷ Li, Z., Zhang, B., Jia, S., Ma, M. & Hao, J., Novel supramolecular organogel based on β -cyclodextrin as a green drug carrier for enhancing anticancer effects. *J MOL LIQ* **250** 19 (2018).

¹⁸⁸ Lupi, F. R. *et al.*, Olive oil/policosanol organogels for nutraceutical and drug delivery purposes. *FOOD FUNCT* **4** 1512 (2013).

¹⁸⁹ Sagiri, S. S. *et al.*, Encapsulation of vegetable organogels for controlled delivery applications. *DES MONOMERS POLYM* **16** 366 (2013).

¹⁹⁰ Esposito, C. L., Kirilov, P. & Roullin, V. G., Organogels, promising drug delivery systems: an update of state-of-the-art and recent applications. *J CONTROL RELEASE* **271** 1 (2018).

¹⁹¹ Vintiloiu, A. & Leroux, J., Organogels and their use in drug delivery — A review. *J CONTROL RELEASE* **125** 179 (2008).

¹⁹² Venkatesan, G. A. & Sarles, S. A., Droplet immobilization within a polymeric organogel improves lipid bilayer durability and portability. *LAB CHIP* **16** 2116 (2016).

¹⁹³ Gao, H. *et al.*, Adaptive and freeze-tolerant heteronetwork organohydrogels with enhanced mechanical stability over a wide temperature range. *NAT COMMUN* **8** 15911 (2017).

¹⁹⁴ Lai, H. Y., Leon, A. D., Pangilinan, K. & Advincula, R., Superoleophilic and under-oil superhydrophobic organogel coatings for oil and water separation. *PROG ORG COAT* **115** 122 (2018).

¹⁹⁵ Tezcan Demirel, Y., Yati, I., Donmez, R. & Bulbul Sonmez, H., Clean-up of oily liquids, fuels and organic solvents from the contaminated water fields using poly(propylene glycol) based organogels. *CHEM ENG J* **312** 126 (2017).

¹⁹⁶ Co, E. D. & Marangoni, A. G., Organogels: An Alternative Edible Oil-Structuring Method. *Journal of the American Oil Chemists' Society* **89** 749 (2012).

¹⁹⁷ Liu, M., Wang, S. & Jiang, L., Nature-inspired superwettability systems. *NAT REV MATER* **2** 17036 (2017).

¹⁹⁸ Yao, X., Ju, J., Yang, S., Wang, J. & Jiang, L., Temperature-Driven Switching of Water Adhesion on Organogel Surface. *ADV MATER* **26** 1895 (2014).

¹⁹⁹ Lv, J., Yao, X., Zheng, Y., Wang, J. & Jiang, L., Antiadhesion Organogel Materials: From Liquid to Solid. *ADV MATER* **29** 1703032 (2017).

²⁰⁰ Liu, H., Zhang, P., Liu, M., Wang, S. & Jiang, L., Organogel-based Thin Films for Self-Cleaning on Various Surfaces. *ADV MATER* **25** 4477 (2013).

²⁰¹ Zhang, P. *et al.*, Grooved Organogel Surfaces towards Anisotropic Sliding of Water Droplets. *ADV MATER* **26** 3131 (2014).

²⁰² Urata, C. *et al.*, Textured Organogel Films Showing Unusual Thermoresponsive Dewetting, Icephobic, and Optical Properties. *ADV MATER INTERFACES* **6** 1801358 (2019).

²⁰³ Kim, B., Hong, L., Chung, Y., Kim, D. & Lee, C., Solvent-Resistant PDMS Microfluidic Devices with Hybrid Inorganic/Organic Polymer Coatings. *ADV FUNCT MATER* **19** 3796 (2009).

²⁰⁴ Lee, J. N., Park, C. & Whitesides, G. M., Solvent Compatibility of Poly(dimethylsiloxane)-Based Microfluidic Devices. *ANAL CHEM* **75** 6544 (2003).

²⁰⁵ Lee, J., Kim, M. J. & Lee, H. H., Surface Modification of Poly(dimethylsiloxane) for Retarding Swelling in Organic Solvents. *LANGMUIR* **22** 2090 (2006).

- ²⁰⁶ Pirner, D., Dulle, M., E. J. Mauer, M. & Förster, S., Reinforcement of nanostructured organogels by hydrogen bonds. *RSC ADV* **6** 42730 (2016).
- ²⁰⁷ García-Iglesias, M., de Waal, B. F. M., de Feijter, I., Palmans, A. R. A. & Meijer, E. W., Nanopatterned Superlattices in Self-Assembled C2-Symmetric Oligodimethylsiloxane-Based Benzene-1,3,5-Tricarboxamides. *Chemistry – A European Journal* **21** 377 (2015).
- ²⁰⁸ Gronwald, O., Snip, E. & Shinkai, S., Gelators for organic liquids based on self-assembly: a new facet of supramolecular and combinatorial chemistry. *CURR OPIN COLLOID IN* **7** 148 (2002).
- ²⁰⁹ Ayer, M. A., Schrettl, S., Balog, S., Simon, Y. C. & Weder, C., Light-responsive azo-containing organogels. *SOFT MATTER* **13** 4017 (2017).
- ²¹⁰ Hu, X., Shi, J. & Thomas, S. W., Photolabile ROMP gels using ortho-nitrobenzyl functionalized crosslinkers. *POLYM CHEM-UK* **6** 4966 (2015).
- ²¹¹ Gumbley, P., Hu, X., Lawrence III, J. A. & Thomas III, S. W., Photoresponsive Gels Prepared by Ring-Opening Metathesis Polymerization. *MACROMOL RAPID COMM* **34** 1838 (2013).
- ²¹² Theis, S. *et al.*, Metallo-Supramolecular Gels that are Photocleavable with Visible and Near-Infrared Irradiation. *Angewandte Chemie International Edition* **56** 15857 (2017).
- ²¹³ Dashan, I., Elverici, M., Balta, D. K., Temel, B. A. & Temel, G., Versatile light-responsive organogels: Evaluation of their dye releasing and photoinitiation behaviors. *Journal of Polymer Science Part A: Polymer Chemistry* **57** 1275 (2019).
- ²¹⁴ Li, L., Scheiger, J. M. & Levkin, P. A., Design and Applications of Photoresponsive Hydrogels. *ADV MATER* **31** 1807333 (2019).
- ²¹⁵ Li, L. *et al.*, Inherent Photodegradability of Polymethacrylate Hydrogels: Straightforward Access to Biocompatible Soft Microstructures. *ADV FUNCT MATER* **29** 1902906 (2019).
- ²¹⁶ Han, Y., Shen, H., Zhao, M. & Sun, W., Flavour binding mechanism between a typical meat flavour compound (nonanal) and porcine myofibrillar proteins with consideration of conformational changes. *International Journal of Food Science & Technology* **53** 1954 (2018).
- ²¹⁷ Yilbas, B. S., Al-Sharafi, A., Ali, H. & Al-Aqeeli, N., Dynamics of a water droplet on a hydrophobic inclined surface: influence of droplet size and surface inclination angle on droplet rolling. *RSC ADV* **7** 48806 (2017).
- ²¹⁸ Carbaugh, D. J., Wright, J. T., Parthiban, R. & Rahman, F., Photolithography with polymethyl methacrylate (PMMA). *SEMICONDUCTOR SCI TECH* **31** 25010 (2015).
- ²¹⁹ Advancing sustainable materials management: 2018 fact sheet. United States Environmental Protection Agency (EPA)—Office of Land and Emergency Management.
- ²²⁰ Stubbins, A., Law, K. L., Muñoz, S. E., Bianchi, T. S. & Zhu, L., Plastics in the Earth system. *SCIENCE* **373** 51 (2021).
- ²²¹ MacLeod, M., Arp, H. P. H., Tekman, M. B. & Jahnke, A., The global threat from plastic pollution. *SCIENCE* **373** 61 (2021).
- ²²² Zhang, Y. *et al.*, Atmospheric microplastics: A review on current status and perspectives. *EARTH-SCI REV* **203** 103118 (2020).
- ²²³ Al-Salem, S. M., Lettieri, P. & Baeyens, J., The valorization of plastic solid waste (PSW) by primary to quaternary routes: From re-use to energy and chemicals. *PROG ENERG COMBUST* **36** 103 (2010).
- ²²⁴ Ignatyev, I. A., Thielemans, W. & Vander Beke, B., Recycling of Polymers: A Review. *CHEMSUSCHEM* **7** 1579 (2014).
- ²²⁵ Thiounn, T. & Smith, R. C., Advances and approaches for chemical recycling of plastic waste. *Journal of Polymer Science* **58** 1347 (2020).

- ²²⁶ Hong, M. & Chen, E. Y., Chemically recyclable polymers: a circular economy approach to sustainability. *GREEN CHEM* **19** 3692 (2017).
- ²²⁷ Al-Salem, S. M., Lettieri, P. & Baeyens, J., Recycling and recovery routes of plastic solid waste (PSW): A review. *WASTE MANAGE* **29** 2625 (2009).
- ²²⁸ Brems, A., Baeyens, J. & Dewil, R., Recycling and recovery of post-consumer plastic solid waste in a European context. *THERM SCI* **16** 669 (2012).
- ²²⁹ García, J. C., Marcilla, A. & Beltrán, M., The effect of adding processed PVC on the rheology of PVC plastisols. *Polymer (Guilford)* **39** 2261 (1998).
- ²³⁰ Kao, C. C., Ghita, O. R., Hallam, K. R., Heard, P. J. & Evans, K. E., Mechanical studies of single glass fibres recycled from hydrolysis process using sub-critical water. *Composites Part A: Applied Science and Manufacturing* **43** 398 (2012).
- ²³¹ Zia, K. M., Bhatti, H. N. & Ahmad Bhatti, I., Methods for polyurethane and polyurethane composites, recycling and recovery: A review. *Reactive and Functional Polymers* **67** 675 (2007).
- ²³² Kowalska, E., Wielgosz, Z. & Pelka, J., Use of Post-Life Waste and Production Waste in Thermoplastic Polymer Compositions. *Polymers and Polymer Composites* **10** 83 (2002).
- ²³³ Fortman, D. J. *et al.*, Approaches to Sustainable and Continually Recyclable Cross-Linked Polymers. *ACS SUSTAIN CHEM ENG* **6** 11145 (2018).
- ²³⁴ Butler, E., Devlin, G. & McDonnell, K., Waste Polyolefins to Liquid Fuels via Pyrolysis: Review of Commercial State-of-the-Art and Recent Laboratory Research. *WASTE BIOMASS VALORI* **2** 227 (2011).
- ²³⁵ Kaitz, J. A., Lee, O. P. & Moore, J. S., Depolymerizable polymers: preparation, applications, and future outlook. *MRS COMMUN* **5** 191 (2015).
- ²³⁶ Anuar Sharuddin, S. D., Abnisa, F., Wan Daud, W. M. A. & Aroua, M. K., A review on pyrolysis of plastic wastes. *ENERG CONVERS MANAGE* **115** 308 (2016).
- ²³⁷ John Scheirs, Walter Kaminsky, Feedstock Recycling and Pyrolysis of Waste Plastics: Converting Waste Plastics into Diesel and Other Fuels, 24 March 2006, 10.1002/0470021543
- ²³⁸ McKay, G., Dioxin characterisation, formation and minimisation during municipal solid waste (MSW) incineration: review. *Chemical engineering journal (Lausanne, Switzerland : 1996)* **86** 343 (2002).
- ²³⁹ McNeill, I. C. & Sadeghi, S. M. T., Thermal stability and degradation mechanisms of poly(acrylic acid) and its salts: Part 1—Poly(acrylic acid). *POLYM DEGRAD STABIL* **29** 233 (1990).
- ²⁴⁰ Zekry, M., Nassar, I., Salim, H. & Abdallah, A., The Potential of super absorbent polymers from diaper wastes to enhance water retention properties of the soil. *Soil & Environment* **39** 27 (2020).
- ²⁴¹ Al-Jabari, M., Ghyadah, R. A. & Alokely, R., Recovery of hydrogel from baby diaper wastes and its application for enhancing soil irrigation management. *J ENVIRON MANAGE* **239** 255 (2019).
- ²⁴² Lépine, L. & Gilbert, R., Thermal degradation of polyacrylic acid in dilute aqueous solution. *POLYM DEGRAD STABIL* **75** 337 (2002).
- ²⁴³ Ching, T. W. *et al.*, Microwave-Assisted Hydrothermal Decomposition of Super Absorbent Polymers. *ACS SUSTAIN CHEM ENG* **8** 14504 (2020).
- ²⁴⁴ Chazovachii, P. T. *et al.*, Giving superabsorbent polymers a second life as pressure-sensitive adhesives. *NAT COMMUN* **12** (2021).
- ²⁴⁵ Moriguchi, T. & Arita, Y. Process for producing acrylic acid. U.S. Patent 8404887B2 (March 26, 2013).
- ²⁴⁶ Li, L. *et al.*, Inherent Photodegradability of Polymethacrylate Hydrogels: Straightforward Access to Biocompatible Soft Microstructures. *ADV FUNCT MATER* **29** 1902906 (2019).
- ²⁴⁷ Vinu, R. & Madras, G., Kinetics of sono-photooxidative degradation of poly(alkyl methacrylate)s. *ULTRASON SONOCHEM* **18** 608 (2011).

-
- ²⁴⁸ Ohara, T. *et al.*, in *Ullmann's Encyclopedia of Industrial Chemistry*, pp. 1.
- ²⁴⁹ Chang, E. P., Viscoelastic windows of pressure-sensitive adhesives. *The Journal of Adhesion* **34** 189 (1991).
- ²⁵⁰ Lee, H. A., Park, E. & Lee, H., Polydopamine and its derivative surface chemistry in material science: a focused review for studies at KAIST. *ADV MATER* **32** 1907505 (2020).

